

Peptide-based probes for protein N-Methyltransferases Zhang, Y.

Citation

Zhang, Y. (2022, June 2). *Peptide-based probes for protein N-Methyltransferases*. Retrieved from https://hdl.handle.net/1887/3307258

Version: Publisher's Version

License: License agreement concerning inclusion of doctoral thesis in the

Institutional Repository of the University of Leiden

Downloaded from: https://hdl.handle.net/1887/3307258

Note: To cite this publication please use the final published version (if applicable).

Peptide-Based Probes for Protein N-Methyltransferases

Yurui Zhang

张宇睿

Ph.D. thesis, Leiden University, 2022 Yurui Zhang was supported by the China Scholarship Council. Cover design: Yurui Zhang Layout: Yurui Zhang Thesis was printed by Proefschriftmaken: www.proefschriftmaken.nl

Peptide-Based Probes for Protein N-Methyltransferases

Proefschrift

ter verkrijging van
de graad van doctor aan de Universiteit Leiden,
op gezag van rector magnificus prof.dr.ir. H. Bijl,
volgens besluit van het college voor promoties
te verdedigen op donderdag 2 juni 2022

door

klokke 11:15 uur

Yurui Zhang

Geboren te Datong, China
in 1991

Promotor: Prof.dr. N.I. Martin

Co-promotor: Dr. M.J. van Haren

Promotiecommissie: Prof.dr. G.P. van Wezel

Prof.dr. L.H. Heitman

Prof.dr. M.T.C. Walvoort (Rijksuniversiteit Groningen)

Dr. S.J. Pomplun

Dr. S.A.K. Jongkees (Vrije Universiteit Amsterdam)

Table of contents

Chapter 1	1
Introduction	
Chapter 2	15
Transition state analogues as inhibitors of PRMTs	
Chapter 3	33
Structural studies provide new insights into the role of lysine acetylation	
on substrate recognition by CARM1 and inform the design of potent	
peptidomimetic inhibi-tors	
Chapter 4	49
A Direct Assay for Measuring Activity and Inhibition of Coactivator	
Associated Arginine Methyltransferase 1	
Chapter 5	67
Macrocyclic Peptides as Allosteric Inhibitors of Nicotinamide	
N-Methyltransferase	
Chapter 6	89
Summary Samenvatting	89
Supplementary materials for Chapter 2-5 Appendix I - IV	97
Appendix Supplementary materials for Chapter 2	98
Appendix II Supplementary materials for Chapter 3	101
Appendix III Supplementary materials for Chapter 4	109
Appendix IV Supplementary materials for Chapter 5	115
Curriculum vitae	127
List of Publications	128

Chapter 1

Introduction

1. Introduction to protein methyltransferases

Protein methyltransferases (PMTs) are responsible for the methylation of amino acid residues in a number of proteins including histones. PMTs that act on histones are in turn highly involved in the regulation of gene expression and transcription. Protein methylation can occur on lysine, arginine, histidine, or glutamine side chains as well as on α -N-terminal residues. All PMTs use a common mechanism of catalysis, in which the universal methyl donor S-adenosyl-L-methionine (AdoMet) and the target protein substrate bind the enzyme to form a ternary complex and, after transfer of the methyl group, the methylated protein substrate and the demethylated cofactor S-adenosyl-L-homocysteine (AdoHcy) are released from the active site. Methyltransferase enzymes share high homology in the active site residues that interact with the AdoMet cofactor, but can be distinguished by their ability to methylate specific amino acids of a small selection of protein substrates.

The methylation of lysine side chains and N-terminal amino acids result in mono-, di and trimethylated products,³ while the arginine side chain can be monomethylated or symmetrically or asymmetrically dimethylated on its quanidyl group.⁴ Histidine can be monomethylated on its imidazole nitrogen atom⁵ and glutamine can be monomethylated to N⁵-methylated glutamine (Figure 1).⁶ Histone methylation has been extensively investigated since it was first recognized in the early 2000s and it has since been shown to be vital in mediating cell signalling and a range of cellular functions.⁷⁻¹⁰ For example, histone H3 methyltransferases control the DNA methylation ¹¹ and the lysine methyltransferase Dot1p is involved in telomere silencing.¹² Aberrant expression of PMTs and their concomitant deleterious effects can be observed in cancer¹³, diabetes,¹⁴ and neurological diseases.¹⁵ Due to their role in a variety of key cellular functions, the discovery of selective inhibitors of PMTs has increasingly become an avenue of interest for therapeutic development ¹⁶, ^{17.} Inhibitors of protein lysine methyltransferases, such as UNC0642 (G9a/GLP) against breast cancer, 18 EPZ005687 (EZH2) against lymphoma cells, 19 and CPI-1205 (EZH2) against B-cell lymphoma²⁰ have been investigated in preclinical trials. In addition, protein arginine methyltransferases inhibitors, MS049 (PRMT4/6),²¹ TP-064 (CARM1),²² and EPZ020411 (PRMT6),²³ are highly selective chemical tools for inhibiting specific protein arginine methyltransferases (PRMTs). The different histone protein methylations regulate gene expression and transcription through a dynamic interplay of chromatin readers, writers, and erasers.^{24, 25} To gain a deeper understanding of the mechanistic processes related to histone methylation, peptide-based probes are valuable tools for understanding the roles of specific enzymes in the complexity of epigenetics. In this thesis, the development of peptide-based probes specific for the PRMT family of methyltransferases is discussed. Inspired by naturally occurring PRMT substrates, the general

methodology to design the peptide probes is based on the substitution and modification of the guanidine moiety of the target arginine residue. Through this methodology, the peptide based probes retain the selectivity and specificity of the peptide substrate, while the guanidine side chain modification mimics the methyltransferase transition state, turning a substrate into an inhibitor. These tool compounds provide detailed insight into the interactions of peptide substrate and AdoMet cofactor in the active site of the targeted methyltransferase.

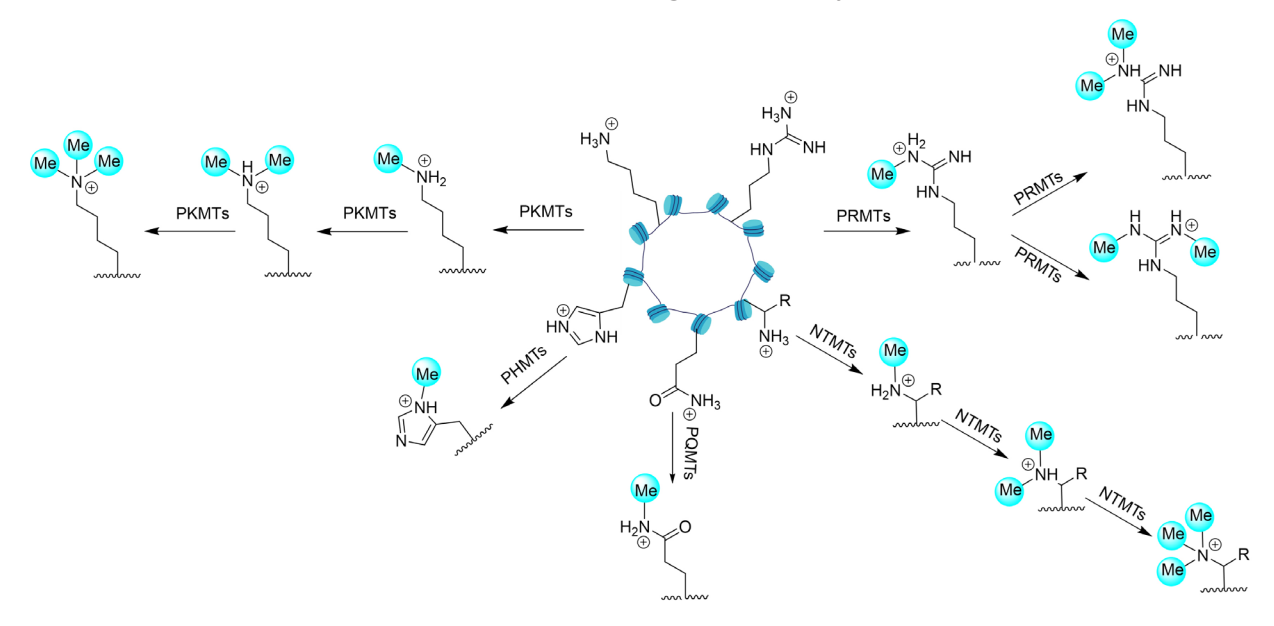


Figure 1. The different types of histone protein methyltransferases and their products. Protein lysine methyltransferases (PKMTs) form mono-, di- or tri-methylated lysine, Protein arginine methyltransferases (PRMTs) form mono-, asymmetrically or symmetrically dimethylated arginine; Protein histidine methyltransferases (PHMTs) form monomethylated histidine; Protein glutamine methyltransferase (PQMTs) form N⁵-methylated glutamine; and Protein N-terminal methyltransferases (NTMTs) form mono-, di-, or tri-methylated N-terminal.

2. Peptide Based Inhibitors and Mechanistic Probes for Protein Arginine Methyltransferases

Protein arginine methyltransferases catalyse the transfer of the methyl group from cofactor AdoMet to the guanidine moiety in the sidechain of arginine residues of protein substrates. After binding of the substrate and the cofactor to the catalytic domain of the PRMT, the methyl group is transferred from AdoMet to the arginine side chain following an S_N2 -like mechanism, to yield the products S-adenosyl-L-homocysteine (AdoHcy) and the methylated protein substrate (Figure 2). There are three distinct types of PRMTs found in mammalian cells,⁴ classified by their methylated product resulting in either ω - N^G -monomethylarginine (MMA), symmetric ω - N^G , N^G -dimethylarginine (sDMA), or asymmetric ω - N^G , N^G -dimethylarginine (aDMA).

and aDMA, and include PRMT1, PRMT3, PRMT4 (CARM1), PRMT6, or PRMT8⁴. The type II PRMT5 and PRMT9 form MMA and sDMA, ^{4, 27} while PRMT7 is the only type-III PRMT known to date that exclusively produces MMA. PRMT1 was the first mammalian PRMT discovered and is responsible for about 85% of total protein arginine methylation activity. ²⁸ Type-I and type-II PRMTs are responsible for the majority of arginine methylation in humans and their aberrant expression has been linked to different cancers, such as prostate cancer²⁹ and leukemia^{29, 30} as well as other pathologies including cardiovascular disease. ^{31, 32} Considering the impact of histone methylation on gene regulation and by extension epigenetic processes, PRMTs have been most heavily researched as potential therapeutical targets in a variety of cancers. ³³⁻³⁵

Figure 2. The overview of the PRMT binding site (residue numbering shown for PRMT4) bound to cofactor AdoMet in blue and a protein substrate in red indicating the interactions with the active site residues and the formation of monomethylated arginine (MMA) and subsequently asymmetrically or symmetrically dimethylated arginine (aDMA and sDMA) produced by the different types of PRMTs.

2.1 Peptide probes with substituted guanidino groups

The first peptide-based probes targeting PRMTs focussed on the substitution of the guanidine moiety in the arginine side chain in the context of a peptide fragment of a protein substrate. ³⁶⁻³⁸ Starting from the sequence of a known PRMT substrate to achieve selectivity, a variety of different substitution of the ω -nitrogen of the target arginine residue were explored to evaluate the effects on the methylating activity of the target PRMT. The first generation N^{η}-substituted arginyl peptides prepared in our group investigated the effects of substituent electronics and sterics on the second methylation step performed by PRMT1. The introduction of

ethyl, or mono-, di- and tri-fluoroethyl groups on one of the terminal nitrogens of the target arginine in the R1 peptide resulted in the inhibition of PRMT1 with IC₅₀ values in the micromolar range (13-29 µM) (Figure 3A).³⁶ Peptides R1-1, -2, -3, and -4 demonstrated a 5- to 24-fold increase in potency compared to the products of the methylation process (i.e. the aDMA or sDMA-containing peptides). Notably, the potency of the probes against PRMT1 increased with an increasing number of fluorine atoms. In addition, comparable activity was observed against PRMT6, but only weak inhibition of CARM1 was found. Inspired by these results, a second generation of Nⁿ-substituted PRMT probes were explored that expanded the range of substitutions on target arginine specifically examining steric, electronic, and pKa and effects (Figure 3B). PRMT1 demonstrated methylating activity towards R4, R5, R6, and R7, but only low levels of methylated product were found for R1 and R3 and no product was observed for R2 in which the arginine residue was modified with a strongly electon withdrawing nitro group. A similar approach was subsequently applied to another PRMT substrate, the HIV-Tat protein. A variety of modifications were introduced onto arginine residue 52 in the HIV-Tat⁴⁸⁻⁶⁰ peptide sequence (Figure 3C) and their effects on enzyme activity analysed. These peptide probes were found to be substrate inhibitors of PRMT1 and PRMT6 and the results obtained demonstrated that a wide range of substitutions were accepted by the PRMTs.

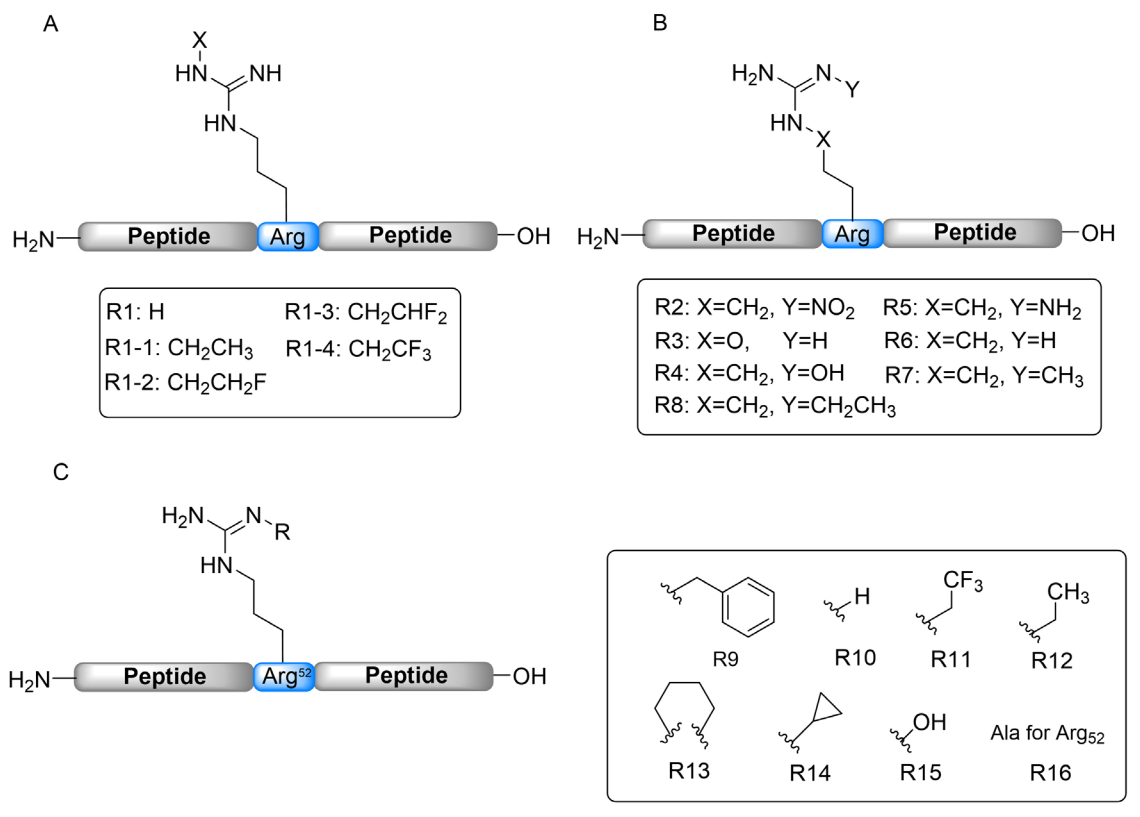


Figure 3. The peptide-based Nⁿ-substituted arginine analogues. A and B showed the guanidino modified peptide inhibitors; C. HIV-Tat⁴⁸⁻⁶⁰Arg⁵² guanidino modified peptide inhibitors.

2.2 Chloroacetylated arginines in peptide-based covalent inhibitors of PRMT1

Figure 4. A. Structure of H4 peptide based covalent inhibitors R17 and R18. B. Structure of H4 activity-based probes (ABPs) R17-1 (biotin-conjugated R17) and R18-1 (fluorescein-conjugated R18).

Covalent inhibitors have been increasingly considered a viable option in clinic and more frequently enter the market.^{39, 40} The covalent interaction with its target blocks the enzyme permanently and the enzyme's activity can be recovered only through de novo protein production. While this can be a downside when de novo production is fast or when prolonged effects are undesirable, covalent inhibitors do have the potential to alter disease pharmacology.³⁹ Recently, several covalent inhibitors of PRMT5 and PRMT6 have been described, showing promising activity outperforming the most potent competitive inhibitors. 41, 42 The crystal structure of the target enzyme plays a vital role in the design of the covalent inhibitors to select the correct spacers and warheads to evaluate. The work on covalent PRMT inhibitors was initiated by the group of Thompson who designed and synthesized two histone H4-based peptides consisting of the first 21 amino acids of the H4 tail and contained a chloroacetamide warhead on Arg¹⁷ or a fluoroacetamide on Arg¹⁸ (Figure 4). To investigate their potencies, the chloroacetamide peptides were incubated with PRMT1 showing that R17 (IC₅₀ 1.8 \pm 0.1 μ M) is about 52-fold more potent than R18 (IC₅₀ 94 \pm 17 μ M). Also of note, while R17 exhibited irreversible inactivation of PRMT1, the fluoroacetamide in R18 was found to be a competitive inhibitor.43

The covalent chloroacetamide-containing H4 peptide R17 was subsequently conjugated at the N-terminus to biotin (R17-1) or fluorescein (R17-2) turning the

peptides into PRMT1-targeting activity-based probes (ABPs) (Figure 4).⁴⁴ ABPs can be used as chemical tools for the investigation of novel functions, binding partners, expression levels or cellular localisation of enzymes as well as for the screening of inhibitors.⁴⁵⁻⁴⁷ The results indicated that N-terminal labelling of R17 did not affect the compound's inhibition of PRMT1. Both ABPs showed good labelling of PRMT1 in MCF-7 cells and R17-2 was found efficient to enrich and isolate the PRMT1.⁴⁴

2.3 Peptide-based probes mimicking the methyltransferase transition state

In an attempt to develop more potent PRMT inhibitors, our group reported a series of small bisubstrate molecules with a guanidine group attached to the adenosine unit of cofactor AdoMet with different linker lengths. While this approach resulted in potent inhibitor with somewhat surprising selectivity, the bisubstrate inhibitors were subsequently optimized towards further enhancing their selectivity through the incorporation of a PRMT-specific peptide sequence. This strategy was initially applied on PRMT4 (also known as coactivator-associated arginine methyltransferase 1 (CARM1)). The CARM1 transition state (TS) mimics were designed and prepared based on the peptide sequence of its known substrate poly(A)-binding protein 1(PABP1) (Figure 5). Different linkers between the adenosine and guanidine moieties were also evaluated revealing the three-carbon linker to most closely mimic the distance between the AdoMet adenosine moiety and the substrate arginine guanidino group. The PABP1 PABP1 and PABP1 TS mimics showed a nanomolar range of inhibition against CARM1 with up to ~300-fold selectivity over PRMT1.

Figure 5. The structure of transition state mimic peptide inhibitors based on CARM1 substrate poly(A)-binding protein 1 (PABP1).

Co-crystal structures obtained with CARM1 and these PABP1 inspired adenosine-peptide conjugates (Figure 6) showed that they effectively mimic the TS of the first methylation step performed by PRMTs. ⁴⁹ These structural results provided new insights into the binding interactions of the PRMTs with the specific peptide

substrate. This approach to generating PRMT-specific TS mimics is in principle also applicable to all PRMTs. In this regard, part of the work contained in this thesis was aimed at extending this approach to other PRMTs.

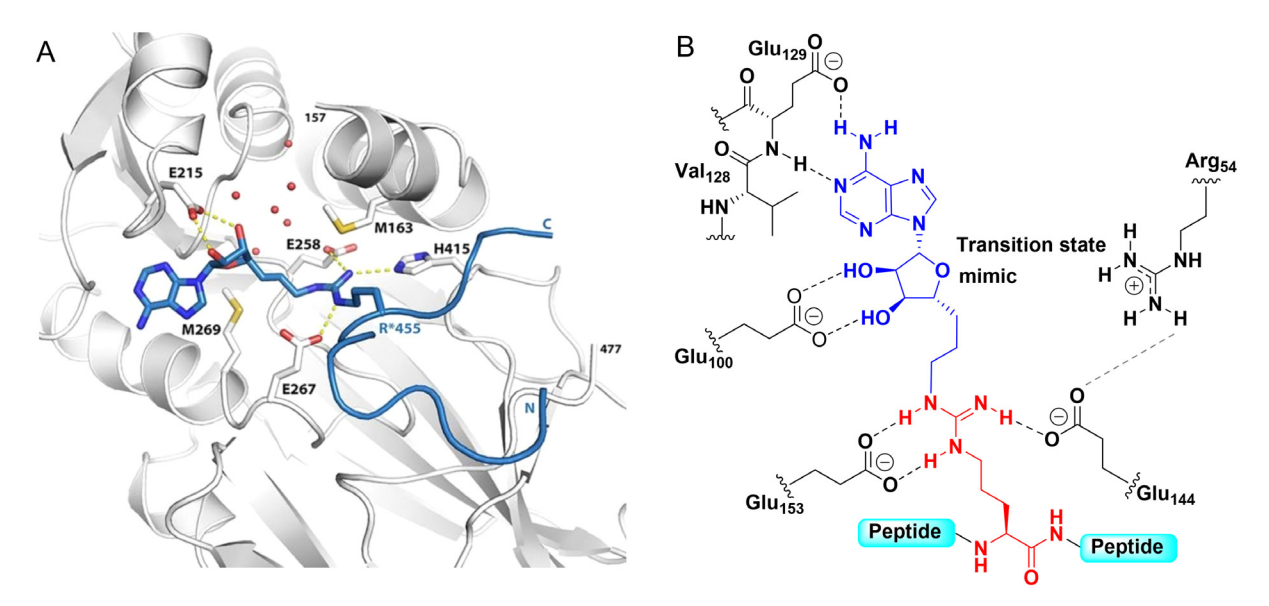


Figure 6. A.The crystal structure of CARM1 and PABP1 peptide substrates. B. Transition state mimic bind to CARM1 catalytic pocket.

3. Thesis Outline

In Chapter 2, the general applicability of the PRMT TS mimic methodology is reported. Specifically, TS mimicking adenosine-peptide conjugates were designed and synthesized to target PRMT1.⁵⁰ Based on the previous work targeting CARM1,⁴⁹ the three-carbon spacer was selected to covalently connect arginine side chains in histone H4¹⁻⁷ and H4¹⁻⁸ peptides to the adenosine moiety. Both sequences were evaluated with a free and an acetylated N-terminus and the ability of the corresponding TS mimics to inhibit PRMT1 compared to the asymmetrically dimethylated arginine (aDMA) product. In all cases the H4 transition state mimics showed inhibition of PRMT1 and PRMT6 with micromolar IC₅₀ values. Interestingly, the extra C-terminal lysine present in H4¹⁻⁸ decreased the selectivity of the compounds towards PRMT1 over PRMT6.

Chapter 3 describes the development of a new series of CARM1 TS mimics based on the sequence of histone H3 around target arginine R¹⁷. To examine the impact of neighbouring lysine acetylation in histone H3 on the recognition of arginine residues by CARM1, adenosine-linked peptides were synthesized with the neighbouring lysine residue K¹⁸ present as either the free amine or in its acetylated form. The potent inhibition observed for both H3¹⁰⁻²⁵ and H3¹⁰⁻²⁵(K¹⁸Ac) TS mimics, led to further evaluation of shorter peptidomimetics by sequentially omitting N- and C-terminal residues to generate the corresponding deca-, octa-

, hexa-, and tetra-peptide analogues 7–14 (See Chapter 3, Table 1). Each of these truncated peptidomimetics were prepared with and without acetylation of the neighboring Lys^{18} residue to probe the interplay between peptide sequence and lysine acetylation on recognition by and inhibition of CARM1. Inhibition studies subsequently showed the most potent inhibition for the hexapeptide with nanomolar IC_{50} values. Structural studies performed with the H3-based TS mimics provide insight into the effect of acetylation on CARM1-binding. The findings point to the intriguing possibility that crosstalk between lysine acetylation and arginine methylation may also serve to reinforce PRMT specificity beyond the primary sequence of the peptide substrate.

The development of a direct, specific, and convenient analytical method for measuring the activity of CARM1 is described in Chapter 4. The LC-MS based method we developed applies multiple reaction monitoring (MRM) for the detection and quantification of a methylated peptide substrate. The assay presents a significant simplification over existing ELISA and radiometric methods while benefitting from high sensitivity and convenient sample preparation. The application of the MRM LC-MS method has been demonstrated by assaying the inhibitory activity of a selection of known CARM1 inhibitors, showing good comparability with previously published data.

Chapter 5, reports the development of peptide-based inhibitors for a different class of methyltransferase, nicotinamide N-methyltransferase (NNMT). NNMT is an AdoMet-dependent small molecule methyltransferase responsible for the methylation of pyridinyl compounds including nicotinamide (vitamin b3) and is implicated as a driver of both metabolic disease and many cancers. Macrocyclic peptide-based NNMT inhibitors were identified using an mRNA-peptide display technique known as the random nonstandard peptides integrated discovery (RaPID) system. The most highly enriched cyclic peptides from both L-tyrosine and D-tyrosine initiating libraries were synthesized using Fmoc- solid phase peptide synthesis (SPPS) and subsequently evaluated for their inhibitory activity against NNMT. Interestingly, while good inhibition of NNMT was observed, none of the macrocyclic peptides identified in our study exhibit significant competition with the substrates of NNMT; AdoMet or nicotinamide. These findings indicate that rather than binding in the active site, the macrocyclic peptides may instead bind at an allosteric site on the enzyme. Furthermore, in cell-based assays, administration of our macrocyclic peptides was found to result in a significant reduction in the production of MNA by endothelial HAEC cells and A549 lung carcinoma cells.

References

- 1. Schneider, R.; Bannister, A. J., Protein N-methyltransferase assays in the study of gene transcription. Methods 2002, 26 (3), 226-32.
- 2. Huang, R., Chemical Biology of Protein N-Terminal Methyltransferases. Chembiochem 2019, 20 (8), 976-984.
- 3. Murray, K., The Occurrence of i ε -N-Methyl Lysine in Histones. Biochemistry 1964, 3 (1), 10-15.
- 4. Bedford, M. T.; Clarke, S. G., Protein arginine methylation in mammals: who, what, and why. Molecular cell 2009, 33 (1), 1-13.
- 5. Kwiatkowski, S.; Drozak, J., Protein Histidine Methylation. Current protein & peptide science 2020, 21 (7), 675-689.
- 6. Tessarz, P.; Santos-Rosa, H.; Robson, S. C.; Sylvestersen, K. B.; Nelson, C. J.; Nielsen, M. L.; Kouzarides, T., Glutamine methylation in histone H2A is an RNA-polymerase-I-dedicated modification. Nature 2014, 505 (7484), 564-8.
- 7. Briggs, S. D.; Xiao, T.; Sun, Z. W.; Caldwell, J. A.; Shabanowitz, J.; Hunt, D. F.; Allis, C. D.; Strahl, B. D., Gene silencing: trans-histone regulatory pathway in chromatin. Nature 2002, 418 (6897), 498.
- 8. Frederiks, F.; Tzouros, M.; Oudgenoeg, G.; van Welsem, T.; Fornerod, M.; Krijgsveld, J.; van Leeuwen, F., Nonprocessive methylation by Dot1 leads to functional redundancy of histone H3K79 methylation states. Nature structural & molecular biology 2008, 15 (6), 550-7.
- 9. Pokholok, D. K.; Harbison, C. T.; Levine, S.; Cole, M.; Hannett, N. M.; Lee, T. I.; Bell, G. W.; Walker, K.; Rolfe, P. A.; Herbolsheimer, E.; Zeitlinger, J.; Lewitter, F.; Gifford, D. K.; Young, R. A., Genome-wide map of nucleosome acetylation and methylation in yeast. Cell 2005, 122 (4), 517-27.
- 10. Rea, S.; Eisenhaber, F.; O'Carroll, D.; Strahl, B. D.; Sun, Z.-W.; Schmid, M.; Opravil, S.; Mechtler, K.; Ponting, C. P.; Allis, C. D.; Jenuwein, T., Regulation of chromatin structure by site-specific histone H3 methyltransferases. Nature 2000, 406 (6796), 593-599.
- 11. Tamaru, H.; Selker, E. U., A histone H3 methyltransferase controls DNA methylation in Neurospora crassa. Nature 2001, 414 (6861), 277-283.
- 12. van Leeuwen, F.; Gafken, P. R.; Gottschling, D. E., Dot1p Modulates Silencing in Yeast by Methylation of the Nucleosome Core. Cell 2002, 109 (6), 745-756.
- 13. Han, D.; Huang, M.; Wang, T.; Li, Z.; Chen, Y.; Liu, C.; Lei, Z.; Chu, X., Lysine methylation of transcription factors in cancer. Cell Death & Disease 2019, 10 (4), 290.
- 14. Sun, G. D.; Cui, W. P.; Guo, Q. Y.; Miao, L. N., Histone lysine methylation in diabetic nephropathy. Journal of diabetes research 2014, 2014, 654148.
- 15. Arrowsmith, C. H.; Bountra, C.; Fish, P. V.; Lee, K.; Schapira, M., Epigenetic protein families: a new frontier for drug discovery. Nature Reviews Drug Discovery 2012, 11 (5), 384-400.

- 16. Schapira, M.; Arrowsmith, C. H., Methyltransferase inhibitors for modulation of the epigenome and beyond. Current Opinion in Chemical Biology 2016, 33, 81-87.
- 17. Schapira, M., Chemical Inhibition of Protein Methyltransferases. Cell Chemical Biology 2016, 23 (9), 1067-1076.
- 18. Liu, X. R.; Zhou, L. H.; Hu, J. X.; Liu, L. M.; Wan, H. P.; Zhang, X. Q., UNC0638, a G9a inhibitor, suppresses epithelial-mesenchymal transition-mediated cellular migration and invasion in triple negative breast cancer. Molecular medicine reports 2018, 17 (2), 2239-2244.
- 19. Knutson, S. K.; Wigle, T. J.; Warholic, N. M.; Sneeringer, C. J.; Allain, C. J.; Klaus, C. R.; Sacks, J. D.; Raimondi, A.; Majer, C. R.; Song, J.; Scott, M. P.; Jin, L.; Smith, J. J.; Olhava, E. J.; Chesworth, R.; Moyer, M. P.; Richon, V. M.; Copeland, R. A.; Keilhack, H.; Pollock, R. M.; Kuntz, K. W., A selective inhibitor of EZH2 blocks H3K27 methylation and kills mutant lymphoma cells. Nat Chem Biol 2012, 8 (11), 890-6.
- 20. Harb, W.; Abramson, J.; Lunning, M.; Goy, A.; Maddocks, K.; Lebedinsky, C.; Senderowicz, A.; Trojer, P.; Bradley, W. D.; Flinn, I., A phase 1 study of CPI-1205, a small molecule inhibitor of EZH2, preliminary safety in patients with B-cell lymphomas. Annals of Oncology 2018, 29, iii7.
- 21. Shen, Y.; Szewczyk, M. M.; Eram, M. S.; Smil, D.; Kaniskan, H.; de Freitas, R. F.; Senisterra, G.; Li, F.; Schapira, M.; Brown, P. J.; Arrowsmith, C. H.; Barsyte-Lovejoy, D.; Liu, J.; Vedadi, M.; Jin, J., Discovery of a Potent, Selective, and Cell-Active Dual Inhibitor of Protein Arginine Methyltransferase 4 and Protein Arginine Methyltransferase 6. J Med Chem 2016, 59 (19), 9124-9139.
- 22. Nakayama, K.; Szewczyk, M. M.; Dela Sena, C.; Wu, H.; Dong, A.; Zeng, H.; Li, F.; de Freitas, R. F.; Eram, M. S.; Schapira, M.; Baba, Y.; Kunitomo, M.; Cary, D. R.; Tawada, M.; Ohashi, A.; Imaeda, Y.; Saikatendu, K. S.; Grimshaw, C. E.; Vedadi, M.; Arrowsmith, C. H.; Barsyte-Lovejoy, D.; Kiba, A.; Tomita, D.; Brown, P. J., TP-064, a potent and selective small molecule inhibitor of PRMT4 for multiple myeloma. Oncotarget 2018, 9 (26), 18480-18493.
- 23. Mitchell, L. H.; Drew, A. E.; Ribich, S. A.; Rioux, N.; Swinger, K. K.; Jacques, S. L.; Lingaraj, T.; Boriack-Sjodin, P. A.; Waters, N. J.; Wigle, T. J.; Moradei, O.; Jin, L.; Riera, T.; Porter-Scott, M.; Moyer, M. P.; Smith, J. J.; Chesworth, R.; Copeland, R. A., Aryl Pyrazoles as Potent Inhibitors of Arginine Methyltransferases: Identification of the First PRMT6 Tool Compound. ACS medicinal chemistry letters 2015, 6 (6), 655-659.
- 24. Greer, E. L.; Shi, Y., Histone methylation: a dynamic mark in health, disease and inheritance. Nature Reviews Genetics 2012, 13 (5), 343-357.
- 25. Taverna, S. D.; Li, H.; Ruthenburg, A. J.; Allis, C. D.; Patel, D. J., How chromatin-binding modules interpret histone modifications: lessons from professional pocket pickers. Nature structural & molecular biology 2007, 14 (11), 1025-1040.

- 26. Pahlich, S.; Zakaryan, R. P.; Gehring, H., Protein arginine methylation: Cellular functions and methods of analysis. Biochimica et biophysica acta 2006, 1764 (12), 1890-903.
- 27. Wolf, S. S., The protein arginine methyltransferase family: an update about function, new perspectives and the physiological role in humans. Cellular and molecular life sciences: CMLS 2009, 66 (13), 2109-21.
- 28. Tang, J.; Frankel, A.; Cook, R. J.; Kim, S.; Paik, W. K.; Williams, K. R.; Clarke, S.; Herschman, H. R., PRMT1 is the predominant type I protein arginine methyltransferase in mammalian cells. The Journal of biological chemistry 2000, 275 (11), 7723-30.
- 29. Hong, H.; Kao, C.; Jeng, M. H.; Eble, J. N.; Koch, M. O.; Gardner, T. A.; Zhang, S.; Li, L.; Pan, C. X.; Hu, Z., Aberrant expression of CARM1, a transcriptional coactivator of androgen receptor, in the development of prostate carcinoma and androgen independent status. Cancer: Interdisciplinary International Journal of the American Cancer Society 2004, 101 (1), 83-89.
- 30. So, C. W.; Caldas, C.; Liu, M.-M.; Chen, S.-J.; Huang, Q.-H.; Gu, L.-J.; Sham, M. H.; Wiedemann, L. M.; Chan, L. C., EEN encodes for a member of a new family of proteins containing an Src homology 3 domain and is the third gene located on chromosome 19p13 that fuses to MLL in human leukemia. Proceedings of the National Academy of Sciences 1997, 94 (6), 2563-2568.
- 31. Couto, E. S. A.; Wu, C. Y.; Citadin, C. T.; Clemons, G. A.; Possoit, H. E.; Grames, M. S.; Lien, C. F.; Minagar, A.; Lee, R. H.; Frankel, A.; Lin, H. W., Protein Arginine Methyltransferases in Cardiovascular and Neuronal Function. Molecular neurobiology 2020, 57 (3), 1716-1732.
- 32. Cai, S.; Liu, R.; Wang, P.; Li, J.; Xie, T.; Wang, M.; Cao, Y.; Li, Z.; Liu, P., PRMT5 Prevents Cardiomyocyte Hypertrophy via Symmetric Dimethylating HoxA9 and Repressing HoxA9 Expression. Frontiers in Pharmacology 2020, 11 (2140).
- 33. Elakoum, R.; Gauchotte, G.; Oussalah, A.; Wissler, M. P.; Clément-Duchêne, C.; Vignaud, J. M.; Guéant, J. L.; Namour, F., CARM1 and PRMT1 are dysregulated in lung cancer without hierarchical features. Biochimie 2014, 97, 210-8.
- 34. Jarrold, J.; Davies, C. C., PRMTs and Arginine Methylation: Cancer's Best-Kept Secret? Trends in molecular medicine 2019, 25 (11), 993-1009.
- 35. Wang, S. M.; Dowhan, D. H.; Muscat, G. E. O., Epigenetic arginine methylation in breast cancer: emerging therapeutic strategies. Journal of molecular endocrinology 2019, 62 (3), R223-r237.
- 36. Lakowski, T. M.; t Hart, P.; Ahern, C. A.; Martin, N. I.; Frankel, A., N η -substituted arginyl peptide inhibitors of protein arginine N-methyltransferases. ACS chemical biology 2010, 5 (11), 1053-63.
- 37.t Hart, P.; Thomas, D.; van Ommeren, R.; Lakowski, T. M.; Frankel, A.; Martin, N. I., Analogues of the HIV-Tat peptide containing N η -modified arginines as potent inhibitors of protein arginine N-methyltransferases. MedChemComm 2012, 3

- (10), 1235-1244.
- 38. Thomas, D.; Koopmans, T.; Lakowski, T. M.; Kreinin, H.; Vhuiyan, M. I.; Sedlock, S. A.; Bui, J. M.; Martin, N. I.; Frankel, A., Protein Arginine N-Methyltransferase Substrate Preferences for Different N η -Substituted Arginyl Peptides. ChemBio-Chem 2014, 15 (11), 1607-1613.
- 39. Strelow, J. M., A Perspective on the Kinetics of Covalent and Irreversible Inhibition. SLAS DISCOVERY: Advancing the Science of Drug Discovery 2016, 22 (1), 3-20.
- 40. Ghosh, A. K.; Samanta, I.; Mondal, A.; Liu, W. R., Covalent Inhibition in Drug Discovery. ChemMedChem 2019, 14 (9), 889-906.
- 41. Lin, H.; Wang, M.; Zhang, Y. W.; Tong, S.; Leal, R. A.; Shetty, R.; Vaddi, K.; Luengo, J. I., Discovery of Potent and Selective Covalent Protein Arginine Methyltransferase 5 (PRMT5) Inhibitors. ACS Medicinal Chemistry Letters 2019, 10 (7), 1033-1038.
- 42. Shen, Y.; Li, F.; Szewczyk, M. M.; Halabelian, L.; Park, K.-s.; Chau, I.; Dong, A.; Zeng, H.; Chen, H.; Meng, F.; Barsyte-Lovejoy, D.; Arrowsmith, C. H.; Brown, P. J.; Liu, J.; Vedadi, M.; Jin, J., Discovery of a First-in-Class Protein Arginine Methyltransferase 6 (PRMT6) Covalent Inhibitor. Journal of Medicinal Chemistry 2020, 63 (10), 5477-5487.
- 43. Obianyo, O.; Causey, C. P.; Osborne, T. C.; Jones, J. E.; Lee, Y. H.; Stallcup, M. R.; Thompson, P. R., A chloroacetamidine-based inactivator of protein arginine methyltransferase 1: design, synthesis, and in vitro and in vivo evaluation. Chembiochem 2010, 11 (9), 1219-23.
- 44. Obianyo, O.; Causey, C. P.; Jones, J. E.; Thompson, P. R., Activity-based protein profiling of protein arginine methyltransferase 1. ACS chemical biology 2011, 6 (10), 1127-35.
- 45. Greenbaum, D.; Baruch, A.; Hayrapetian, L.; Darula, Z.; Burlingame, A.; Medzihradszky, K. F.; Bogyo, M., Chemical approaches for functionally probing the proteome. Molecular & cellular proteomics: MCP 2002, 1 (1), 60-8.
- 46. Berger, A. B.; Vitorino, P. M.; Bogyo, M., Activity-based protein profiling: applications to biomarker discovery, in vivo imaging and drug discovery. American journal of pharmacogenomics: genomics-related research in drug development and clinical practice 2004, 4 (6), 371-81.
- 47. Leung, D.; Hardouin, C.; Boger, D. L.; Cravatt, B. F., Discovering potent and selective reversible inhibitors of enzymes in complex proteomes. Nature biotechnology 2003, 21 (6), 687-91.
- 48. van Haren, M.; van Ufford, L. Q.; Moret, E. E.; Martin, N. I., Synthesis and evaluation of protein arginine N-methyltransferase inhibitors designed to simultaneously occupy both substrate binding sites. Organic & Biomolecular Chemistry 2015, 13 (2), 549-560.
- 49. van Haren, M. J.; Marechal, N.; Troffer-Charlier, N.; Cianciulli, A.; Sbardella, G.;

Cavarelli, J.; Martin, N. I., Transition state mimics are valuable mechanistic probes for structural studies with the arginine methyltransferase CARM1. Proceedings of the National Academy of Sciences of the United States of America 2017, 114 (14), 3625-3630.

50. Zhang, Y.; van Haren, M. J.; Martin, N. I., Peptidic transition state analogues as PRMT inhibitors. Methods 2020, 175, 24-29.

Chapter 2

Transition state analogues as inhibitors of PRMTs

Published in

Methods (2020)

DOI: 10.1016/j.ymeth.2019.08.003

Abstract

Protein arginine N-methyltransferases (PRMTs) methylate arginine residues in target proteins using the ubiquitous methyl donor S-adenosyl-L-methionine (AdoMet) as a cofactor. PRMTs play important roles in both healthy and disease states and as such inhibition of PRMTs has gained increasing interest. A primary challenge in the development of PRMT inhibitors is achieving specificity for the PRMT of interest as the active sites are highly conserved for all nine members of the PRMT family. Notably, PRMTs show very little redundancy in vivo due to their specific sets of protein substrates. However, relatively little is known about the interactions of PRMTs with their protein substrates that drive this substrate specificity. We here describe the extended application of a methodology recently developed in our group for the production of peptide-based transition state mimicking PRMT inhibitors. Using this approach, an adenosine moiety, mimicking that of the AdoMet cofactor, is covalently linked to the quanidine side chain of a target arginine residue contained in a peptidic fragment derived from a PRMT substrate protein. Using this approach, histone H4 tail peptide-based transition state mimics were synthesized wherein the adenosine group was linked to the Arg3 residue. H4R3 is a substrate for multiple PRMTs, including PRMT1 and PRMT6. The inhibition results obtained with these new H4-based transition state mimics show low micromolar IC₅₀ values against PRMT1 and PRMT6, indicating that the methodology is applicable to the broader family of PRMTs.

Introduction

The methylation of arginines in proteins is performed by the family of protein arginine N-methyltransferases (PRMTs). The family consists of nine members which are classified into three categories; type I PRMTs, which form asymmetrically dimethylated arginine (aDMA), type II PRMTs, which form symmetrically dimethylated arginine (sDMA) and the much less common type III PRMTs which only form monomethylated arginine (MMA). Within these categories the members are differentiated by their protein substrate specificity and cellular localizations. In common with the majority of small molecule and peptide methyltransferase the PRMTs employ the ubiquitous methyl donor S-adenosyl-L-methionine (AdoMet) as a cofactor. In all PRMTs the methylation of the target arginine residue is facilitated by the presence of two conserved glutamate residues that serve to lock the guanidine moiety in close proximity to the AdoMet cofactor's methyl group. These features in PRMT enzymes result in a highly conserved active site configuration (Figure. 1A).

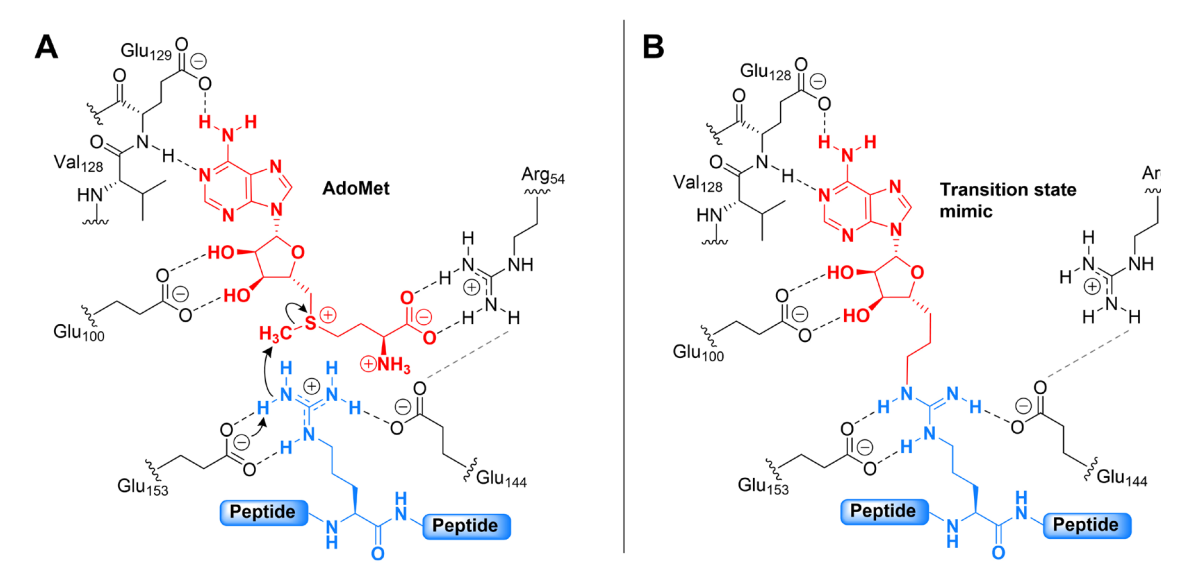


Figure. 1. A) Schematic representation of the conserved residues in the PRMT active site interacting with the AdoMet cofactor (in red) and the guanidine of the target arginine residue (in blue) (PRMT1 numbering). B) The design of the transition state mimics is based on the covalent linkage of the adenosine group (as shown in red) to the arginine sidechain in a peptide (as shown in blue). This approach leads to binding interactions with the conserved active site residues of both the AdoMet cofactor and peptide substrate binding pockets.

PRMTs are involved in a variety of cellular functions in both healthy and disease states. Cellular functions include the regulation of gene transcription, nuclear transport, DNA repair, protein-protein interactions and RNA processing.^{4,5} Upon methylation of histone tails, gene transcription can be activated or repressed, depending on the arginine residue and the type of methylation (aDMA or sDMA).⁶

Notably, most PRMTs are implicated in one or more types of cancer and inhibition of PRMTs has been shown to inhibit cancer cell growth.⁷ In addition, several studies have indicated the involvement of PRMTs in cardiovascular disease,^{8,9} pulmonary disease ^{10,11} and viral infection.^{12,13} Therefore, the development of inhibitors against PRMTs has gained interest over the past decade as also evidenced by recently initiated clinical trials initiated with inhibitors against PRMT5 for the treatment of solid tumours and non-Hodgkin's lymphoma.¹⁴

A major challenge in the development of PRMT inhibitors is how to achieve specificity for a given PRMT considering the highly conserved active site architecture shared among all members of this methyltransferase family. To this end, technologies that can provide new insights into PRMT-substrate interactions can be of great value. We here describe such an approach wherein known PRMT substrate peptides are converted into PRMT specific inhibitors. In an attempt to obtain general PRMT inhibitors, we previously synthesized a series of small molecule bisubstrate compounds with a quanidine group attached to the adenosine unit with different linker lengths.¹⁵ For these compounds, we observed surprising selectivity among the PRMTs tested. Building on those results, we hypothesized that enhanced specificity could be achieved by linking the adenosine unit to the target arginine residue of a given PRMT substrate peptide (Figure. 1B). The adenosine-peptide conjugates mimic the transition state of the first methylation step, making the approach applicable to all three types of PRMTs. In addition, by binding in the protein substrate binding pocket, more information could be gathered about the binding interactions of the PRMTs with their (specific) protein substrates.

This approach was initially validated on coactivator-associated arginine methyltransferase 1 (CARM1 also known as PRMT4).¹⁶ Transition state analogues were prepared based on a peptide sequence of its known substrate PABP1. Biochemical evaluation showed nanomolar inhibition against CARM1 with up to 300-fold selectivity over PRMT1. Subsequent co-crystallization experiments quickly led to high resolution crystal structures of CARM1 bound to the transition state analogue revealing the interactions in both the cofactor's and peptide binding sites. The fact that the crystals of the complex were readily obtained was attributed to the stabilizing effect the transition state mimics have on the enzyme by binding in the different substrate binding pockets simultaneously.

Following up on our promising initial results with transition state analogues designed for CARM1, we here describe the application of a similar approach for generating transition state mimics as inhibitors of PRMT1. PRMT1 is the most abundant PRMT and it is estimated that 85% of all methylated arginine residues in the proteome are methylated by PRMT1. PRMT1 preferentially methylates the

RGG motif in target proteins and is found primarily in the cytoplasm. Alternative splicing variants show different activities, substrate specificity and cellular localizations. PRMT1 substrates are diverse and include histones (H2AR3 and H4R3), splicing factors, DNA damage proteins, RNA-binding proteins, transcription factors, viral proteins and signaling proteins. As a player in human disease, PRMT1 is overexpressed in different types of cancer and is further involved in pulmonary disease and cardiovascular disease. A well-known substrate of PRMT1 is Arg on the histone H4 tail (H4R3), which is often used as a marker in studies concerning the role of PRMT1. The design of the compounds here described focuses on H4R3. As this residue is also a substrate of several other PRMTs (at least in vitro) we additionally included PRMT6 in the biochemical evaluation of the new H4R3 based transition state analogues. In contrast with PRMT1, PRMT6 is exclusively found in the nucleus.

Similar to PRMT1, it preferentially methylates the RGG motif and known substrates include histone tails (H2AR3, H2AR29, H3R2, H3R8, H3R42 and H4R3), chromatin proteins, DNA-binding proteins and viral proteins.^{2,24} PRMT6 is overexpressed in bladder, lung and prostate cancer and associated with pulmonary disorders.^{7,11,25} Interestingly, PRMT6 is reportedly downregulated in melanoma and reduces HIV-1 production and viral replication.²⁶⁻²⁸

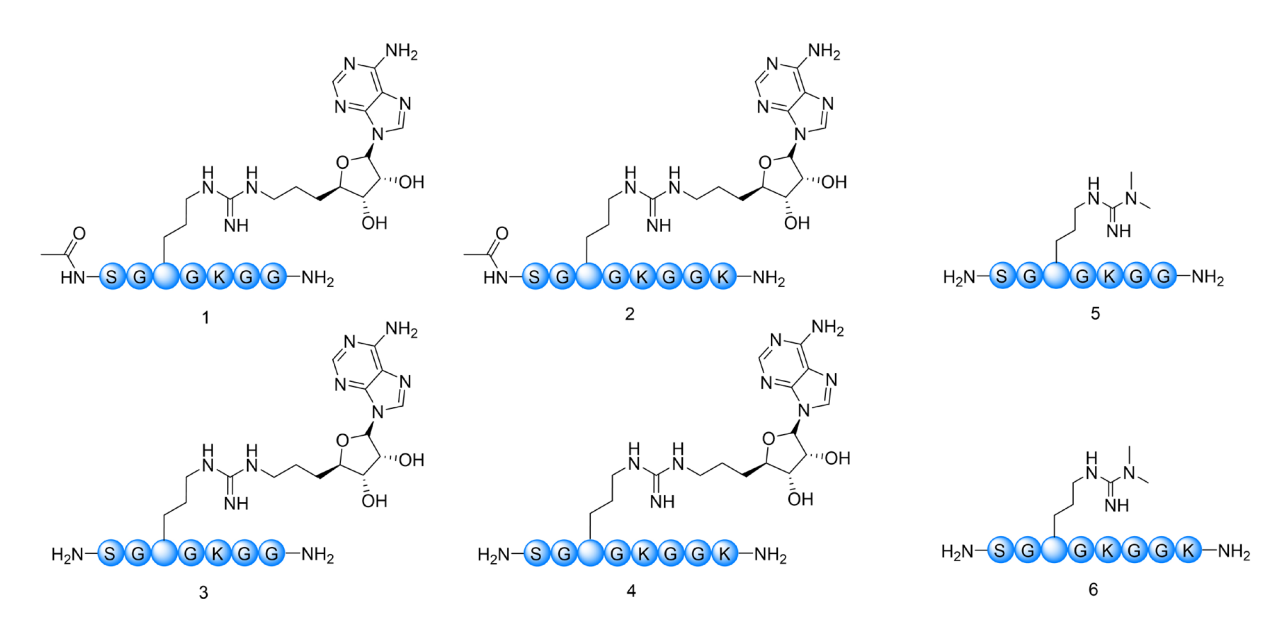


Figure. 2. Schematic representations of the structures of compounds 1–6. Compounds 1, 2 and 5 are based on residues 1–7 of the histone H4 tail and compounds 3, 4 and 6 are based on residues 1–8 of the histone H4 tail.

Above all, for installation of the adenosine unit a fully saturated three-carbon spacer was used to link to the arginine side-chain. This linker was found to be most effective among the small molecule bisubstrate inhibitors tested against PRMT1

and PRMT6 in previous work.¹⁵ As a control we also prepared the corresponding asymmetrically dimethylated arginine containing peptides of sequences H4¹⁻⁷ (5) and H4¹⁻⁸ (6). The structures of peptides 1–6 are presented in Figure. 2.

Results and discussion

We here describe methodology for the synthesis of PRMT1 inhibiting transition state mimics through the covalent linkage of the adenosine moiety to PRMT1 target peptides. Using chemistry developed in our group,²⁹ the adenosine moiety can be conveniently linked to the arginine side chain of any target peptide, making the methodology widely applicable to the entire family of PRMTs.

The design of the H4R3-based transition state analogues here described is based on the N-terminal 7 or 8 amino acids of the H4 tail peptide. Because the target arginine is close to the N-terminus, the N-terminal serine residue was evaluated as both the free amine as well as in its acetylated form to investigate the effect of the N-terminus on the inhibitory activity of the modified peptides. The sequences designed around H4R3 were selected on the basis of the kinetic data on methylation of the histone H4 tail by PRMT1 as reported by Thompson and coworkers.³⁰ The results of their study revealed that the best catalytic efficiency was achieved with a sequence of histone 4 covering the first 21 residues (H4¹⁻²¹). A slight reduction in turnover was found for two mid-sequence truncations of H4¹⁻²¹ where either residues 11–13 or 9–15 were eliminated. Conversely, sequences H4^{1–13} and H4¹⁻¹⁵ showed a greatly reduced methylation rate. These findings suggest that binding of the H4 tail is driven by two contributing parts: one part that interacts at the methylation site (residues 1–8) and one part that binds at a more distal binding pocket containing several negatively charged residues. Without the positive residues (H4¹⁶⁻²¹) to bind in this negatively charged region of the enzyme, 'linker residues' 9–15 seem to hinder more than attribute to the methylation process. Therefore, sequences H4¹⁻⁷ and H4¹⁻⁸ were selected with a C-terminal amide and both a free or acetylated N-terminus. The rationale for examining the H4 ¹⁻⁷ peptide in addition to the H4¹⁻⁸ peptide was to elucidate the contribution of the Lys⁸ residue in binding.

The methodology here described provides a flexible and generally applicable approach for the preparation of transition state analogues of PRMTs based on peptidic fragments of their respective protein substrates. By using an orthogonally protected ornithine residue at the position of the target arginine, the peptides can be synthesized by SPPS and modified on the resin. Conveniently, given that the intermediate peptides are manipulated on resin, no intermediate purification steps are necessary and all reagents can simply be washed away. Also of note is the possibility of using this approach to specifically modify a single arginine reside

when synthesizing peptides containing multiple arginines.

Key to this methodology is thiourea building block 13 that can be prepared in six steps with good to excellent yields, the details of which are presented in the supplementary information. For groups interested in applying this methodology the building block is also available on request. Also of note, if desired, variants of the thiourea building block can also be prepared with either a two-carbon spacer or an unsaturated three-carbon spacer, as we have previously described.¹⁶

Table 1. Inhibitory activity of compounds 1–6 against PRMT1 and PRMT6.

Compound	Sequence	IC ₅₀ values (μM) ^a	
		PRMT 1	PRMT 6
1	H ₂ N-SGR*GKGG-CONH ₂	2.51 ± 0.24	4.82 ± 0.96
2	AcNH-SGR*GKGG-CONH ₂	5.36 ± 0.52	10.98 ± 2.25
3	H ₂ N-SGR*GKGGK-CONH ₂	4.66 ± 0.65	2.26 ± 0.72
4	AcNH-SGR*GKGGK-CONH2	1.33 ± 0.25	1.22 ± 0.34
5 ^b	H ₂ N-SGR(aDMA)GKGG-CONH ₂	> 50	> 50
6 ^b	H ₂ N-SGR(aDMA)GKGGK-CONH ₂	> 50	> 50

 $^{^{\}rm a}$ IC₅₀ values from duplicate data obtained from seven concentrations \pm standard deviations. The R* indicates the position where the adenosine group is incorporated. $^{\rm b}$ In compounds 5 and 6, the central arginine residue is present in asymmetrically dimethylated form. The full IC₅₀ curves were shown in the Appendix I

As reported in Table 1, compounds 1–4 display low micromolar inhibition against both PRMT1 and PRMT6. H4^{1–7} analogues 1 and 2 show a 2-fold higher potency against PRMT1 over PRMT6. In addition, the free N-terminus in 1 results in slightly higher inhibition than the acetylated N-terminus in 2. For H4^{1–8} analogues 3 and 4 the findings are the opposite of those found for compounds 1 and 2. Compound 3 is slightly more active against PRMT6 over PRMT1, but no significant difference is observed for compound 4 between PRMT1 and 6. Against both enzymes, the acetylated peptide 4 is more active than peptide 3 with a free N-terminus. Notably, no significant inhibition was observed for the asymmetrically dimethylated control peptides 5 and 6 when tested at 50 μ M, indicating that the inhibitory activity observed for 1–4 is driven by the incorporation of the adenosine moiety. To gain additional insight into the binding of these transition state analogues to both PRMT1 and PRMT6, structural studies are now underway the results of which will be presented in due course.

As previously reported, 16 a key advantage of the methodology here presented

is that the transition state analogues can be used to facilitate co-crystallization of PRMTs with mimics of their protein substrates without the need for a cofactor analogue. Obtaining crystal structures of PRMTs bound to their peptidic substrate can give valuable insight into the interactions in the binding site of the peptide substrate, providing information that is crucial for the development of selective small molecule inhibitors. It is known that the co-crystallization of PRMTs with their substrates is often very challenging due to the necessity of including an analogue of the AdoMet cofactor. AdoMet itself cannot be used as this would result in the formation of the (di-)methylated product. Often AdoMet analogues S-adenosyl-L-homocysteine (AdoHcy), the product of the methylation reaction, or sinefungin are used to obtain structures of the ternary complex of enzyme, cofactor and substrate. However, the use of AdoHcy in co-crystallization studies of PRMTs is limited for obtaining mechanistical insight as it would only stabilize the PRMT in the conformation it adopts after the methyltransfer takes place. In addition, other AdoMet analogues introduce unnatural interactions into the active site, the effects of which can be difficult to interpret. Furthermore, the crystallization of a ternary complex is often more challenging than for a binary complex of substrate and enzyme. This is evidenced by the limited number of structures of PRMTs bound to their protein substrate. In fact, for only CARM1 and PRMT5 have high resolution crystal structures been reported that show the peptide substrate bound to the enzyme. 16,31,32 In the only structure published to date for PRMT1 bound to a substrate peptide only the target arginine residue was resolved in the active site while in similar studies with PRMT7 only the target arginine glycine segment of a larger substrate peptide was visible. 33,34

In conclusion, the results of compounds 1–6 show that our peptide transition state analogue methodology is generally applicable throughout the family of PRMTs. Where previous studies focused on PRMT4, we here demonstrate the applicability of the methodology in generating peptide based bisubstrate inhibitors for PRMT1 and PRMT6 as well. Future efforts will be directed to examining the applicability of peptides 1–4 in co-crystallization studies with PRMT1 and 6 as well as further application of the methodology towards other PRMTs.

Experimental Procedures

Materials and methods

All reagents employed were of American Chemical Society (ACS) grade or finer and were used without further purification unless otherwise stated. The Pbf-thiourea building block and its precursors 8-13 were synthesized according to previously described procedures. All known compounds prepared had NMR spectra and HRMS data consistent with the assigned structures. All reactions and fractions

from column chromatography were monitored by thin layer chromatography (TLC) using plates with a UV fluorescent indicator (normal SiO_2 , Merck 60 F 254). One or more of the following methods were used for visualization: UV absorption by fluorescence quenching; phosphomolybdic acid: ceric sulfate: sulfuric acid: H_2O (10 g:1.25 g: 12 mL:238 mL) staining; KMnO₄ staining; PPh₃ staining; ninhydrin staining. Flash chromatography was performed using Merck type 60, 230–400 mesh silica gel.

The final compounds 1-6 were purified by preparative HPLC performed on a BESTATechnik system with a Dr. Maisch Reprosil Gold 120 C18 column (25 × 250 mm, 10 µm) and equipped with a ECOM Flash UV detector monitoring at 214 nm. Compounds were eluted with a water-methanol gradient moving from 0% to 100% methanol (0.1% TFA) over 60 minutes at a flow-rate of 12.0 mL·min⁻¹ with UV detection at 214 nm. Purity of compounds 1-4 was confirmed to be ≥95% by HPLC. HPLC analyses were performed on a Shimadzu Prominence-i LC-2030 system with a Dr. Maisch ReproSil Gold 120 C18 column (4.6 × 250 mm, 5 or 10 µm) at 30°C and equipped with a UV detector monitoring at 214 and 254 nm. Compounds were eluted with a water- methanol gradient moving from 0% to 100% methanol (0.1% TFA) over 50 minutes at a flow rate of 1.0 mL·min⁻¹ with UV detection (214 nm and 254 nm). Compounds 5 and 6 were analyzed on a Shimadzu LC-20AD system with a Shimadzu Shim-Pack GIST-AQ C18 column (3.0 x 150 mm, 3 µm) at 30°C and equipped with a UV detector monitoring at 214 and 254 nm. This system was connected to a Shimadzu 8040 triple quadrupole mass spectrometer (ESI ionization). Compounds were eluted with a water-methanol gradient moving from 0% to 100% methanol (0.1% FA) over 15 minutes at a flow rate of 0.5 mL·min - 1 with UV detection (214 nm and 254 nm) and MS detection.

HRMS analyses were performed on a Thermo Scientific Dionex UltiMate 3000 HPLC system with a Phenomenex Kinetex C18 column (2.1 x 150 mm, 2.6 µm) at 35 °C and equipped with a diode array detector. The following solvent system, at a flow rate of 0.3 mL min⁻¹, was used: solvent A, 0.1 % formic acid in water; solvent B, 0.1% formic acid in acetonitrile. Gradient elution was as follows: 95:5 (A/B) for 1 min, 95:5 to 5:95 (A/B) over 9 min, 5:95 to 2:98 (A/B) over 1 min, 2:98 (A/B) for 1 min, then reversion back to 95:5 (A/B) over 2 min, 95:5 (A/B) for 1 min. This system was connected to a Bruker micrOTOF-Q II mass spectrometer (ESI ionisation) calibrated internally with sodium formate.

Synthesis of the building block. Installation of the adenosine moiety at the target arginine residue in the peptides prepared required access to a specific thiourea building block (Compound 13, Scheme 1), The preparation of this thiourea begins from commercially available 2,3-O-isopropylidine adenosine alcohol 7 as we previously reported. Briefly, 7 is first transformed into unsaturated ethyl ester 8 in

a one-pot oxidation and Wittig reaction. Subsequently, the ester is reduced to alcohol 9 using diisobutylaluminium hydride (DiBAL-H). The alcohol is converted to phthalimide-protected amine 11 via a Mitsunobu reaction with phthalimide and subsequent deprotection using methylamine resulting in amine 12. The amine is then reacted with 2,2,4,6,7-pentamethyldihydrobenzofuran-5-sulfonyl isothiocyanate (Pbf-NCS) ²⁹ to form the Pbf-protected thiourea building block 13.

Scheme 1. Synthesis of Pbf-protected thiourea building block 13. Reagents and conditions: (a) IBX, Ph₃P=CHCO₂Et, DMSO, 79%; (b) DIBAL-H, hexane, DCM, 78%; (c) phthalimide, PPh₃, diethyldiazocarboxylate, THF, 94%; (d) MeNH₂, EtOH, 94%; (e) 10% Pd/C, H₂ (g), EtOH, 98%; (f) Pbf-NCS, Et₃N, DCM, 83%.

Ethyl-(E)-3-((3aR,6R,6aR)-6-(6-amino-9H-purin-9-yl)-2,2-dimethyltetrahydrofu-ro[3,4-d][1,3]dio xol -4-yl)acrylate (8)

2',3'-O-isopropylideneadenosine 7 (12.3 g, 40 mmol) was dissolved in DMSO (100 mL) and 2-iodoxybenzoic acid (IBX) (27.8 g, 100 mmol) and $Ph_3P=CHCOOC_2H_5$ (42.8 g, 100 mmol) were added. The mixture was stirred at room temperature for 72 h. Water (500 mL) was added and the mixture was extracted with EtOAc (2 × 500 mL). The combined organic layers were dried with Na_2SO_4 , the mixture was concentrated and purified by column chromatograph (4% MeOH in EtOAc) to give compound 8 (11.9 g, 79%) as a white powder.

(E)-3-((3aR,6R,6aR)-6-(6-amino-9H-purin-9-yl)-2,2-dimethyltetrahydrofu-ro[3,4-d][1,3]dioxol-4-yl)prop-2-en-1-ol (9)

Compound 8 (4.5 g, 12 mmol) was dissolved in DCM (30 mL), then cooled down to -78°C and a 1 M solution of DIBAL-H in hexane (100 mL) was added dropwise. The mixture was stirred at -78°C for 2 h and then quenched with MeOH (65 mL). A saturated aqueous solution of potassium sodium tartrate monohydrate (Rochelle

salt, 550 mL) was added and the resulting suspension was stirred vigorously at room temperature overnight, then extracted with EtOAc (2 \times 500 mL). The combined organic phases were dried (Na₂SO₄) and concentrated. The crude was purified by column chromatograph (4-6% MeOH gradient in EtOAc) to give compound 9 (3.1 g, 78%) as a white powder.

2-((E)-3-((3aR,6R,6aR)-6-(6-amino-9H-purin-9-yl)-2,2-dimethyltetrahydrofu-ro[3,4-d][1,3]dioxol -4-yl)allyl)isoindoline-1,3-dione (10)

To a solution of compound 9 (2.4 g, 7 mmol) in THF (60 ml), phthalimide (1.0 g, 7 mmol) and Ph_3P (1.8 g, 7 mmol) were added. DEAD (1.3 ml, 7 mmol) was added dropwise to a stirred suspension of mixture. After stirring for 2 h at room temperature during which a colorless solid started to precipitate. Stirring was continued for 1 h, after which the mixture was cooled to 0°C for 30 minutes and the product was filtered off. The residue was washed with Et_2O (3 × 50 mL) and dried in vacuum to give 10 (3.1 g, 94%) as white powder.

9-((3aR,4R,6aR)-6-((E)-3-aminoprop-1-en-1-yl)-2,2-dimethyltetrahydrofuro[3,4-d][1,3]d ioxol -4-yl)-9H-purin-6-amine (11)

To compound 10 (1.5 g, 3.2 mmol) was dissolved in a solution of 33% CH_3NH_2 in ethanol and the mixture was stirred at room temperature overnight. The mixture was concentrated, and redissolved in chloroform (40 mL) and extracted with 10% acetic acid (50 mL). The aqueous phase was washed with chloroform (3 × 40 mL), then adjusted adjusted with 2N NaOH to pH >12 and extracted with chloroform (4 × 40 mL). The combined organic phases were dried (Na_2SO_4) and concentrated to give 11 (990 mg, 94%) as white powder.

9-((3aR,4R,6aR)-6-(3-aminopropyl)-2,2-dimethyltetrahydrofuro[3,4-d][1,3]diox-ol-4-yl)-9H-purin-6-amine (12)

To a solution of compound 11 (880 mg, 2.6 mmol) in methanol (20 mL), water (5 mL) and acetic acid (5 drops), Pd-C (20 wt%, 90 mg) was added and the mixture was stirred overnight under a hydrogen atmosphere until MS showed complete conversion. The mixture was filtered through celite, washed with methanol, and concentrated to give 12 (870 mg, 98%) a yellow solid.

N-((3-((3aR,6R,6aR)-6-(6-amino-9H-purin-9-yl)-2,2-dimethyltetrahydrofu-ro[3,4-d][1,3]dioxol-4-yl)propyl)carbamothioyl)-2,2,4,6,7-pentamethyl-2,3-dihydrobenzofuran-5-sulfon amide (13)

Compound 12 (670 mg, 2 mmol) was dissolved in DCM (10 mL) and cooled to 0

°C. Trimethylamine (0.56 mL, 4 mmol) was added, followed by dropwise addition of a 0.1 M solution of Pbf-NCS (24 mL, 2.4 mmol) in DCM. After 75 min, the mixture was diluted with DCM (100 mL) and washed with water (3 × 75 mL) and brine (3 × 75 mL), dried with Na₂SO₄ and concentrated. The crude was purified by column chromatograph (2-4% MeOH gradient in DCM) to give compound 13 (1.1 g, 83%) as a white powder.

Scheme 2. On-resin modification procedure for the synthesis of transition state analogues 1–4, presented for H4^{1–8} peptides 3 and 4. The H4^{1–7} peptides 1 and 2 were prepared following the same route. Reagents and conditions: a) Pd(PPh₃)₄, phenylsilane, DCM, Ar (g), dark, rt, 1 h; b) 13, EDCI, DCM, N₂ (g), rt, 90 min; c) TFA/TIPS/H₂O (95:2.5:2.5), rt, 1 h.

Peptides Synthesis. In preparing the peptides, the target arginine in the sequence was replaced by an Alloc-protected ornithine residue, which allows for orthogonal deprotection and modification of the required residue. As a representative example Scheme 2 illustrates the synthetic route used in preparing transition state mimics 3 and 4. To begin, the Alloc-protected ornithine peptides were synthesized manually following standard Fmoc solid phase peptide synthesis (SPPS) protocols using Rink Amide tentagel resin. The peptide couplings were performed in N,Ndimethylformamide (DMF) at ambient temperature for 1 h using standard Fmocprotected amino acids with (2-(1H-benzotriazol-1-yl)-1,1,3,3-tetramethyluronium hexafluorophosphate (HBTU) as the activator and di-isopropylethylamine (DiPEA) as base. Deprotection of the Fmoc protecting group was done with 20% piperidine in DMF. Each step was checked by means of a Kaiser test 35,36 to ensure completion of the reaction. After coupling and Fmoc deprotection of the last residue the resin was split and one half treated with di-tert-butyldicarbonate (Boc₂O) to generate resin bound intermediate 16 while the other half was acetylated with acetic anhydride to yield intermediate 17. Resin bound 16 and 17 were subsequently converted to the corresponding adenosine-linked arginine peptides

On-resin installation of the adenosine unit. The on-resin conjugation of the adenosine thiourea building block (13) to the peptides is described here for the synthesis of compounds 3 and 4. The same procedure is used to synthesize compounds 1 and 2.

Peptides were Alloc-deprotected on the resin using tetrakis(triphenylphosphine)-palladium(0) and phenylsilane in DCM. The mixture was shaken for 1 hour under argon atmosphere and protected from light. Upon completion of deprotection, the resin is drained, washed with DCM (5 × 10 mL), 0.5% diethyldithiocarbamic acid sodium salt (5 × 10 mL), DMF (5 × 10 mL) and DCM (5 × 10 mL). Subsequently, the adenosine thiourea building block 13 (105 mg, 0.13 mmol, 1.3 eq) was coupled to the free amine using 1-ethyl-3-(3-dimethylaminopropyl)- carbodiimide (EDCI) (34.5 mg, 0.15 mmol, 1.5 eq) in DMF (10 mL) for 1.5 hours at room temperature. The mixture was drained and the resin was washed with DCM (3×10 mL), DMF (3×10 mL) and DCM (2×10 mL). Finally, the peptides were deprotected and cleaved from the resin using a standard cleavage cocktail of TFA/TIPS/H₂O (95:2.5:2.5). Precipitation in MTBE/hexane (1:1) yielded the crude peptide, which was purified by preparative HPLC. The purity and identity were confirmed by analytical HPLC and High-resolution Mass Spectrometry.

Synthesis of aDMA-peptides 5 and 6. Asymmetrically dimethylated arginine (aDMA) - containing peptides 5 and 6 were synthesized on a CEM Liberty Blue™ Automated Microwave Peptide Synthesizer. Peptide couplings were performed by using Fmoc-protected amino acid (4.0 eq), Oxyma (8.0 eq) and DIC (4.0 eq) in DMF (5 mL). Each coupling took 2 minutes at 90°C, followed by Fmoc deprotection using 20% piperidine in DMF for 4 minutes at 90°C. Special building block Fmoc-Adma(Pbf)-OH was coupled at room temperature overnight using 2 equivalents of amino acid.

After completion of the peptide synthesis, the peptides were deprotected and cleaved from the resin using a standard cleavage cocktail of TFA/TIPS/H2O (95:2.5:2.5). Precipitation in MTBE/hexane (1:1) yielded the crude peptide, which was purified by preparative HPLC. The purity and identity were confirmed by analytical HPLC and High-resolution Mass Spectrometry.

Biochemical evaluation. Methyltransferase inhibition assays were performed using commercially available chemiluminescent assay kits for PRMT1 and PRMT6 (BPS Bioscience, San Diego, CA, USA). The inhibition reactions were performed in duplicate at room temperature for 1 h using 96-well plates precoated with histone $\rm H4^{1-24}$ peptides as the substrate in a total volume of 50 µl containing proprietary assay buffer, 20 µM AdoMet, enzyme: PRMT1 (10 ng per reaction) and PRMT6 (200 ng per reaction) and inhibitors with concentration ranges of 0.0128–200 µM

in water. Positive controls were performed by addition of pure water instead of inhibitor solution. Blank and substrate controls were conducted in the absence of enzyme and AdoMet, respectively. After incubation for 1 h at room temperature, the wells were washed and blocked, primary antibody was added to each well and incubated for an additional 1 h. After washing and blocking, a secondary HRP-labelled antibody was added and incubated for another 30 min. After a final washing and blocking step, the HRP-substrate mixture was added to the wells and the luminescence was measured immediately using a Tecan spark plate reader. All the measurements were performed in duplicate and the luminescence data analysed using GraphPad Prism 7. Blank data was subtracted from the luminescence data and the results were subsequently normalized with the highest value in the concentration range defined as 100% inhibition. The percentage of inhibition activity was plotted as a function of inhibitor concentration and fit using non-linear regression analysis of the sigmoidal dose-response curve generated using the normalized data and a variable slope following equation:

$$Y = \frac{100}{(1 + 10^{((logIC50 - X)*Hillslope~))})}$$

where Y=percent activity, X=the logarithmic concentration of the compound, Hillslope=slope factor or Hill coefficient. The IC_{50} value was determined by the half maximal inhibitory concentration. The standard deviations were reported using the symmetrical CI function.

References

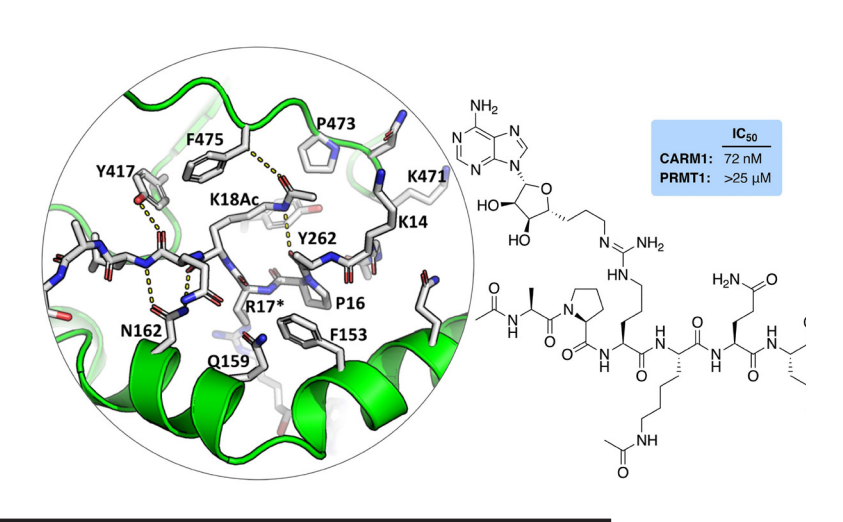
- 1. M.T. Bedford, P. Pably, C. Eckerich, F.O. Fackelmayer and F. Herrmann, Human protein arginine methyltransferases in vivo distinct properties of eight canonical members of the PRMT family, J. Cell Sci., 2009, 122, 667–677.
- 2. H. Wei, R. Mundade, K.C. Lange and T. Lu, Protein arginine methylation of non-histone proteins and its role in diseases, Cell Cycle, 2014, 13, 32–41.
- 3. H.L. Rust, C.I. Zurita-Lopez, S. Clarke and P.R. Thompson, Mechanistic studies on transcriptional coactivator protein arginine methyltransferase 1, Biochemistry, 2011, 50, 3332–3345.
- 4. M.T. Bedford and S.G. Clarke, Protein arginine methylation in mammals: who, what, and why, Mol. Cell, 2009, 33, 1–13.
- 5. Y. Morales, T. Cáceres, K. May and J.M. Hevel, Biochemistry and regulation of the protein arginine methyltransferases (PRMTs), Arch. Biochem. Biophys., 2016, 590, 138–152.
- 6. A.Di Lorenzo and M.T. Bedford, Histone arginine methylation, FEBS Lett., 2011, 585, 2024–2031.
- 7. Y. Yang and M.T. Bedford, Protein arginine methyltransferases and cancer, Nat. Rev. Cancer, 2013, 13, 37–50.
- 8. S. Franceschelli, A. Ferrone, M. Pesce, G. Riccioni and L. Speranza, Biological functional relevance of asymmetric dimethylarginine (ADMA) in cardiovascular disease, Int. J. Mol. Sci., 2013, 4, 24412–24421.
- 9. J.E. Nahon, C. Groeneveldt, J.J. Geerling, M. van Eck and M. Hoekstra, Inhibition of protein arginine methyltransferase 3 activity selectively impairs liver X receptordriven transcription of hepatic lipogenic genes in vivo, Br. J. Pharmacol., 2018, 175, 3175–3183.
- 10. D. Zakrzewicz and O. Eickelberg, From arginine methylation to ADMA: a novel mechanism with therapeutic potential in chronic lung diseases, BMC Pulm. Med., 2009, 9, 1–7.
- 11. D. Zakrzewicz, A. Zakrzewicz, K.T. Preissner, P. Markart and M. Wygrecka, Protein arginine methyltransferases (PRMTs): promising targets for the treatment of pulmonary disorders, Int. J. Mol. Sci., 2012, 13, 12383–12400.
- 12. B. Xie, C.F. Invernizzi, S. Richard and M.A. Wainberg, Arginine methylation of the human immunodeficiency virus type 1 tat protein by PRMT6 negatively affects tat interactions with both cyclin T1 and the tat transactivation region, J. Virol., 2007, 81, 4226–4234.
- 13. S. Pileri, L. Alinari, S. Roy, E.M. Smith, B. Yu, A. De Leo, J.C. Byrd, P.L. Smith, K.V. Mahasenan, J.E. Bradner, S. Sif, T. Motiwala, J.T. Patton, J.-H. Chung, L. Ayers, L. Kim, O. Elemento, C. Li, Y. Wu, S. Majumder, S. Jacob, F. Yan, V. Karkhanis, R.A. Baiocchi, S. Chen-Kiang, C. Agostinelli, R. Lapalombella and C. Quinion, Selective inhibition of protein arginine methyltransferase 5 blocks initiation and maintenance of B-cell transformation, Blood, 2015, 125, 2530–2543.

- 14. Wang, W. Hu and Y. Yuan, Protein arginine methyltransferase 5 (PRMT5) as an anticancer target and its inhibitor discovery, J. Med. Chem., 2018, 21, 9429–9441.
- 15.M. Van Haren, L.Q. Van Ufford, E.E. Moret and N.I. Martin, Synthesis and evaluation of protein arginine N-methyltransferase inhibitors designed to simultaneously occupy both substrate binding sites, Org. Biomol. Chem., 2015, 13, 549-560.
- 16. M.J. van Haren, N. Marechal, N. Troffer-Charlier, A. Cianciulli, G. Sbardella, J. Cavarelli and N.I. Martin, Transition state mimics are valuable mechanistic probes for structural studies with the arginine methyltransferase CARM1, Proc. Natl. Acad. Sci., 2017, 114, 3625–3630.
- 17. J. Tang, P.N. Kao and H.R. Herschman, Protein-arginine methyltransferase i, the predominant protein-arginine methyltransferase in cells, interacts with and is regulated by interleukin enhancer-binding factor 3, J. Biol. Chem., 2000, 275, 19866–19876.
- 18. R.M. Baldwin, A. Morettin, G. Paris, I. Goulet and J. Coté ., Alternatively spliced protein arginine methyltransferase 1 isoform PRMT1v2 promotes the survival and invasiveness of breast cancer cells, Cell Cycle, 2012, 11, 4597–4612.
- 19. C. Poulard, L. Corbo, M and Le Romancer, Protein arginine methylation/demethylation and cancer, Oncotarget, 2016, 7, 67532–67550.
- 20. L. Liu, J. Sun, C. Jiang, Q. He, X. Lan, J. Tian, S. Lu, B. Zhong, R. Bao, Q. Sun, X. Yang and M. Roth, PRMT1 upregulated by epithelial proinflammatory cytokines participates in COX2 expression in fibroblasts and chronic antigen-induced pulmonary inflammation, J. Immunol., 2015, 195, 298–306.
- 21. J.H. Pyun, H.J. Kim, M.H. Jeong, B.Y. Ahn, T.A. Vuong, D.I. Lee, S. Choi, S.H. Koo, H. Cho and J.S. Kang, Cardiac specific PRMT1 ablation causes heart failure through CaMKII dysregulation, Nat. Commun., 2018, 9, 5017.
- 22. K. Murata, W. Lu, M. Hashimoto, N. Ono, M. Muratani, K. Nishikata, J.-D. Kim, S. Ebihara, J. Ishida and A. Fukamizu, PRMT1 deficiency in mouse juvenile heart induces dilated cardiomyopathy and reveals cryptic alternative splicing products, iScience, 2018, 8, 200–213.
- 23. Y. Feng, J. Wang, S. Asher, L. Hoang, C. Guardiani, I. Ivanov and Y.G. Zheng, Histone H4 acetylation differentially modulates arginine methylation by an in cis mechanism, J. Biol. Chem., 2011, 286, 20323–20334.
- 24. A.Frankel, N. Yadav, J. Lee, T.L. Branscombe, S. Clarke, M.T. Bedford, The novel human protein arginine N-methyltransferase PRMT6 is a nuclear enzyme displaying unique substrate specificity, J. Biol. Chem., 2002, 277, 3537–3543.
- 25. R. Henrique, P. Costa-Pinheiro, A. Pereira, J. Ramalho-Carvalho, C. Jerónimo, J. Oliveira, L. Antunes, F.D. Menezes, I. Carneiro and F.Q. Vieira, Deregulated expression of selected histone methylases and demethylases in prostate carcinoma, Endocr. Relat. Cancer, 2013, 21, 51–61.

- 26. K. Limm, C. Ott, S. Wallner, D.W. Mueller, P. Oefner, C. Hellerbrand and A.K. Bosserhoff, Deregulation of protein methylation in melanoma, Eur. J. Cancer, 2013, 49, 1305–1313.
- 27. M.-C. Boulanger, C. Liang, R.S. Russell, R. Lin, M.T. Bedford, M.A. Wainberg and S. Richard, Methylation of tat by PRMT6 regulates human immunodeficiency virus type 1 gene expression, J. Virol., 2005, 79, 124–131.
- 28. D.N. Singhroy, T. Mesplède, A. Sabbah, P.K. Quashie, J.P. Falgueyret and M.A. Wainberg, Automethylation of protein arginine methyltransferase 6 (PRMT6) regulates its stability and its anti-HIV-1 activity, Retrovirology, 2013, 10, 1–10.
- 29. N.I. Martin and R.M.J. Liskamp, Preparation of NG-substituted L-arginine analogues suitable for solid phase peptide synthesis, J. Org. Chem., 2008, 73, 7849–7851.
- 30.T.C. Osborne, O. Obianyo, X. Zhang, X. Cheng and P.R. Thompson, Protein arginine methyltransferase 1: positively charged residues in substrate peptides distal to the site of methylation are important for substrate binding and catalysis, Biochemistry, 2007, 46, 13370–13381.
- 31. Moradei, P.A. Boriack-Sjodin, A. Drew, L. Jin, M.P. Scott, S. Ribich, M.P. Moyer, C. Sneeringer, R.A. Copeland and S.L. Jacques, Structural insights into ternary complex formation of human CARM1 with various substrates, ACS Chem. Biol., 2015, 11, 763–771.
- 32. K. Mavrakis, E.R. McDonald, M.R. Schlabach, E. Billy, G.R. Hoffman, A. DeWeck, D.A. Ruddy, K. Venkatesan, G. McAllister, R. DeBeaumont, S. Ho, Y. Liu, Y. Yan-Neale, G. Yang, F. Lin, H. Yin, H. Gao, D.R. Kipp, S. Zhao, J.T. McNamara, E.R. Sprague, Y.S. Cho, J. Gu, K. Crawford, V. Capka, K. Hurov, J.A. Porter, J. Tallarico, C. Mickanin, E. Lees, R. Pagliarini, N. Keen, T. Schmelzle, F. Hofmann, F. Stegmeier and W.R. Sellers, Abstract LB-017: disordered methionine metabolism in MTAP/CDKN2A-deleted cancers leads to marked dependence on PRMT5, Cancer Res, 2016, 76, LB-017-LB-017.
- 33.X. Zhang and X. Cheng, Structure of the predominant protein arginine methyltransferase PRMT1 and analysis of its binding to substrate peptides, Structure, 2003, 11, 509–520.
- 34. L. Liu, C. Wang, J. Wu, X. Chen, T.B. Caceres, M. Teng, Y. Zhu, Q. Gong, J.M. Hevel Z. Zhang, Y. Shi, J. Chen, J. Peng, J. Wang and X. Zuo, Structural determinants for the strict monomethylation activity by Trypanosoma brucei protein arginine methyltransferase 7, Structure, 2014, 22, 756–768.
- 35. Kaiser, R.L. Colescott, C.D. Bossinger and P.I. Cook, Color test for detection of free terminal amino groups in the solid-phase synthesis of peptides, Anal. Biochem., 1970, 34, 595–598.
- 36. V.K. Sarin, S.B.H. Kent, J.P. Tam and R.B. Merrifield, Quantitative monitoring of solidphase peptide synthesis by the ninhydrin reaction, Anal. Biochem., 1981, 117, 147–157.

Chapter 3

Structural studies provide new insights into the role of lysine acetylation on substrate recognition by CARM1 and inform the design of potent peptidomimetic inhibitors



Published in

ChemBioChem (2021)

DOI: 10.1002/cbic.202100506.

Abstract

The dynamic interplay of post-translational modifications (PTMs) in chromatin provides a communication system for the regulation of gene expression. An increasing number of studies have highlighted the role that such crosstalk between PTMs plays in chromatin recognition. In this study, (bio)chemical and structural approaches were applied to specifically probe the impact of acetylation of Lys¹⁸ in the histone H3 tail peptide on peptide recognition by the protein methyltransferase CARM1. Peptidomimetics that recapitulate the transition state of protein arginine N-methyltransferases, were designed based on the H3 peptide wherein the target Arg¹⁷ was flanked by either a free or an acetylated lysine. Structural studies with these peptidomimetics and the catalytic domain of CARM1 provide new insights into the binding of the H3 peptide within the enzyme active site. While the cocrystal structures reveal that lysine acetylation results in minor conformational differences for both CARM1 and the H3 peptide, acetylation of Lys¹⁸ does lead to additional interactions (Van der Waals and hydrogen bonding) and likely reduces the cost of desolvation upon binding, resulting in increased affinity. Informed by these findings a series of smaller peptidomimetics were also prepared and found to maintain potent and selective CARM1 inhibition. These findings provide new insights both into the mechanism of crosstalk between arginine methylation and lysine acetylation as well as towards the development of peptidomimetic CARM1 inhibitors.

Introduction

Post-translational modifications (PTMs) on the N-terminal tails of histones are involved in the activation or silencing of gene expression and in the signaling of readers and writers. PTMs come in a broad variety including phosphorylation, glycosylation, acetylation, and methylation or larger modifications such as ubiquitination or SUMOylation. PTMs are often reversible and interconnected, resulting in a complex code of modifications, known as crosstalk, in which one modification can result in the blocking, promoting, or recruitment of another.^{1,2} Examples of crosstalk in histones include the effect of serine phosphorylation on lysine acetylation and the effect of lysine acetylation on arginine methylation in histone H3.3,4 In addition, crosstalk can even occur between entirely different regions of chromatin as shown by the crosstalk found between lysine methylation in histone H3 and lysine acetylation in histone H4, the crosstalk between DNA methylation and histone H3 methylation, and the effect of ubiquitination on histone H2B on lysine methylation in H3 and lysine acetylation in histone H2A.⁵⁻⁸ Recent years have witnessed an increasing awareness of the roles played by this complex communication system in a variety of processes in both healthy and diseased states.9-11

In this investigation we focussed our attention on examining the impact of lysine acetylation in histone H3 on the recognition of neighboring arginine residues by coactivator-associated arginine methyltransferase 1 (CARM1). Previous reports on lysine acetylation/arginine methylation crosstalk have shown that the acetylation of lysine residues Lys¹⁸ and Lys²⁷ in histone H3 tails promote subsequent CARM1-mediated methylation of the neighboring arginine residues Arg¹⁷ and Arg²⁶ respectively. ^{12,13} Specifically, the methylation of H3 Arg¹⁷ was shown to be enhanced through acetylation of Lys¹⁸ and to a lesser extent also through acetylation of Lys¹⁴ or Lys²³. In addition, the affinity of CARM1 has been reported to be greater for substrate peptides containing Lys¹⁸Ac and Lys²³Ac (but not Lys¹⁴Ac), suggesting that acetylation of Lys¹⁸ and Lys²³ enhances binding of the H3 substrate for CARM1, leading to increased Arg¹⁷ methylation.¹² However, kinetic analysis of this methylation process revealed that the increased catalytic efficiency of CARM1 for the H3 substrate acetylated at Lys¹⁸ is rather driven by an increase in turnover number (k_{cat}) with no significant change in affinity (K_M) .¹⁴ The CARM1mediated methyl transfer reaction is facilitated by several highly conserved active site residues. Notably, two glutamate residues (E²⁵⁸ and E²⁶⁷, known as the "double E-loop") serve to position the quanidine moiety in close proximity to the methyl group of the S-adenosyl- L-methionine (SAM) cofactor. Additionally, a specific histidine residue (H⁴¹⁵) found in the so-called THW-loop, is crucial for the deprotonation of the quanidine, which in turn allows for the methyl group transfer to occur (Figure 1A). The explanation proposed by the authors for the observed increase in k_{cat} for H3 peptide substrates containing an acetylated lysine next to the target arginine is based on the local electrostatic environment in which a neutral (acetylated) residue will lower the pKa of the catalytic histidine (H⁴¹⁵) and aspartic acid (D¹⁶⁶) residues, thereby stabilizing the transition state and facilitating the proton transfer necessary for the methyl group transfer.¹⁴ For the methylation of H3Arg²⁶ a similar observation was made, wherein mutation of the neighboring positively charged lysine to a neutral methionine residue (K²⁷M), enhanced the methylation of H3Arg²⁶ to a similar extent as acetylation on Lys²⁷.¹³ To compliment these biochemical studies, we here describe structural investigations employing H3-based peptidomimetics designed to directly probe the role of lysine acetylation on substrate recognition by CARM1.

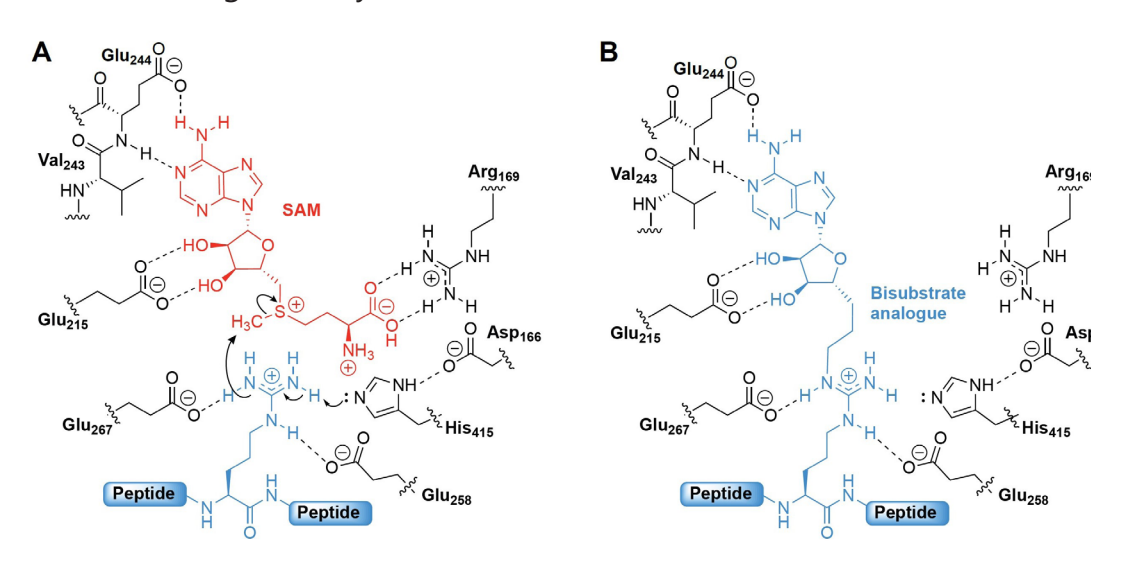
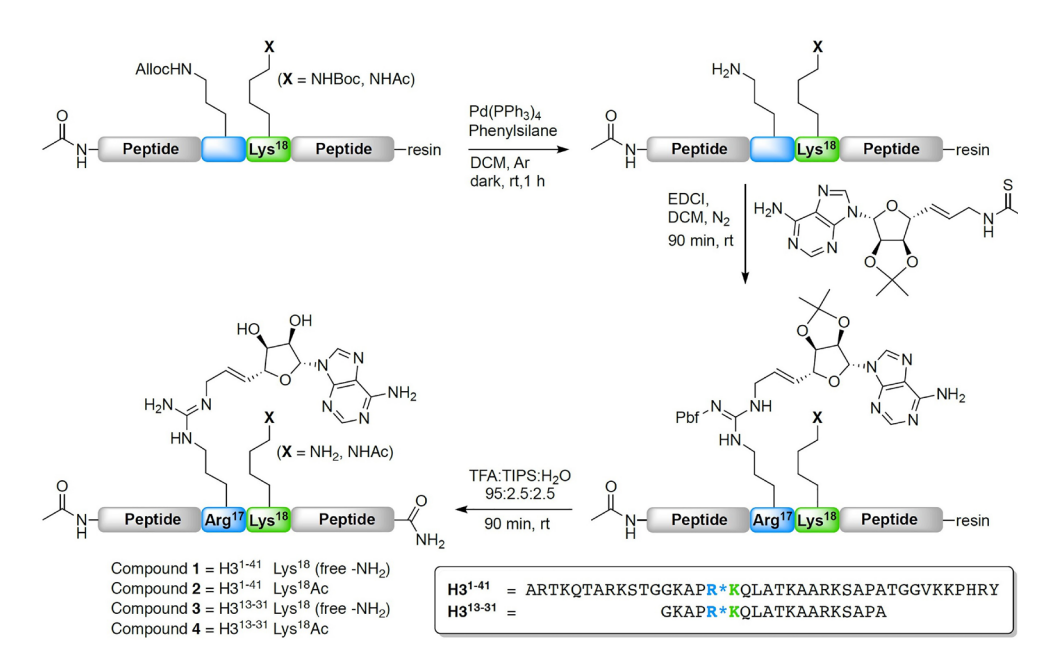


Figure 1. A) CARM1 active site with key active residues interacting with cofactor SAM and the target arginine of a peptide substrate. The double E-loop consists of glutamate residues Glu²⁵⁸ and Glu²⁶⁷. His⁴¹⁵ is involved in substrate recognition as part of the THW-loop and interacts with Asp166 for the deprotonation of the guanidine moiety facilitating methyl group transfer. B) Design strategy used in preparing bi-substrate analogues for structural studies and peptidic inhibitors of CARM1.

Results and Discussion

To gain additional insights into the impact of lysine acetylation on arginine methylation by CARM1, we performed structural studies using a transition-state peptidomimetic strategy recently developed by our group (Figure 1B).¹⁵ By covalently linking the adenosine moiety of the methyl donor SAM to the arginine side chain of a substrate peptide it is possible to generate conjugates that mimic the transition state of the first methylation step performed by the family of protein arginine N-methyltransferases (PRMTs). These peptidomimetics facilitate structural studies with PRMTs by circumventing the need to add SAM mimics (typically SAH or sinefungin) and the formation of ternary complex with substrate peptides.¹⁵

In synthesizing these peptidomimetics the adenosine group is introduced via the arginine guanidine moiety using a convenient on-resin modification procedure wherein the target arginine is initially installed as an Alloc-protected ornithine residue (Scheme 1). After assembly of the peptide using the solid phase peptide synthesis (SPPS), the Alloc group is selectively removed leaving the other protecting groups unaffected and the peptide bound to the resin. The free ornithine side chain amine is subsequently coupled with a Pbf-protected thiourealinked adenosine building block leading to formation of the arginine guanidino group directly linked to the adenosine moiety. Capping of the N-terminus with acetic anhydride followed by deprotection and cleavage from Rink Amide resin yields the modified peptide with amine groups on bothe the N and C-terminus, mimicking those present in the natural substrate.



Scheme 1. General synthetic scheme for the preparation of transition state peptidomimetics with the adenosine moiety covalently linked to the side chain of the CARM1 target arginine. Also indicated is the neighbouring lysine residue in either acetylated or nonacetylated state.

For this study, two pairs of peptidomimetics were prepared based on the residues 1-41 and 13-31 of the histone H3 tail peptide (Scheme 1). In these peptidomimetics the Arg¹⁷ residue was covalently linked to an adenosine moiety via a 3-carbon linker previously shown to be the optimal length for the recognition of such peptidomimetics.¹⁵ To directly examine the influence of lysine acetylation, both sequences were also prepared as the Lys¹⁸Ac variants which were readily prepared by introduction of the corresponding acetylated lysine building block during the SPPS. The two pairs of peptidomimetics thus obtained where designed to address two aspects of H3 substrate recognition by CARM1: for both the H3¹⁻⁴¹ and H3¹³⁻³¹ constructs the presence of free Lys¹⁸ or Lys¹⁸Ac was expected to provide

insight into the role of crosstalk between substrate acetylation and methylation. In addition, the larger H3¹⁻⁴¹ constructs were prepared with the aim of also obtaining additional structural insights into long distance interactions known to be crucial for CARM1 substrate recignition. ^{16,17}

With peptidomimetics 1-4 in hand, co-crystallization studies were performed using an isolated catalytic domain of mmCARM1 (Mus musculus CARM1, residues 130-497). Peptidomimetics 1-4 were initially crystallized using PEG as the main crystallizing agent in line with previous structural studies with CARM1. 15,16 All structures were solved and refined (depending on crystals, resolution ranging from 2.0 to 2.7 Å at ESRF or SOLEIL synchrotron beamlines) in the space group P2₁2₁2 with one copy of the CARM1 tetramer in the asymmetric unit (see Appendix II Table S1). While the resulting structures were solved and refined, the electron density maps displayed poor density beyond the previously established minimal binding sequence, 15,18 indicating high disorder or low occupancy for the peptidomimetics. Our previous experience in solving a number of different PRMT structures (PRMT4, PRMT2, PRMT6) has shown that in some cases PEG molecules can map the peptide binding site and in doing so inhibit, or strongly affect, peptide-binding. 19 To address this challenge we also explored the use of sodium malonate as the primary crystallization reagent instead of PEG. In total, 33 crystal structures of mmCARM1 in complex with the H3 peptidomimetics were solved and refined with PEG as the primary crystallization reagent along with an additional 12 structures obtained when using sodium malonate. 19 These studies revealed sodium malonate to be a superior crystallization reagent for obtaining high quality structures of CARM1 in complex with peptidomimetics 1-4 that were successfully solved and refined in the same space group. The highest resolution structures were obtained with H3¹³⁻³¹ peptidomimetics 3 and 4 (2.54 Å for 3 (Lys¹⁸-NH₂) and 2.2 Å for 4 (Lys¹⁸Ac)). While the electron density maps obtained with 3 and 4 clearly revealed the conformation of 10 residues in all CARM1 complexes (amino acids 13 to 22) the same was not the case for the longer H3¹⁻⁴¹ peptidomimetics 1 and 2. In the case of 1 and 2, the peptidomimetics were found to occupy only two of the active sites of the mmCARM1 tetramer and are unable to displace all SAH molecules natively bound to the protein (the purified mmCARM1 construct naturally contains SAH molecule bound in the active site).

As noted, the H3^{13–31} peptidomimetics 3 and 4 gave well-resolved structures for the first 10 amino acids. Beyond that however, residues 23 to 31 were never seen in the electron density maps, likely due to high levels of disorder. In the structures solved with both 3 and 4, Leu²⁰ of the H3^{13–31} peptidomimetic is the last residue that is clearly seen to be interacting with CARM1 via Van der Waal interactions at Leu⁴¹³. Beyond that, the positioning of Ala²¹ and Thr²² indicates that residues 23–31 of the peptidomimetics are likely located in a region that has no interactions with CARM1

(Figure 2). While the longer H3¹⁻⁴¹-based peptidomimetics failed to give additional structural information regarding long distance substrate interactions with CARM1, the H3¹³⁻³¹ constructs did provide insights into the conformational behavior of the substrate peptides and the impact of lysine acetylation. In keeping with previous reports, the peptide segments of transition-state mimetics 3 and 4 adopt a conformation similar to that observed in the structure of CARM1 bound to sinefungin and a linear H3¹³⁻³⁰ peptide (see Appendix || Figure S1).¹⁸

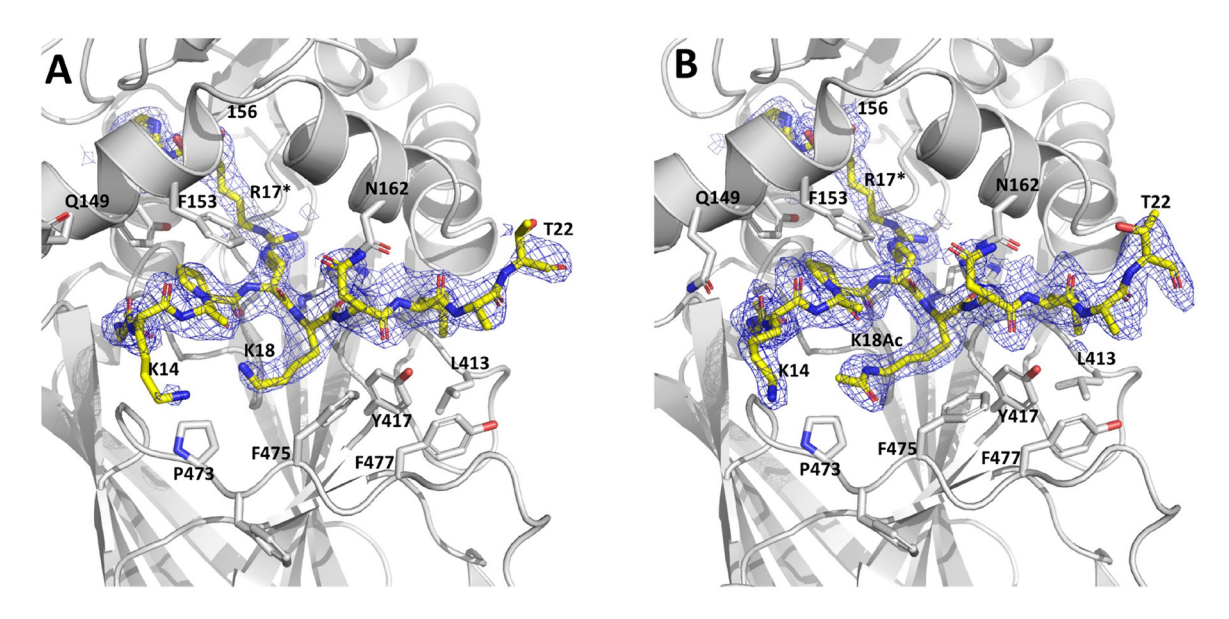


Figure 2. Electron density (2Fobs-Fcalc) weighted maps for subunit A of mmCARM1 bound to: A) peptidomimetic 3 (H3¹³⁻³¹ Lys¹⁸-NH₂), PDB code 7OS4 and B)peptidomimetic 4 (H3¹³⁻³¹ Lys¹⁸Ac), PDB code 7OKP. CARM1 is represented as cartoon and H3 peptidomimetics are represented as stick. Maps are represented as a mesh contouring level set to 1 σ .

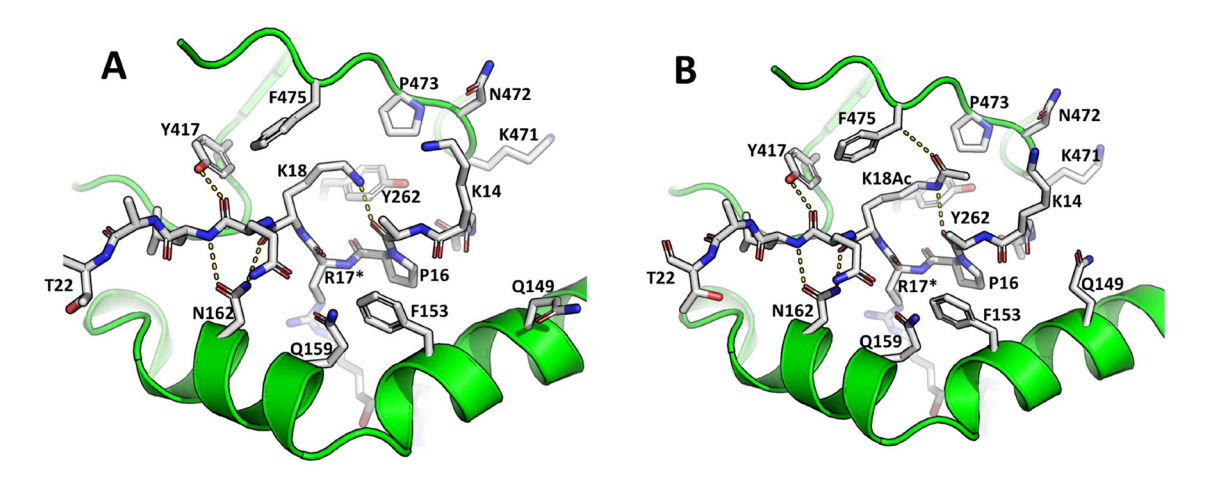


Figure 3. Recognition of peptidomimetics 3 and 4 by mmCARM1. Interactions shown for: A) compound 3 ($H3^{13-31}$ Lys¹⁸-NH₂) PDB code 7OS4 and B) compound 4 ($H3^{13-31}$ Lys¹⁸Ac) PDB code 7OKP. H-bonds are shown as dash lines with cartoon and stick representation of the peptidomimetics bound to mmCARM1.

Interestingly, little conformational change is observed for either CARM1 or the substrate peptidomimetics upon Lys¹⁸ acetylation (Figure 3 and Appendix **II** Figure S2), with both the intra-peptide and peptide-CARM1 interactions observed with Lys¹⁸ peptidomimetic 3 largely maintained with Lys¹⁸Ac peptidomimetics 44. The conformation of the peptide is stabilized by intra-peptide hydrogen bond between Nz atom of Lys¹⁸ and the back bone oxygen of Ala¹⁵ and by additional Van der Waals interactions with Tyr²⁶², Tyr⁴¹⁷ and Phe⁴⁷⁵ in the CARM1active site (Figure 3). While subtle, acetylation of Lys¹⁸ does lead to some additional interactions: (i) a weak C-H-O hydrogen bond involving the O atom of the acetyl functional group and the C β atome of Phe⁴⁷⁵ and (ii) Van der Waals interactions with the proline ring of Pro⁴⁷³ and CH₃ group of Ala¹⁵ (Figure 3). In addition to these stabilizing interactions, acetylation of Lys¹⁸ may reduce the cost of desolvation of the peptides prior to binding and therefore produce an energetic gain in complex formation.

As the noted above, Yue and coworkers have previous proposed that Lys¹⁸ acetylation stabilizes the transition state of the methylation transfer.¹⁴ Our crystal structures do not, however, support this hypothesis as the side chain of Lys¹⁸ is found to be located more than 12 Å away from the active site center. Rather, the structural data presented here indicated that gain in substrate affinity associated with lysine acetylation is likely due to additional interactions (Van der Waals and weak hydrogen bonding) as well as a possible reduction of the desolvation penalty.

Table 1. IC	value and for	compounds	5-14 against	CARM1	and PRMT1
50					

Compound		Pontidomimetic coguence	IC ₅₀ values (μM) ^a		
		Peptidomimetic sequence	CARM1	PRMT1	
5	H3 ¹⁰⁻²⁵	Ac-STGGKAPR*KQLATKAA-NH ₂	0.290 ± 0.015	>2.5	
6	H3 ¹⁰⁻²⁵ (K ¹⁸ Ac)	Ac-STGGKAP R * $K(Ac)QLATKAA-NH2$	0.155 ± 0.007	>5	
7	H3 ¹³⁻²²	$Ac-GKAP$ R * $KQLAT-NH_2$	0.121 ± 0.007	>5	
8	H3 ¹³⁻²² (K ¹⁸ Ac)	Ac-GKAP R * $K(Ac)QLAT-NH2$	0.155 ± 0.012	>5	
9	H3 ¹⁴⁻²¹	$Ac-KAP$ R * $KQLA-NH_2$	0.287 ± 0.034	>2.5	
10	H3 ¹⁴⁻²¹ (K ¹⁸ Ac)	$Ac-KAP$ R * $K(Ac)QLA-NH_2$	0.211 ± 0.023	>25	
11	H3 ¹⁵⁻²⁰	$Ac-AP$ R * $KQL-NH_2$	0.143 ± 0.014	>2.5	
12	H3 ¹⁵⁻²⁰ (K ¹⁸ Ac)	$Ac-AP$ R * $K(Ac)QL-NH_2$	0.072 ± 0.008	>25	
13	H3 ¹⁶⁻¹⁹	$Ac-PR*KQ-NH_2$	0.346 ± 0.031	>5	
14	H3 ¹⁶⁻¹⁹ (K ¹⁸ Ac)	$Ac-PR*K(Ac)Q-NH_2$	0.699 ± 0.081	>25	

 $^{^{}a}$ IC₅₀ values reported in μ M from duplicate data obtained from a minimum of 7 different concentrations \pm standard error of the mean (s.e.m.). The R* indicates the Arg¹⁷ residue where the adenosine group is incorporated.

Informed by our structural findings obtained with the H3¹³⁻³¹-based peptidomimetics 3 and 4, we next prepared a series of smaller peptidomimetics

and evaluated their inhibitory activity against CARM1. These peptidomimetics were centred around Arg¹⁷ which was again covalently linked to an adenosine group via its side chain quanidine moiety. Two peptidomimetics based on H3¹⁰⁻²⁵ (compounds 5 and 6) were first prepared and assessed as inhibitors of CARM1 assessed (Table 1). The potent inhibition observed for both 5 and 6, led us to also investigate shorter peptidomimetics by sequentially omitting N- and C-terminal residues to generate the corresponding deca-, octa-, hexa-, and tetra-peptide analogues 7–14. Again, each of these truncated peptidomimetic were prepared with and without acetylation of the neighboring Lys¹⁸ residue to probe the interplay between peptide sequence and lysine acetylation on recognition by/inhibition of CARM1. Inhibition studies subsequently revealed that all compounds retain potent inhibition with IC₅₀ values in the nM range. Interestingly, the most potent inhibition measured was for the acetylated hexapeptide-based peptidomimetic 12. This hexapeptide motif appears to be an optimum for achieving inhibition as either elongation to the octapeptide or truncation to the tetrapeptide was found to result in measurable increases in IC_{50} values. Interestingly, lysine acetylation also reduces the capacity of these peptidomimetics to engage with other PRMTs. To assess selectivity, peptidomimetics 5-14 were evaluated against PRMT1, which in all cases revealed a high degree of selectivity for CARM1 inhibition. These findings are in line with expectations given that the H3 peptide sequence used in this study is known to be methylated by CARM1 and not by PRMT1.²⁰

As shown in Table 1, Lys 18 acetylation led to a decrease in IC $_{50}$ for compounds 6, 10, and 12 suggesting an increase in binding affinity. As noted above, in addition to stabilizing interactions with the enzyme active site, acetylation of Lys¹⁸ may reduce the cost of desolvation of the peptide prior to binding and therefore produce an energetic gain in complex formation. Notable is the potent inhibition obtained for hexapeptide 12 (H3¹⁵⁻²⁰ K¹⁸Ac) which retains the main interactions with CARM1 and intra-peptide interactions revealed by our co-crystal structures. It is plausible that the larger peptidomimetics display a lowered inhibition/reduced affinity because they must pay a high desolvation penalty (particularly for Lys¹⁴) in order to bind that is not compensated for by additional interactions with CARM1. We do note that in the case of decapeptide analogues 7 and 8 the finding that the acetylated species exhibits a slightly higher IC₅₀ does not adhere to this explanation and remains to be understood. Our structural insights also provide an explanation for the reduced inhibition observed for the tetrapeptide analogues 13 and 14: deletion of Ala¹⁵ is likely to significantly destabilize peptide binding as intra-peptide interactions between Ala¹⁵ and Lys¹⁸ (which stabilize the tight turn conformation of the peptide) are lost and in this context, acetylation of Lys¹⁸ is not sufficient to restore binding affinity. Also of note for peptidomimetics 5-14 is the finding that acetylation of Lys¹⁸ consistently results in an increased inhibitory selectivity towards CARM1 vs PRMT1 (Table 1). This finding points to the intriguing possibility that crosstalk between lysine acetylation and arginine methylation may also serve to reinforce PRMT specificity beyond the primary sequence of the peptide substrate.

While our studies provide new in vitro insights, the structural basis of crosstalk between H3K¹⁸ acetylation and CARM1 methylation remains to be further elucidated in vivo. Notable in this regard is recent work by O'Malley and co-workers who combined cryo-electron microscopy and biochemical approaches in studying the ER-coactivator complex.²¹ These investigations revealed that CARM1 recruitment induces p300 conformational change and promotes H3K¹⁸Ac and that increased histone H3K¹⁸ acetylation in turn enhanced CARM1-mediated H3R¹⁷ methylation.

Conclusion

We here report the use of peptide-based transition state mimetics centred around the Arg¹⁷/Lys¹⁸ of the histone H3 tail peptide to study crosstalk between lysine acetylation and arginine methylation and its impact on substrate recognition by CARM1. Structural studies with these peptidomimetics and the catalytic domain of CARM1 reveal that little conformational change is observed in the protein and on the peptide substrates conformations upon Lys¹⁸ acetylation. Rather, the increase in affinity associated with Lys¹⁸ acetylation is likely due to additional weak interactions with mmCARM1, intra-peptide interactions that stabilize the active conformation of the substrate peptide, and a possible reduction of the desolvation cost associated with substrate binding when Lys¹⁸ is acetylated. Building from these findings, shorter peptidomimetics were also synthesized and evaluated as CARM1 inhibitors. The truncation approach used led to the discovery of potent inhibitors containing only two residues flanking the central Arg-Lys pair on either side with peptidomimetics 11 and 12 exhibiting IC₅₀ values of 143 and 72 nM respectively. Taken together, the findings reported in this study provide valuable new insights both into the mechanistic understanding of crosstalk and its role in CARM1 mediated methylation as well as in the design of potent CARM1-selective peptidomimetic inhibitors.

Experimental Section

All reagents employed were of American Chemical Society grade or finer and were used without further purification unless otherwise stated. The final compounds were purified via preparative HPLC performed on a BESTA-Technik system with a Dr. Maisch Reprosil Gold 120 C18 column (25×250 mm, $10 \mu m$) and equipped with a ECOM Flash UV detector monitoring at 214 nm. The following solvent system, at a flow rate of 12 mL min⁻¹, was used: solvent A:0.1% TFA in water/acetonitrile 95/5; solvent B: 0.1% TFA in water/acetonitrile 5/95. Gradient elution was as follows:

95:5 (A/B) for 5 min, 95:5 to 0:100 (A/B) over 40 min, 0:100 (A/B) for 5 min, then reversion back to 95:5 (A/B) over 2 min, 95:5 (A/B) for 8 min.

Purity was confirmed to be \geq 95% by LCMS performed on a Shimadzu LC-20AD system with a Shimadzu Shim-Pack GIST-AQ C18 column (3.0×150 mm, 3 µm) at 30°C and equipped with a UV detector monitoring at 214 and 254 nm. This system was connected to a Shimadzu 8040 triple quadrupole mass spectrometer (ESI ionisation). The following solvent system, at a flow rate of 0.5 mL min⁻¹, was used: solvent A, 0.1% formic acid in water; solvent B, acetonitrile. Gradient elution was as follows: 95:5 (A/B) for 2 min, 95:5 to 0:100 (A/B) over 23 min, 0:100 (A/B) for 1 min, then reversion back to 95:5 (A/B) over 1 min, 95:5 (A/B) for 3 min.

HRMS analyses were performed on a Shimadzu Nexera X2 UHPLC system with a Waters Acquity HSS C18 column (2.1×100 mm, 1.8 μm) at 30°C and equipped with a diode array detector. The following solvent system, at a flow rate of 0.5 mL min⁻¹, was used: solvent A, 0.1% formic acid in water; solvent B, 0.1% formic acid in acetonitrile. Gradient elution was as follows: 95:5 (A/B) for 1 min, 95:5 to 15:85 (A/B) over 6 min, 15:85 to 0:100 (A/B) over 1 min, 0:100 (A/B) for 3 min, then reversion back to 95:5 (A/B) for 3 min. This system was connected to a Shimadzu 9030 QTOF mass spectrometer (ESI ionisation) calibrated internally with Agilent's API-TOF reference mass solution kit (5.0 mM purine, 100.0 mMammonium trifluoroacetate and 2.5 mM hexakis(1H,1H,3H-tetrafluoropropoxy) phosphazine) diluted to achieve a mass count of 10000.

Synthetic procedures. Compounds 1–14 were synthesized by using a methodology developed in our group enabling the on-resin preparation of peptides containing substituted arginine residues. 15 Specifically, Histone H3-derived peptides were synthesized by using standard Fmoc solid-phase peptide synthesis (SPPS) techniques after which the adenosine group was introduced. The peptides were synthesized on 0.1 mmol scale using Rink Amide AM resin (146 mg with a resin loading of 0.684 mmol g⁻¹). The arginine in the sequence was replaced with an Alloc-protected ornithine. The lysine was introduced as Fmoc-Lys(Boc)-OH to obtain the free lysine or as Fmoc-Lys(Ac)-OH to obtain the peptides with the acetylated lysine residue. Peptide couplings were performed using standard Fmoc amino acids (4.0 eg), BOP (4.0 eg) and DiPEA (8.0 eg) in DMF (7.5 mL) at ambient temperature for 1 hour. The Fmoc deprotection was performed in two runs by using 20% piperidine in DMF (6 mL) for 5 minutes and 30 minutes, consecutively. After SPPS, the N-terminus was acetylated on resin using acetic anhydride (0.5 mL) and DiPEA (0.85 mL) in DMF (10 mL) for 1 hour at room temperature with nitrogen bubbling. The peptides were kept on the resin for next step.

The peptides were Alloc-deprotected on the resin using tetrakis (triphenylphos-

phine)-palladium(0) and phenylsilane in DCM following a literature procedure.²² Upon the completion of Alloc deprotection, the adenosine thiourea building block15 (105 mg, 0.13 mmol, 1.3 eq) was coupled to the amine group of ornithine side-chain using 1-ethyl-3-(3-dimethylaminopropyl)carbodiimide (EDCI) (34.5 mg, 0.15 mmol, 1.5 eq) in DCM (10 mL). The mixture was stirred for 1.5 hours at room temperature, drained and the resin was washed with DCM (3×10 mL), DMF (3×10 mL) and DCM (2×10 mL). Peptides were deprotected and cleaved from the resin using cleavage cocktail (TFA/TIPS/H2O 95: 2.5 : 2.5). Precipitation in MTBE/Petroleum ether (1:1) yielded the crude peptide, which was purified by preparative HPLC. The purity and identity were confirmed by analytical HPLC and High-resolution Mass Spectrometry, the results of which are presented in the Appendix II for all final compounds.

Enzymatic activity assays. The commercially available PRMT1 and CARM1 chemiluminescent assay kits (BPS Bioscience, Dan Diego, CA, USA) were used for evaluation of methyltransferase inhibition as previously described.²² The enzymatic reactions were performed in duplicate at room temperature using 96-wells plates precoated with histone substrates. The reaction volume is 50 µL containing proprietary assay buffer, 20 µM SAM, enzyme: PRMT1 (10 ng per reaction) and CARM1 (200 ng per reaction). Against CARM1, the inhibitors were dissolved in water and tested at varying concentration ranging from 0.0128 to 200 µM. For selectivity, inhibitors were tested against PRMT1 at three fixed concentrations (2.5, 5 and 25 µM). Positive controls were performed by addition of water instead of inhibitor. Blank and substrates controls were performed in the absence of enzyme and SAM, respectively. Before the reactions were initiated by the addition of SAM, the inhibitors were incubated with the enzyme for 15 min at room temperature. After incubation for one hour with PRMT1 or two hours with CARM1, the wells were washed and blocked and incubated with primary antibody (1:100) for 1 h. After washing and blocking, the wells were incubated with secondary HRP-labelled antibody (1:1000) for 30 minutes. After a final washing and blocking, the HRP chemiluminescent substrate mixture was added to the wells and the luminescence was measured immediately using a Tecan spark plate reader. All the measurements were performed in duplicate and the data was analysed using GraphPad Prism 9.

All the luminescence data were corrected with the blank values and the data was subsequently normalized with the highest value in the concentration range defined as 100% activity. The percentage of inhibition activity was plotted as a function of inhibitor concentration and fit using non-linear regression analysis of the sigmoidal dose -response curve generated using the normalized data and a variable slope following Equation (1):

$$Y = \frac{100}{(1+10^{(logIC\ 50-X)*Hillslope\)})}$$
(1)

where Y=percentage activity, X=the logarithmic concentration of the inhibitors, Hill Slope=slope factor or Hill coefficient. The IC $_{50}$ value was determined by the half maximal inhibitory concentration. The IC $_{50}$ values measured for SAH, which served as a reference compound, are similar to those reported. Full IC $_{50}$ curves and comparative K $_{i}$ values for compounds 5–14 and SAH are presented in the Appendix II .

CARM1 cloning, expression, and purification. The Mus musculus CARM1 gene sequence corresponding to the PRMT core (residues 130 to 497, mmCARM1^{130–497}) were amplified by PCR from the original GST-CARM1 construct.²⁴ The sequences were cloned in the pDONR207TM (Invitrogen) vector using a BP reaction (Gateway® Cloning, Life Technologies). The positive clones were confirmed by sequencing (GATC). The sequences were subcloned in a pDEST20TM vector using a LR reaction. The resulting recombinant protein harbour an amino-terminal glutathione Stransferase (GST) tag followed by a Tobacco etch virus (TEV) protease cleavage site. DH10Bac competent cells containing the baculovirus genome were transformed with the pDEST20TM-CARM1 plasmids and plated onto LB agar media containing 15 mg.mL⁻¹ tetracycline, 7 mg mL⁻¹ gentamicin, 50 mg.mL⁻¹ kanamycin, 25 mg mL⁻¹ X-Gal and 40 mg mL⁻¹ IPTG. Bacmid DNA purified from recombinationpositive white colonies was transfected into Sf9 cells using the Lipofectin reagent (Invitrogen). Viruses were harvested 10 days after transfection. Sf9 cells were grown at 300 K in suspension culture in Grace medium (Gibco) using Bellco spinner flasks. 1 L of sf9 cell culture (at 0.8×10^6 cells mL⁻¹) was infected with recombinant GSTmmCARM1 virus with an infection multiplicity of 1. Cells were harvested 48 h postinfection. Cell lysis was performed by sonication in 50 mL buffer A [50 mM Tris-HCl pH 8.0, 250 mM NaCl, 5% glycerol, 5 mM TCEP, 0.01% NP40 and antiproteases (Roche, CompleteTM, EDTA-free)] and cellular debris were sedimented by centrifugation of the lysate at 40,000×g for 30 min. The supernatant was incubated overnight at 277 K with 2 mL glutathione Sepharose resin (GE Healthcare). After a short centrifugation, the supernatants were discarded, and the beads were poured in an Econo-column (Bio-Rad). After two wash steps with 10 mL buffer A, 2 mL buffer A supplemented with in-house produced TEV protease were applied to the columns and digestion was performed 4 hours at 303 K with gentle mixing. The digest was concentrated with an Amicon Ultra 10 K (Milipore), loaded on a gelfiltration column (HiLoad 16/60 Superdex S200, GE Healthcare) and eluted at 1 mL.min⁻¹ with buffer B [20 mM Tris-HCl pH 8.0, 100 mM NaCl, 1 mM TCEP] using an ÄKTA Purifier device (GE Healthcare). Fractions containing mmCARM1130-497 were pooled and concentrated to 7.75 mg mL⁻¹.

Crystallization. Transition state mimics were solubilized in water before addition to

the protein solution (2 mg mL $^{-1}$) at the final concentration of 2 mM. The protein-peptide solution was incubated 30 minutes at room temperature before use. Vapor diffusion method utilizing hanging drop trays with a 0.5 mL reservoir was used for crystallization. Typically, 2 μ L of protein-ligand solution were added to 1 μ L of well solution consisting of 1–1.5 M disodium malonate, 100 mM MES pH 5.5–7 and 200 mM NaCl. Crystals grew in a few days at 293 K.

X-ray structure determination. Crystals were flash-frozen in liquid nitrogen after a brief transfer to 5 μL reservoir solution containing 25% (v/v) Glycerol as a cryoprotectant and were stored in liquid nitrogen. The diffraction data sets were collected using CBI X-ray home source (Rigaku FR-X and EIGER 4 M), SOLEIL PROXIMA1 and ESRF ID30-B beamlines, using a Pilatus 6 M, EIGER 4 M, EIGER X4M (Dectris) detector and processed with XDS²⁵ and HKL-2000.²⁶ The crystals belonged to the P2₁2₁2 space group with four monomers of CARM1 in the asymmetric unit. The structures were solved by molecular replacement using CARM1 structure as a probe.¹⁶ Model building and refinement were carried out using Coot²⁷ and PHENIX.²⁸ TLS refinement with 6 groups per polypeptide chain was used. All other crystallographic calculations were carried out with the CCP4 package.²⁹ Structure figures were generated with PyMOL (http://www.pymol.org).

References

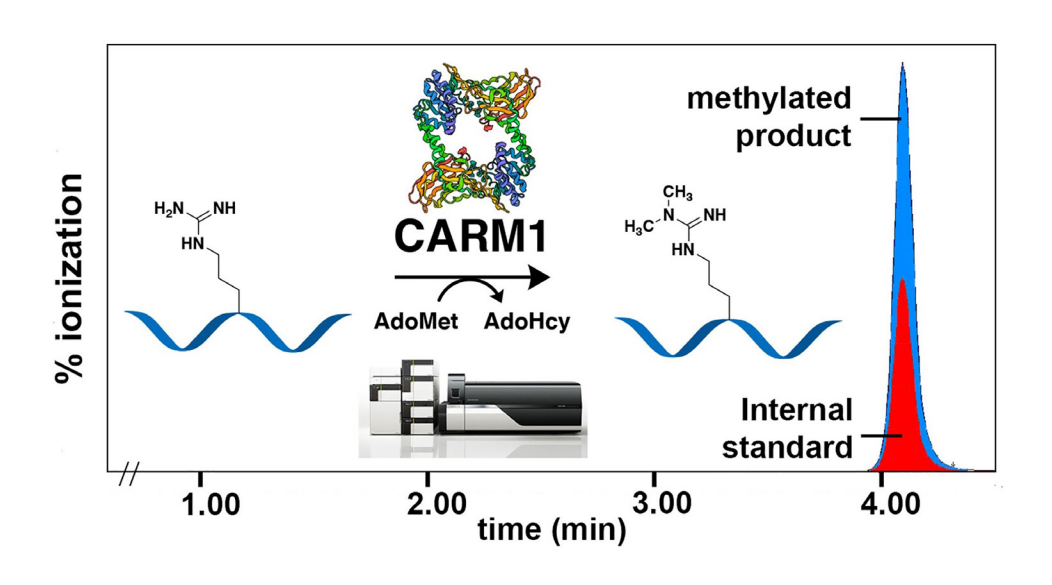
- 1. T. Hunter, The age of crosstalk: phosphorylation, ubiquitination, and beyond, Mol. Cell. 2007, 28, 730–738.
- 2. A. S. Venne, L. Kollipara, R. P. Zahedi, The next level of complexity: crosstalk of posttranslational modifications, Proteomics 2014, 14, 513–524.
- 3. W. S. Lo, R. C. Trievel, J. R. Rojas, L. Duggan, J. Y. Hsu, C. D. Allis, R. Marmorstein, S. L. Berger, Phosphorylation of serine 10 in histone H3 is functionally linked in vitro and in vivo to Gcn5-mediated acetylation at lysine 14, Mol. Cell. 2000, 5, 917–926.
- 4. K. P. Nightingale, S. Gendreizig, D. A. White, C. Bradbury, F. Hollfelder, B. M. Turner, Cross-talk between histone modifications in response to histone deacetylase inhibitors: MLL4 links histone H3 acetylation and histone H3K4 methylation, J. Biol. Chem. 2007, 282, 4408–4416.
- 5. L. Li, Y. Wang, Cross-talk between the H3K36me3 and H4K16ac histone epigenetic marks in DNA double-strand break repair, J. Biol. Chem. 2017, 292, 11951–11959.
- 6. O. Castillo-Aguilera, P. Depreux, L. Halby, P. B. Arimondo, L. Goossens, DNA Methylation Targeting: The DNMT/HMT Crosstalk Challenge, Biomol. Eng. 2017, 7.
- 7. Y. Shi, M. J. Long, M. M. Rosenberg, S. Li, A. Kobjack, P. Lessans, R. T. Coffey, L. Hedstrom, Boc 3 Arg-Linked Ligands Induce Degradation by Localizing Target

- Proteins to the 20S Proteasome, ACS Chem. Biol. 2016, 11, 3328-3337.
- 8. F. Wojcik, G. P. Dann, L. Y. Beh, G. T. Debelouchina, R. Hofmann, T. W. Muir, Functional crosstalk between histone H2B ubiquitylation and H2A modifications and variants, Nat. Commun. 2018, 9, 1394.
- 9. R. S. Blanc, S. Richard, Arginine Methylation: The Coming of Age, Mol. Cell. 2017, 65, 8–24.
- 10. Z. Zhao, A. Shilatifard, Epigenetic modifications of histones in cancer, Genome Biol. 2019, 20, 245.
- 11. B. M. Lorton, D. Shechter, Cellular consequences of arginine methylation, Cell. Mol. Life Sci. 2019, 76, 2933–2956.
- 12. S. Daujat, U. M. Bauer, V. Shah, B. Turner, S. Berger, T. Kouzarides, Crosstalk between CARM1 methylation and CBP acetylation on histone H3, Curr. Biol. 2002, 12, 2090–2097.
- 13. Z. Zhang, B. C. Nikolai, L. A. Gates, S. Y. Jung, E. B. Siwak, B. He, A. P. Rice, B. W. O'Malley, Q. Feng, Crosstalk between histone modifications indicates that inhibition of arginine methyltransferase CARM1 activity reverses HIV latency, Nucleic Acids Res. 2017, 45, 9348–9360.
- 14. W. Yue, M. Hassler, S. M. Roe, V. Thompson-Vale, L. H. Pearl, Insights into histone code syntax from structural and biochemical studies of CARM1 methyltransferas, EMBO J. 2007, 26, 4402–4412.
- 15. M. J. van Haren, N. Marechal, N. Troffer-Charlier, A. Cianciulli, G. Sbardella, J. Cavarelli, N. I. Martin, Transition state mimics are valuable mechanistic probes for structural studies with the arginine methyltransferase CARM1, Proc. Natl. Acad. Sci. USA 2017, 114, 3625–3630.
- 16. N. Troffer-Charlier, V. Cura, P. Hassenboehler, D. Moras, J. Cavarelli, Functional insights from structures of coactivator-associated arginine methyltransferase 1 domains, EMBO J. 2007, 26, 4391–4401.
- 17. J. Mailliot, Étude Structurale de l'histoneméthyltransférase "CARM1" et de Ses Complexes Biologiquement Significatifs: Des Structures 3D Vers La Conception Rationnelle de Composés à Action Pharmacologique, PhD Thesis, University of Strasbourg. 2013.
- 18. P. A. Boriack-Sjodin, L. Jin, S. L. Jacques, A. Drew, C. Sneeringer, M. P. Scott, M. P. Moyer, S. Ribich, O. Moradei, R. A. Copeland, Structural Insights into Ternary Complex Formation of Human CARM1 with Various Substrates, ACS Chem. Biol. 2016, 11, 763–771.
- 19. N. Marechal, Etude Structurale Des Protéines Arginine Méthyltransferases, PhD Thesis, University of Strasbourg, 2018.
- 20. B. T. Schurter, S. S. Koh, D. Chen, G. J. Bunick, J. M. Harp, B. L. Hanson, A. Henschen-Edman, D. R. Mackay, M. R. Stallcup, D. W. Aswad, Methylation of histone H3 by coactivator-associated arginine methyltransferase 1, Biochemistry 2001, 40, 5747–5756.

- 21. P. Yi, Z. Wang, Q. Feng, C. K. Chou, G. D. Pintilie, H. Shen, C. E. Foulds, G. Fan, I. Serysheva, S. J. Ludtke, M. F. Schmid, M. C. Hung, W. Chiu, B. W. O'Malley, Structural and Functional Impacts of ER Coactivator Sequential Recruitment, Mol. Cell 2017, 67, 733–743 e734.
- 22. Y. Zhang, M. J. van Haren, N. I. Martin, Peptidic transition state analogues as PRMT inhibitors, Methods 2020, 175, 24–29.
- 23. M. van Haren, L. Q. van Ufford, E. E. Moret, N. I. Martin, Synthesis and evaluation of protein arginine N-methyltransferase inhibitors designed to simultaneously occupy both substrate binding sites, Org. Biomol. Chem. 2015, 13, 549–560.
- 24. D. Chen, H. Ma, H. Hong, S. S. Koh, S. M. Huang, B. T. Schurter, D. W. Aswad, M. R. Stallcup, Regulation of transcription by a protein methyltransferase, Science 1999, 284, 2174–2177.
- 25. W. Kabsch, XDS, Acta Crystallogr. Sect. D 2010, 66, 125–132.
- 26. Z. Otwinowski, W. Minor, Processing of X-ray diffraction data collected in oscillation mode, Methods Enzymol. 1997, 276, 307–326.
- 27. P. Emsley, K. Cowtan, Coot: model-building tools for molecular graphics, Acta Crystallogr. Sect. D 2004, 60, 2126–2132.
- 28. P. D. Adams, P. V. Afonine, G. Bunkoczi, V. B. Chen, I. W. Davis, N. Echols, J. J. Headd, L. W. Hung, G. J. Kapral, R. W. Grosse-Kunstleve, A. J. McCoy, N. W. Moriarty, R. Oeffner, R. J. Read, D. C. Richardson, J. S. Richardson, T. C. Terwilliger, P. H. Zwart, PHENIX: a comprehensive Python-based system for macromolecular structure solution, Acta Crystallogr. Sect. D 2010, 66, 213–221.
- 29. M. D. Winn, C. C. Ballard, K. D. Cowtan, E. J. Dodson, P. Emsley, P. R. Evans, R. M. Keegan, E. B. Krissinel, A. G. Leslie, A. McCoy, S. J. McNicholas, G. N. Murshudov, N. S. Pannu, E. A. Potterton, H. R. Powell, R. J. Read, A. Vagin, K. S. Wilson, Overview of the CCP4 suite and current developments, Acta Crystallogr. Sect D 2011, 67, 235–242.

Chapter 4

A Direct Assay for Measuring Activity and Inhibition of Coactivator Associated Arginine Methyltransferase 1



Accepted by Biochemistry

Abstract

Coactivator-associated arginine methyltransferase 1 (CARM1) is a member of the family of protein arginine methyltransferases. CARM1 catalyzes methyl group transfer from the cofactor S-adenosyl-L-methionine (AdoMet) to both histone and non-histone protein substrates. CARM1 is involved in a range of cellular processes, mainly involving RNA transcription and gene regulation. As the aberrant expression of CARM1 has been linked to tumorigenesis, the enzyme is a potential therapeutic target, leading to the development of inhibitors and tool compounds engaging with CARM1. In order to evaluate the effects of these compounds on the activity of CARM1, sensitive and specific analytical methods are needed. While different methods are currently available to assess the activity of methyltransferases, these assays mainly focus on either the measurement of the cofactor product S-adenosyl-L-homocysteine (AdoHcy) or employ radioactive or expensive reagents, each with their own advantages and limitations. To complement the tools currently available for analysis of CARM1 activity, we here describe the development of a convenient assay employing peptide substrates derived from poly(A)-binding protein 1 (PABP1). This operationally straightforward LC-MS/MS based approach allows for the direct detection of substrate methylation with minimal workup. The method was validated and its value in characterizing CARM1 activity and inhibition demonstrated through a comparative analysis involving a set of established small molecule and peptide-based CARM1 inhibitors.

Introduction

Cofactor-associated arginine methyltransferase 1 (CARM1) is a member of the family of protein arginine N-methyltransferases (PRMTs), responsible for the methylation of arginine residues in a variety of nuclear protein substrates, including histone tails, RNA binding proteins and splicing factors.^{1, 2} Arginine methylation in histones and other nuclear proteins plays an important role in regulating a range of cellular processes, including gene regulation, signal transduction, RNA processing, and DNA repair.^{3, 4} PRMTs can be classified into three types based on their primary product formation: type I PRMTs result in both ω -N^G-monomethyl arginine (MMA) and asymmetrically ω-N^G,N^G dimethylated arginine (aDMA), type II PRMTs catalyze the formation of MMA and symmetrical $\omega - N^G, N^G$ –dimethylarginine (sDMA), while type III PRMTs exclusively form MMA.^{5, 6} As a type I PRMT, CARM1 catalyzes the transfer of the methyl group from S-adenosyl-L-methionine (AdoMet) to first generate MMA followed directly by a second methylation step resulting in the formation of aDMA (Figure 1). The methyl group transfer from AdoMet to the protein substrate generates the by-product S-adenosyl-L-homocysteine (AdoHcy), which in turn can inhibit CARM1 as a feedback inhibitor.⁷

Figure 1. CARM1 catalyzes the methylation of arginine residues in substrate proteins and peptides to generate monomethyl arginine (MMA) and asymmetric dimethyl arginine (aDMA).

The aberrant expression of CARM1 has been linked to a variety of disease states, most prominently in the field of cancer. CARM1 overexpression is linked to ovarian, colorectal, prostate, and lung cancers. In addition, CARM1 was found to promote cell proliferation of ER α -positive breast cancer cells. These findings

have led to interest in CARM1 as a potential therapeutic target for the treatment of cancer. To facilitate the development of inhibitors of CARM1, reliable, specific, and rapid analytical methods for characterizing its activity are vital. Generally, analytical methods for the detection of methyltransferase activity focus on the detection of enzymatic by-product AdoHcy. Several high-throughput assays are available for the detection of AdoHcy, either directly by chromatographic means, ¹² or indirectly, using enzyme-coupled assays in which AdoHcy formation leads to a luminescent or fluorescent signal. 13,14 Using such an approach, we recently investigated the use of a commercially available assay kit (MTase Glo) for the purposes of studying CARM1 activity but were not able to achieve consistent results (data not shown). We attribute this to the previously noted high background signal encountered with this method owing to the auto-methylating ability of CARM1 at its own arginine residue R551.15 These findings suggested to us that methods relying on the detection of AdoHcy formation are not optimal for the quantification of CARM1 activity. For this reason, we were inspired to develop of an alternative assay focused on the direct detection of the methylated products formed by CARM1.

Substrate methylation can be quantified using existing methods for example through the use of radio-labeled ³H-AdoMet¹⁶ to measure direct methyl group addition or indirectly through the use of antibodies developed against specific methylated epitopes.¹⁷ There are, however, several disadvantages to these assays. While compatible with high-throughput screening (HTS), radiometric approaches require strict operating conditions, radio-protected equipment, and specific laboratory setups. In comparison, while antibody-based ELISA assays avoid the use of radioactivity, they are expensive and involve complex experimental protocols that are not suitable for high-throughput screening. To address these shortcomings, we here describe the development of a rapid, straightforward, and sensitive CARM1-specific assay. Specifically, our method relies upon the direct detection of the dimethylated products formed when substrate peptides derived from poly(A)-binding protein 1 (PABP1) are incubated with CARM1 and AdoMet. Using an LC-MS based approach, the enzymatic products are readily detected via multiple reaction monitoring (MRM) and quantified by comparison to a hexadeuteromethylated species serving as internal standard. MRM is a technique widely used in quantitative proteomics because of its high selectivity using two levels of mass detection, high sensitivity, and wide dynamic range. 18 We further demonstrate the suitability of this rapid and direct analytical method in characterizing CARM1 inhibition by evaluating a number of established CARM1 inhibitors. Notably, the results obtained with our assay were found to compare well with those obtained when using a more operationally complex antibody-based chemiluminescent method. The analytical method here reported provides high selectivity and sensitivity in the characterization of CARM1 activity and offers a simplified approach to screening for inhibitors of CARM1.

Result and Discussion

Analytical method development

To achieve a rapid and direct analytical method for the quantification of CARM1 activity, we have developed an LC-MS method using multiple reaction monitoring (MRM) analysis and optimized to obtain maximal detection sensitivity and accuracy. In search of a peptide substrate suitable for use in an LC-MS based activity assay for CARM1, we initially focused our attention on peptides derived from histone H3. Tail peptides from H3 are well-characterized substrates of CARM1, with preferential methylation occurring at arginine residue H3R17. 19, 20-22 To assess the suitability of H3 peptides with the envisioned LC-MS detection method, we first synthesized H3¹⁶⁻³⁰, incorporating an asymmetrically dimethylated arginine residue at arginine 17. Subsequent Analysis of the H3¹⁶⁻³⁰ R¹⁷aDMA peptide by LC-MS was found to produce a distribution of m/z values rather than a major single precursor ion owing to the presence of other arginine and lysine residues in the sequence. This in turn led to a significant reduction in signal as even when selecting for the major precursor ion, approximately 75% of total signal was lost. No significant improvement was observed when using buffers at different pH in an attempt to tune the charge distribution of the peptide (data not shown). We therefore opted to evaluate different substrate peptides not based on H3 but rather derived from poly(A)-binding protein 1 (PABP1), a protein known to be efficiently methylated by CARM1 at arginine residues 455 and 460.^{23,24} Notably, the PABP1 sequences PABP1 447-459 and PABP1 456-466 do not include any additional positively charged residues other than the arginine residues R⁴⁵⁵ and R⁴⁶⁰, respectively. To this end, PAPB1⁴⁴⁷⁻⁴⁵⁹ R⁴⁵⁵aDMA and PAPB1⁴⁵⁶⁻⁴⁶⁶ R⁴⁶⁰aDMA were synthesized and analyzed by LC-MS. Based on peak shape and signal intensity, PAPB1456-466 R460 aDMA was identified as the preferred analyte and used for optimization. In contrast to the histone H3 sequence, mass analysis of this PABP1 sequence yielded a single major peak (m/z = 620.850, corresponding to $[M+2H]^{2+}$) which was subsequently selected as the precursor ion for further MRM optimization (see Figure. S1 and S2 in the Appendix III).

During the optimization of the MRM method, we examined the influence of mobile phase composition and pH, column temperature, and flow rate on the elution profile of the PAPB1⁴⁵⁶⁻⁴⁶⁶ R⁴⁶⁰aDMA standard. Initial attempts employed isocratic elution with a mobile phase consisting of 25% acetonitrile containing 20 mM NH₄Ac (pH 7, flow rate is 0.5 mL·min⁻¹ at 30 $^{\circ}$ C) and 20 mM NH₄Ac (pH 9, flow rate is 0.5 mL·min⁻¹ at 30 $^{\circ}$ C), respectively. These conditions yielded a broad saw-like peak for the peptidic analyte. When the mobile phase was changed to

25% acetonitrile containing 0.1% formic acid (pH 2), a smooth peak resulted but still gave a broad signal with significant peak tailing. To improve peak shape, we subsequently evaluated gradients of acetonitrile in aqueous formic acid (0.1%). This led to an optimized method employing a gradient moving from 20% to 92% acetonitrile in aqueous formic acid (0.1%) (pH 2) which reliably gave a sharp and symmetrical peak for PAPB1⁴⁵⁶⁻⁴⁶⁶ R⁴⁶⁰aDMA. Variation of the slope of the gradient (between 6 and 20 minutes) did not significantly affect the peak shape, allowing for a convenient run time of 6 minutes. Subsequently, we examined the column temperature (up to 60 °C) and flow rate (0.5 and 1 mL·min ^{- 1)}, but this provided no significant improvement. The final conditions were therefore set on a method with a run time of 6 minutes and a gradient of 20% to 92% acetonitrile in water containing 0.1% formic acid with a flow rate of 0.5 mL·min ^{- 1} at 30 °C. The MRM parameters generated for the PAPB1⁴⁵⁶⁻⁴⁶⁶ R⁴⁶⁰aDMA through an automated methodology of the mass spectrometer were incorporated in the LC-MS method.

Internal standards. As an internal standard we prepared the hexadeuterated form of the analyte, PAPB1 $^{456-466}$ R 460 -d $_6$ -aDMA. In doing so, any changes in the analyte signal resulting from variation in the workup or the analytical method (e.g. due to matrix effects, ion suppression, precipitation, or non-specific binding) can be corrected for. Isotopically labeled compounds have the same chromatographic behavior and show the same ionization and fragmentation pattern as their non-labeled counterparts, but can be separated based on their mass difference. The synthesis of PAPB1 $^{456-466}$ R 460 -d $_6$ -aDMA was conducted as for the non-deuterated species with the exception that a hexadeuterated aDMA building block was required which was prepared following protocols previously reported by our group. ^{25,26}

Optimization of the Enzymatic activity assay. The conditions of the enzymatic activity assay were optimized with respect to buffer composition, reaction time, and work-up. The optimized buffer consists of 20 mM Tris buffer (pH 8) containing 50 mM NaCl, 1 mM EDTA, 3 mM MgCl₂, 0.1 mg/ml BSA, and 1mM DTT. The addition of DTT was vital for avoiding disulfide bond formation and the addition of BSA was found necessary to keep CARM1 in its active form by blocking aggregation and reducing unspecific binding of the CARM1 to the well plate. Sample work-up consisted of quenching the enzyme reaction by addition of 0.1% formic acid solution (known to be compatible with the MS conditions of the assay²⁷) and addition of the internal standard.

In order to maximize the signal for the enzymatic reaction, a screen was performed to establish both the optimal concentration of enzyme and incubation time. For CARM1, the half maximal effective concentration (EC_{50}) determination was performed using CARM1 enzyme at concentrations of 0.875, 1.75, 3.5, 7, 14,

28, 56 and 112 ng/ μ L. Substrates were fixed at 100 μ M PAPB1 ⁴⁵⁶⁻⁴⁶⁶ and 10 μ M AdoMet and samples were taken every 15 minutes for 2 hours. The CARM1 EC₅₀ value was thus established to be 11.68 \pm 0.33 ng/ μ L (see Figure. S3 in the Appendix |||), which is in good agreement with the final concentration of CARM1 used in the commercially available chemiluminescent assay kit (BPS Bioscience, Catalog #52041L; CARM1 concentration is 10 ng/ µL or 200 ng per reaction). For the determination of the $K_{\mbox{\scriptsize M}}$ value of PABP1 $^{456\mbox{\scriptsize -}466}$, formation of the methylated product was analyzed in the presence of a fixed concentration of 100 µM AdoMet and PABP1 $^{456-466}$ applied over a concentration range of 0.05 μ M to 100 μ M. For the determination of the K_M value of AdoMet, the methylated substrate was analyzed in the presence of a fixed concentration of 100 µM PABP1 and AdoMet concentrations ranging from 0.05 μM to 100 μM . The K_M values thus obtained were 12.03 \pm 2.28 μ M for PABP1⁴⁵⁶⁻⁴⁶⁶ and 5.46 \pm 0.01 μ M for AdoMet (see Figure. S3 in the Appendix III). Based on these findings, when performing the subsequent inhibition studies CARM1 was used at a concentration of 11.68 ng/µL while the substrate concentrations were fixed at 12 µM PABP1 and 10 µM AdoMet.

Inhibitor studies. We next applied the assay in assessing the inhibition of CARM1 by a number of known inhibitors of varying potencies including AdoHcy (1), MS023 (2), MS049 (3), TP064 (4), and a series of recently reported peptidomimetic CARM1 inhibitors (5-9) (Figure. 2). 28, 29-32 For the purpose of generating IC₅₀ curves for these inhibitors, concentration ranges were set according to previously reported IC₅₀ values. The inhibitors were first incubated with CARM1 for 15 minutes at room temperature before the enzyme reaction was initiated by addition of the AdoMet/PABP1 456-466 substrate mixture. On the basis of the residual CARM1 activity measured, inhibition curves were generated and the IC₅₀ values determined (Table 1). In order to evaluate the suitability of the method for the determination of CARM1 inhibition, the IC₅₀ values were compared with those obtained using a commercially available chemiluminescent ELISA kit. The conditions used with this kit are comparable to those used here in terms of enzyme concentrations, but a slightly lower AdoMet concentration is applied in the kit (1 µM versus 10 µM). In addition, the peptide substrate and detection method employed in the ELISA kit are inherently different. The kit employs a histone H3 derived peptide that is covalently linked to the bottom of the well plate and as such no substrate concentration is given. Product formation in turn is detected using specific antibodies that recognize aDMA formation at arginine residue H3R17.

The results of the inhibitor screen are summarized in Table 1 and show that the potency trend for the IC_{50} values obtained with the MRM LC-MS assay corresponds very well with that obtained with the ELISA based method (Table 1). The absolute IC_{50} values measured via the MRM LC-MS assay were found to be generally 2-4 times higher than those obtained via the ELISA assay, an effect we ascribe to the

differences in assay conditions and methodology. The most notable differences between the MRM LC-MS and ELISA assays lie in the AdoMet concentrations and peptide substrates used. The MRM LC-MS method here reported uses a 10-fold higher concentration of AdoMet which likely impacts the IC₅₀ values measured. Furthermore, MRM LC-MS assay detects the CARM1 catalyzed methylation of a PAPB1 derived substrate while the ELISA method employs an H3 based peptide substrate. Notably, the published $_{\rm KM}$ value of CARM1 for such H3 substrates (112 μ M)³³ is 10-fold higher than that of PABP1 based substrates (K_M, = 12 μ M, this work). In the context of inhibition assays, the higher affinity of CARM1 for PABP1 based substrates versus those derived from H3 is also likely to impact the relative IC₅₀ values measured for competitive inhibitors.

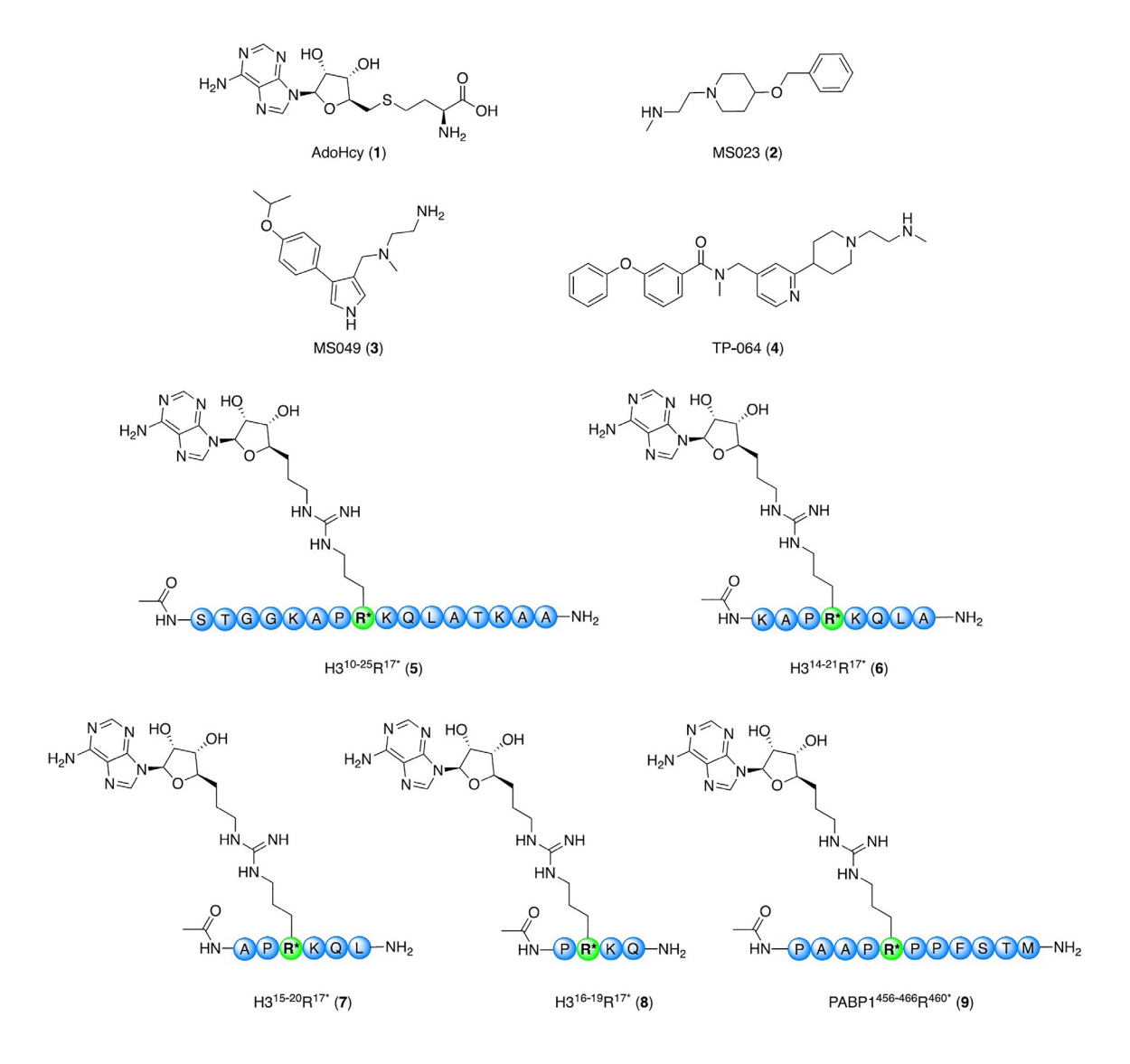


Figure 2. Overview of the chemical structures of reported small molecule CARM1 inhibitors AdoHcy (1), MS023 (2), MS049 (3) and TP064 (4) and peptidomimetic inhibitors H3¹⁰⁻²⁵R^{17*} (5), H3¹⁴⁻²¹R^{17*} (6), H3¹⁵⁻²⁰R^{17*} (7), H3¹⁶⁻¹⁹R^{17*} (8), and PABP1⁴⁵⁶⁻⁴⁶⁶R^{460*} (9).

Table 1. Inhibition data for compounds 1-9 against CARM1 tested by MRM and ELISA assay

Inhibitor		CARM1 IC ₅₀ values (μM) ^a		
Number	Compound name	MRM LC-MS Assay	ELISA Assay	
1	AdoHcy	0.873 ± 0.339	$0.276 \pm 0.074 \text{ (ref 27)}$	
2	MS023	0.327 ± 0.034	0.101 ± 0.011 (this work)	
3	MS049	0.082 ± 0.008	$0.028 \pm 0.003 \text{ (this work)}$	
4	TP064	0.162 ± 0.010	$0.037 \pm 0.008 \text{ (this work)}$	
5	$H3^{10-25}R^{17*}$	0.770 ± 0.098	$0.290 \pm 0.021 \text{ (ref 20)}$	
6	$H3^{14-21}R^{17*}$	0.403 ± 0.028	$0.287 \pm 0.048 \text{ (ref 20)}$	
7	$H3^{15-20}R^{17*}$	0.617 ± 0.057	$0.143 \pm 0.020 \text{ (ref 20)}$	
8	$H3^{16-19}R^{17*}$	1.456 ± 0.021	$0.346 \pm 0.044 \text{ (ref 20)}$	
9	PABP1456-466 R460*	0.212 ± 0.025	$0.090 \pm 0.016 \text{ (ref 27)}$	

 ${}^{a}IC_{50}$ values reported in μM from duplicate data obtained from a minimum of 7 different concentrations \pm standard error of the mean (s.e.m.). Full inhibition curves are provided in the Appendix III.

Conclusion

We here describe the development of a direct, specific, and convenient analytical method for measuring the activity of CARM1. The LC-MS based method applies multiple reaction monitoring (MRM) for the detection and quantification of a methylated peptide substrate (PAPB1⁴⁵⁶⁻⁴⁶⁶ R⁴⁶⁰aDMA). The assay presents a significant simplification over existing ELISA and radiometric methods while benefitting from high sensitivity and convenient sample preparation. Compared with the widely used radiolabeled AdoMet assay, the MRM LC-MS assay is not restricted by specialized operational and laboratory conditions. We have also demonstrated the application of the MRM LC-MS method in assaying the inhibitory activity of a selection of known CARM1 inhibitors by generating CARM1 inhibition curves. The IC₅₀ values obtained were found to be comparable with published values and with values obtained with the commercially available ELISA kit. Considering the growing body of evidence for CARM1 as a therapeutic target, the MRM LC-MS assay here described represents a valuable addition to the tools available for the identification of CARM1 inhibitors. Furthermore, the 6-minute run time of the MRM LC-MS assay allows for the convenient assessment of focused libraries number in the tens-to-hundreds of compounds. While HTS campaigns for CARM1 inhibitor identification typically rely on alternative methods such as radiometric detection, the CARM1-specificity of the MRM LC-MS assay makes it very well suited for hit validation purposes. In addition, the approach here described should be widely applicable in the development of assays for other methyltransferases provided that compatible substrates are available.

Experimental Procedures

Building block Synthesis. The Fmoc- d_6 -aDMA(Pbf)-OH building block was synthesized from commercially available Fmoc-Orn(Boc)-OH 9 following the synthetic route for Fmoc-aDMA(Pbf)-OH as previously described (Scheme 1)²⁵. Briefly, compound 9 was transformed into allyl ester 10 catalyzed with allyl alcohol, HOBt, DMAP and DCC in THF. Subsequently, allyl ester 10 was treated with TFA/DCM (2:1) to remove the Boc group and reacted with 2,2,4,6,7-pentamethyldihydrobenzofuran-5-sulfonyl isothiocyanate (Pbf-NCS) to form Pbf-protected thiourea 11. Finally, compound 11 was reacted with dimethyl-d₆-amine hydrochloride in the presence of 1-ethyl-3-(3-dimethylaminopropyl)-carbodiimide (EDCI) to form the intermediate guanidine species which was treated directly with tetrakis(triphenylphosphine) palladium(0) to form Pbf-protected Fmoc building block 12 which used for solid phase peptide synthesis.

Scheme 1. Synthesis of Fmoc-d6-aDMA. a. allyl alcohol, HOBt, DMAP, DCC, THF, overnight, (yield 62%); b. TFA/DCM(2:1),1h; c. Pbf-NCS in DCM (0.1 M), 2h, (yield 60%); d. EDCl, bis(methyl-d3)amine hydrochloride, DCM, overnight; e. Pd(PPh₃)₄, N-methylaniline, N₂, overnight, (yield 85% over 2 steps).

(E) - N2 - (((9 H - fluoren - 9 - yl) methoxy) carbonyl) - N $^{\circ}$, N $^{\circ}$ - bis (meth-yl-d3)-N $^{\circ}$ -((2,2,4,6,7-pentamethyl-2,3-dihydrobenzofuran-5-yl)sulfonyl)arginine (12)

To a solution of compound 3 (610 mg, 0.86 mmol) in DCM (30 mL), 1-ethyl-3-(3-dimethylaminopropyl)carbodiimide (269 mg, 1.73 mmol) and bis(methyl- d_3)amine hydrochloride (151 mg, 1.73 mmol) were added. The mixture was stirred overnight at room temperature. The mixture was diluted with DCM (50 mL), washed with 10% citric acid (2 x 20 mL) and saturated sodium bicarbonate (2 x 20 mL) and dried over sodium sulfate. The organic solvent was removed and the residue was redissolved in THF (40 mL). The mixture was treated with N-methylaniline (238 μ L, 2.31 mmol), followed by addition of tetrakis(triphenylphosphine) palladium(0) (41.4 mg, 0.04

mmol). The mixture was protected from light and stirred under nitrogen at room temperature. After TLC indicated completion of the allyl ester removal, the solvent was removed under reduced pressure and purified by column chromatography (2% methanol in DCM) to yield compound 4 (500 mg, 85%) as a white foam. HRMS (m/z): [M+H] $^+$ calculated for C₃₆H₃₉D₆N₄O₇S $^+$, 683.3385, found 683.3345. 1 H NMR (500 MHz, CDCl₃) δ 8.17 (s, 1H), 7.64 (d, J = 7.6 Hz, 2H), 7.48 (dd, J = 7.6, 4.5 Hz, 2H), 7.28 (m, J = 7.3 Hz, 2H), 7.19 – 7.15 (m, 2H), 6.00 (d, J = 7.7 Hz, 1H), 4.22 (m, J = 7.1, 3.1 Hz, 2H), 4.15 (d, J = 6.4 Hz, 1H), 4.08 (t, J = 7.3 Hz, 1H), 3.30 – 3.07 (m, 2H), 2.84 (s, 2H), 2.38 (s, 3H), 2.32 (s, 3H), 1.98 (s, 3H), 1.81 – 1.48 (m, 4H), 1.35 (s, 6H). 13 C NMR (126 MHz, CDCl₃) δ 174.33, 161.58, 161.28, 160.98, 160.79, 160.67, 156.89, 155.62, 143.84, 143.73, 141.36, 139.87, 135.23, 135.18, 135.13, 134.10, 130.67, 129.01, 128.25, 128.21, 128.17, 127.90, 127.27, 125.89, 125.30, 120.09, 118.72, 87.59, 77.42, 77.16, 76.91, 67.56, 53.36, 47.10, 45.05, 42.92, 29.50, 28.53, 24.96, 19.42, 18.07, 12.49.

CARM1 Cloning, Expression, and Purification. The mus musculus CARM1 (mmCARM1) gene sequence corresponding to the PRMT core (residues 130 to 497, mmCARM1₁₃₀₋₄₉₇) were amplified by PCR from the original GST-CARM1 construct.¹⁹ The sequences were cloned in the pDONR207[™] (Invitrogen) vector using a BP reaction (Gateway® Cloning, Life Technologies). The positive clones were confirmed by sequencing (GATC). The sequences were subcloned in a pDEST20[™] vector using an LR reaction. The resulting recombinant protein is harboring an amino-terminal glutathione S-transferase (GST) tag followed by a Tobacco etch virus (TEV) protease cleavage site. DH10Bac competent cells containing the baculovirus genome were transformed with the pDEST20[™]-CARM1 plasmids and plated onto LB agar media containing 15 mg.mL⁻¹ tetracycline, 7 mg.mL⁻¹ gentamicin, 50 mg.mL⁻¹ kanamycin, 25 mg.mL⁻¹ X-Gal and 40 mg.mL⁻¹ IPTG. Bacmid DNA purified from recombinationpositive white colonies was transfected into Sf9 cells using the Lipofectin reagent (Invitrogen). Viruses were harvested 10 days after transfection. Sf9 cells were grown at 300 K in suspension culture in Grace medium (Gibco) using Bellco spinner flasks. 1 L of sf9 cell culture (at 0.8 x 10⁶ cells.mL⁻¹) was infected with recombinant GST-mmCARM1 virus with an infection multiplicity of 1. Cells were harvested 48 h post-infection. Cell lysis was performed by sonication in 50 mL buffer A [50 mM Tris-HCl pH 8.0, 250 mM NaCl, 5% glycerol, 5 mM TCEP, 0.01% NP40 and antiproteases (Roche, Complete[™], EDTA-free)] and cellular debris were sedimented by centrifugation of the lysate at 40,000 x g for 30 min. The supernatant was incubated overnight at 277 K with 2 mL glutathione Sepharose resin (GE Healthcare). After a short centrifugation, the supernatants were discarded, and the beads were poured in an Econo-column (Bio-Rad). After two washing steps with 10 mL buffer A, 2 mL buffer A supplemented with in-house produced TEV protease was applied to the columns and digestion was performed for 4 hours at 303 K with gentle mixing.

The digest was concentrated with an Amicon Ultra 10K (Milipore), loaded on a gelfiltration column (HiLoad 16/60 Superdex S200, GE Healthcare) and eluted at 1 mL.min⁻¹ with buffer B [20 mM Tris-HCl pH 8.0, 100 mM NaCl, 1 mM TCEP] using an ÄKTA Purifier device (GE Healthcare). Fractions containing mmCARM1₁₃₀₋₄₉₇ were pooled and concentrated to 7.75 mg.mL⁻¹.

Peptide Synthesis. The PABP1⁴⁵⁶⁻⁴⁶⁶ peptides (Figure 3) used in the study were prepared via solid phase peptide synthesis (SPPS) using a CEM Liberty Blue microwave-assisted peptide synthesizer. The Fmoc protected Rink amide AM resin (0.1 mmol) was first swollen in 10 mL of a 1:1 mixture of DMF/DCM for 5 min, drained, and treated with 20 vol.% piperidine (10 mL) in DMF for 65 seconds at 90°C, drained and washed with DMF (3 x 5 mL). The resin was then treated with a solution of Fmoc-Met-OH (0.2 M, 2.5 mL, 5 eq), DIC (1 M, 1 mL, 10 eq) and Oxyma (1 M, 0.5 mL, 5 eg) in DMF (4 mL) at 76°C for 15 s before the temperature was increased to 90°C for an additional 110 s before being drained. To achieve maximal yield, each amino acid was double coupled according to the previous cycle. Following Fmoc removal with 20 vol.% piperidine (10 mL) in DMF for 65 seconds at 90°C, the resin was drained and washed with DMF (3 x 5 mL) after which the subsequent amino acids were coupled. All Fmoc amino acids were obtained commercially with the exception of Fmoc-d₆-aDMA(Pbf)-OH which was prepared as described in the supporting information. After coupling and deprotection of the final amino acid, the N-terminus was acetylated on resin using acetic anhydride (0.5 mL) and DiPEA (0.85 mL) in DMF (10 mL) for 120 s at 65°C. Then the resin was washed three times with DMF (10 mL). The final peptides were cleaved from the resin using a mixture of TFA/water/TIPS (95:2.5:2.5) under shaking for 2 hours at room temperature. The resin was filtered over cotton and washed with TFA (2 x 0.5 mL). The crude peptides were precipitated in a mixture of MTBE/Hexane (1:1) and pelleted by centrifugation (5 min at 4500 rpm). The pellet was then washed twice with MTBE/Hexane (1:1) (50 mL), centrifuged (5 min at 4500 rpm), and dried under a nitrogen flow. The crude peptides were purified by prep-HPLC and characterized by LC-MS and HRMS. The final yield of the peptides ranges from 30-40%.

Enzymatic Activity Assay. Enzyme activity assays were performed with CARM1 (11.68 ng/µL or 200 nM) in 20 mM Tris buffer (pH 8) containing 50 mM Tris NaCl, 1 mM EDTA, 3 mM MgCl₂, 0.1 mg/ml BSA and 1 mM dithiothreitol (DTT). The enzyme mixture (20 µL) was added to the substrate mixture (20 µL) containing the PABP1 $^{456-466}$ substrate peptide and AdoMet (final concentrations of 12 µM and 10 µM respectively) followed by incubation for two hours at room temperature. The reaction was subsequently quenched by addition of 30 µL of the reaction mixture to 10 µL of a 0.1 % formic acid solution (pH 2). After addition of the deuterated internal standard in water (100 nM, 40 µL) and mixing for 2 minutes, the samples were centrifuged for 5 minutes at 3000 rpm. 60 µL of the supernatant was

transferred to a new 96-well plate and analyzed.

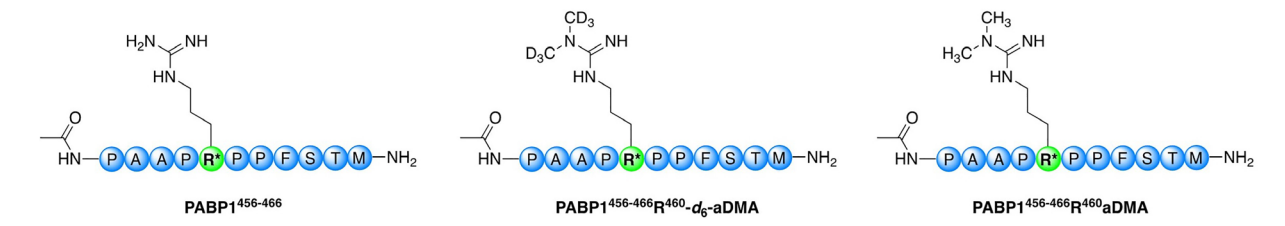


Figure 3. Structures of the PABP1 $^{456-466}$ substrate, the PABP1 $^{456-466}$ -R 460 -d₆-aDMA internal standard and the PABP1 $^{456-466}$ R 460 -aDMA reference standard.

LC-MS method for Analysis of Methylated peptides. LC-MS analysis was performed on a Shimadzu LC-20AD system with a Shimadzu Shim-Pack GIST C18 column (3.0 x 150 mm, 3 μ m particle size) at 30°C connected to a Shimadzu 8040 triple quadrupole mass spectrometer with an electrospray ionization (ESI) source. The products were eluted with a water–acetonitrile gradient moving from 20% to 92% acetonitrile (0.1% FA) over 6 minutes at a flow rate of 0.5 mL·min $^{-1}$. The injection volume was 10 μ L. The ionization source was operated in positive mode using an interface voltage of 4.5 kV, nebulizing gas at 1.5 L/min, drying gas at 15 L/min and a desolvation line (DL) temperature of 250 °C. The MRM parameter optimization was performed using both the analyte (PABP1 $^{456-466}$ R 460 -aDMA) and hexadeuterated internal standard (PABP1 $^{456-466}$ R 460 -d $_6$ -aDMA). The results of this optimization, which include precursor ion scanning, collision energy, Q1 and Q3 scanning, are summarized in Table 2.

Table 2. Optimized MRM parameters for the PABP1 analyte and internal standard^a

Compounds		Q1 (m/z)	Q3 (m/z)	Q1 PreBias (V)	CE (V)	Q1 PreBias (V)
PABP1-aDMA	analyte	620.85	211.00	-28	-29	-22
			140.00	-28	-47	-25
			282.00	-28	-20	-30
PABP1-d ₆ -aDMA	standard	623.75	210.95	-28	-28	-22
			140.00	-24	-45	-26
			282.00	-28	-19	-29

^aThe interface voltage was set at 4.5 kV for all the compounds; dwell time was 100 ms. Q1: quadrupole 1, Q3: quadrupole 3, m: mass, z: charge, CE: collision energy.

Analytical Method Validation (Linearity, Limits of Detection, accuracy, and precision)

Analysis of the PABP1⁴⁵⁶⁻⁴⁶⁶R⁴⁶⁰-aDMA peptide was validated between 16 and 512 nM for within and between run accuracy and precision, the linearity of the calibration curve, the sample recovery, and the limit of detection. Linearity was performed with calibration points consisting of 1, 2, 4, 8, 16, 32, 64, 128, 256,

512 and 1024 nM PABP1 $^{456-466}$ R 460 -aDMA peptide dissolved in water. Samples for analysis were worked up as described above in the enzymatic reaction assay section and analyzed with the LC-MS/MS method. Area ratios of PABP1 $^{456-466}$ R 460 -aDMA and the hexadeuterated internal standard were assessed and plotted versus concentration. Linearity was assessed visually and by calculation of the coefficient of determination R 2 , which should be >0.98. The limit of detection (LOD) was determined by the samples corresponding to a signal-to-noise (S/N) of 3.

Quality control (QC) samples consist of PABP1⁴⁵⁶⁻⁴⁶⁶R⁴⁶⁰-aDMA concentrations of 16, 64, 512 nM and enzymatic reaction buffer (20 mM Tris buffer pH 8, 50 mM NaCl, 1 mM EDTA, 3 mM MgCl₂, 0.1 mg/ml BSA and 1 mM DTT). QC samples for analysis were worked up as described above in the enzymatic reaction assay section and analyzed with the LC-MS/MS method. In order to evaluate the precision and accuracy of the quantification of PABP1⁴⁵⁶⁻⁴⁶⁶R⁴⁶⁰-aDMA, concentration values were recalculated for QC using calibration curves. Intra-run accuracy and precision tests were performed using PABP1⁴⁵⁶⁻⁴⁶⁶R⁴⁶⁰-aDMA concentrations of 16, 64, 512 nM. Accuracy and precision tests were performed in six-fold per concentration in 1 run and in one-fold per concentration in three separate runs. The acceptance criteria of the accuracy results were 85-115% and of the precision results <15%. The limit of detection was calculated to be 1.55 nM and the method was linear between 8 and 512 nM with a R² of 0.996 (Table 3). The lowest concentration giving a reliable and accurate signal was found to be 16 nM.

Table 3. Validation Parameters of the MRM Method for detection of PABP1⁴⁵⁶⁻⁴⁶⁶R⁴⁶⁰-aD-MA

[QC] (nM)	R^2	
8-512	0.	996
	Accuracy (%)	Precision CV (%)
Within run (n=6)		
16	113.7	2.1
64	87.0	4.7
512	94.4	5.6
Between runs (n=3)		
16	106.2	0.1
64	97.5	2.3
512	91.2	4.9
Limit of detection (S/N ≥ 3)	5 nM	

Enzyme Inhibition Assay. The CARM1 inhibition assays were performed using a number of established, commercially available CARM1 inhibitors as well as a series of peptidomimetic inhibitors recently reported our group. When using the assay to characterize CARM1 inhibition, the substrates were set at concentrations near their calculated K_M values (12 μ M for the PABP1 peptide and 10 μ M for AdoMet). The inhibitors were tested at 10 different concentrations that were

selected based on their published IC $_{50}$ values. For commercially available inhibitors that were not soluble in water, stock solutions were prepared in DMSO and diluted to a final DMSO concentration of <1% in the assay mixture. CARM1 (20 μ L) and inhibitors (10 μ L) were incubated for 15 minutes at room temperature, followed by the addition of a mixture of peptide substrate and AdoMet (10 μ L) to start the reaction. The mixture was incubated for two hours at room temperature and the reaction subsequently quenched by addition of 30 μ L of the reaction mixture to 10 μ L of a 0.1 % formic acid solution (pH 2). After addition of the deuterated internal standard in water (100 nM, 40 μ L) and mixing for 2 minutes, the samples were centrifuged for 5 minutes at 3000 rpm. 60 μ L of the supernatant was transferred to a new 96-well plate and analyzed by LC-MS as described above. Negative controls (no enzyme) and positive controls (no inhibitor) were included in each plate.

Data Analysis. The data obtained from the MRM method included a linearity line with ten different concentrations of reference standard (from 8 to 512 nM) and a fixed concentration of internal standard (100 nM). These data points were subjected to weighted regression $(1/x^2)$. The intercept and slope were used for determination of the measured concentrations.

For quantification of the methylated product, the area ratio of analyte to internal standard was calculated and quantified using the linearity line obtained with the reference standards. The concentrations were then converted to enzyme velocity in nmoles produced/hour/mg CARM1 using equation 1 with the concentration the methylated product in nM, time in minutes, and enzyme concentration in mg/L.

$$v = \frac{[product]^{\frac{60}{t}}}{[E]}$$
 (equation 1)

Calculation of V_{max} and K_m was done using Graphpad Prism 6 following nonlinear (Michaelis-Menten) regression analyses using equation 2.

$$v = \frac{V_{max} [S]}{K_m + [S]}$$
 (equation 2)

The k_{cat} was calculated from the V_{max} using equation 3, with V_{max} in nmol/hour/mg enzyme and enzyme concentration in mg/L. To obtain k_{cat} with units of s⁻¹, the maximal velocity (V_{max}) is divided by 3600.

$$k_{cat} = \frac{V_{max}}{[E]}$$
 (equation 3)

The percentage inhibition was plotted as a function of inhibitor concentration and fit using non-linear regression analysis of the sigmoidal dose–response curve

$$Y = \frac{100}{(1+10^{((logIC\ 50-X)\times Hill\ Slope\)})}$$
 (equation 4)

generated using the normalized data and a variable slope following equation 4.

Where Y = percent inhibition, X = the logarithmic concentration of the inhibitors, Hill Slope= slope factor or Hill coefficient. The IC_{50} value was determined by the concentration resulting in half-maximal percent activity. Values reported include the standard errors of the mean (S.E.M., calculated using the symmetrical CI function in Graphpad Prism 6) indicating the precision of the mean values obtained.

References

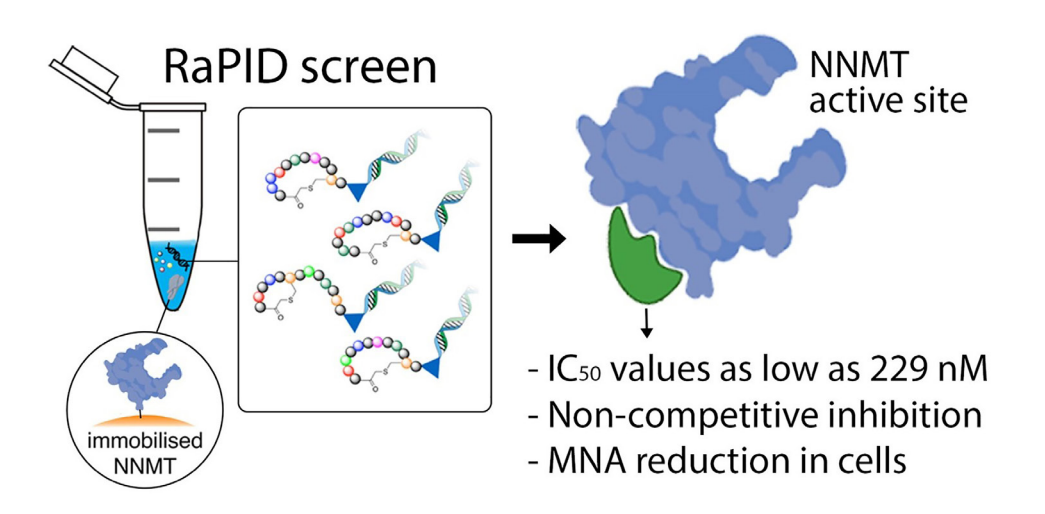
- 1. D. Cheng, J. Côté, S. Shaaban, M. T. Bedford. The Arginine Methyltransferase CARM1 Regulates the Coupling of Transcription and mRNA Processing. Mol. Cell 2007, 25, 71-83.
- 2. U.-M. Bauer, S. Daujat, S. J. Nielsen, K. Nightingale, T. Kouzarides. Methylation at arginine 17 of histone H3 is linked to gene activation. EMBO reports 2002, 3, 39-44.
- 3. A. Jambhekar, A. Dhall, Y. Shi. Roles and regulation of histone methylation in animal development. Nat. Rev. Mol. Cell Biol. 2019, 20, 625-641.
- 4. S. Wei, C. Li, Z. Yin, J. Wen, H. Meng, L. Xue, J. Wang. Histone methylation in DNA repair and clinical practice: new findings during the past 5-years. J. Cancer 2018, 9, 2072-2081.
- 5. M. T. Bedford, S. G. Clarke. Protein arginine methylation in mammals: who, what, and why. Mol. Cell 2009, 33, 1-13.
- S. C. Larsen, K. B. Sylvestersen, A. Mund, D. Lyon, M. Mullari, M.V. Madsen, J. A. Daniel, L. J. Jensen, M. L. Nielsen. Proteome-wide analysis of arginine monomethylation reveals widespread occurrence in human cells. Sci. Signal 2016, 9, rs9.
- 7. J. Fuhrmann, K. W. Clancy, P. R. Thompson. Chemical Biology of Protein Arginine Modifications in Epigenetic Regulation. Chem. Rev. 2015, 115, 5413-5461.
- 8. Y. R. Kim, B. K. Lee, R. Y. Park, N. T. X. Nguyen, J. A. Bae, D. D. Kwon, C. Jung. Differential CARM1 expression in prostate and colorectal cancers. BMC Cancer 2010, 10, 197.
- 9. R. Elakoum, G. Gauchotte, A. Oussalah, M. P. Wissler, C. Clément-Duchêne, J. M. Vignaud, J. L. Guéant, F. Namour. CARM1 and PRMT1 are dysregulated in lung cancer without hierarchical features. Biochimie. 2014, 97, 210-218.
- 10. J. Lin, H. Liu, T. Fukumoto, J. Zundell, Q. Yan, C. H. A. Tang, S. Wu, W. Zhou, D. Guo, S. Karakashev, C. C. A. Hu, K. Sarma, A. V. Kossenkov, R. Zhang. Targeting the IRE1 α /XBP1s pathway suppresses CARM1-expressing ovarian cancer. Nat. Commun. 2021, 12, 5321.
- 11. H. O. Habashy, E. A. Rakha, I. O. Ellis, D. G. Powe. The oestrogen receptor

- coactivator CARM1 has an oncogenic effect and is associated with poor prognosis in breast cancer. Breast Cancer Res. Treat. 2013, 140, 307-316.
- 12. J. Krijt, A. Dutá, V. Kožich. Determination of S-Adenosylmethionine and S-Adenosylhomocysteine by LC–MS/MS and evaluation of their stability in mice tissues. J. Chromatogr. B 2009, 877, 2061-2066.
- 13. K. Hsiao, H. Zegzouti, S. A. Goueli. Methyltransferase-Glo: a universal, bioluminescent and homogenous assay for monitoring all classes of methyltransferases. Epigenomics 2016, 8, 321-339.
- 14. G. Dong, A. Yasgar, D. L. Peterson, A. Zakharov, D. Talley, K. C. C. Cheng, A. Jadhav, A. Simeonov, R. Huang. Optimization of High-Throughput Methyltransferase Assays for the Discovery of Small Molecule Inhibitors. ACS Comb. Sci. 2020, 22, 422-432.
- 15. L. Wang, P. Charoensuksai, N. J. Wats0on, X. Wang, Z. Zhao, C. G. Coriano, L. R. Kerr, W. Xu. CARM1 automethylation is controlled at the level of alternative splicing. Nucleic Acids Res. 2013, 41, 6870-6880.
- 16. H. Hu, K. Qian, M. C. Ho, Y. G. Zheng. Small Molecule Inhibitors of Protein Arginine Methyltransferases. Expert Opin Investig Drugs 2016, 25, 335-358.
- 17. D. Cheng, N. Yadav, R. W. King, M. S. Swanson, E. J. Weinstein, M. T. Bedford. Small Molecule Regulators of Protein Arginine Methyltransferases*. J. Biol. Chem. 2004, 279, 23892-23899.
- 18. V. Lange, P. Picotti, B. Domon, R. Aebersold. Selected reaction monitoring for quantitative proteomics: a tutorial. Mol. Syst. Biol. 2008, 4, 222.
- 19. D. Chen, H. Ma, H. Hong, S. S. Koh, S. M. Huang, B. T. Schurter, D. W. Aswad, M. R. Stallcup. Regulation of transcription by a protein methyltransferase. Science 1999, 284, 2174-2177.
- 20. A. Di Lorenzo, M. T. Bedford. Histone arginine methylation. FEBS Lett. 2011, 585, 2024-2031.
- 21. S. L. Jacques, K. P. Aquino, J. Gureasko, P. A. Boriack-Sjodin, M. Porter Scott, R. A. Copeland, T. V. Riera. CARM1 Preferentially Methylates H3R17 over H3R26 through a Random Kinetic Mechanism. Biochemistry 2016, 55, 1635-1644.
- 22. A. E. Drew, O. Moradei, S. L. Jacques, N. Rioux, A. P. Boriack-Sjodin, C. Allain, M. P. Scott, L. Jin, A. Raimondi, J. L. Handler, H. M. Ott, R. G. Kruger, M. T. McCabe, C. Sneeringer, T. Riera, G. Shapiro, N. J. Waters, L. H. Mitchell, K. W. Duncan, M. P. Moyer, R. A. Copeland, J. Smith, R. Chesworth, S. A. Ribich. Identification of a CARM1 Inhibitor with Potent In Vitro and In Vivo Activity in Preclinical Models of Multiple Myeloma. Sci. Rep. 2017, 7, 17993.
- 23.G. Blobel. A protein of molecular weight 78,000 bound to the polyadenylate region of eukaryotic messenger RNAs. Proc Natl Acad Sci U S A 1973, 70, 924-928.
- 24. J. Lee, M. T. Bedford. PABP1 identified as an arginine methyltransferase substrate using high-density protein arrays. EMBO Rep 2002, 3, 268-273.

- 25. Martin, N. I., and Liskamp, R. M. J. Preparation of NG-Substituted I-Arginine Analogues Suitable for Solid Phase Peptide Synthesis. J. Org. Chem. 2008, 73, 7849-7851.
- 26. M. J. van Haren, N. Marechal, N. Troffer-Charlier, A. Cianciulli, G. Sbardella, J. Cavarelli, N. I. Martin. Transition state mimics are valuable mechanistic probes for structural studies with the arginine methyltransferase CARM1. Proc Natl Acad Sci U S A 2017, 114, 3625.
- 27. R. Wang, Y. Wang, T. C. Edrington, Z. Liu, T. C. Lee, A. Silvanovich, H. S. Moon, Z. L. Liu, B. Li. Presence of small resistant peptides from new in vitro digestion assays detected by liquid chromatography tandem mass spectrometry: An implication of allergenicity prediction of novel proteins? PloS one 2020, 15, e0233745-e0233745.
- 28. Y. Zhang, N. Marechal, M. J. van Haren, N. Troffer-Charlier, V. Cura, J. Cavarelli, N. I. Martin. Structural Studies Provide New Insights into the Role of Lysine Acetylation on Substrate Recognition by CARM1 and Inform the Design of Potent Peptidomimetic Inhibitors. ChemBioChem 2021, 22, 3469-3476.
- 29. Y. Shen, M. M. Szewczyk, M. S. Eram, D. Smil, H. Kaniskan, R. F. de Freitas, G. Senisterra, F. Li, M. Schapira, P. J. Brown, C. H. Arrowsmith, D. Barsyte-Lovejoy, J. Liu, M. Vedadi, J. Jin. Discovery of a Potent, Selective, and Cell-Active Dual Inhibitor of Protein Arginine Methyltransferase 4 and Protein Arginine Methyltransferase 6. J. Med. Chem. 2016, 59, 9124-9139.
- 30. M. S. Eram, Y. Shen, M. Szewczyk, H. Wu, G. Senisterra, F. Li, K. V. Butler, H. Kaniskan, B. A. Speed, C. Dela Seña, A. Dong, H. Zeng, M. Schapira, P. J. Brown, C. H. Arrowsmith, D. Barsyte-Lovejoy, J. Liu, M. Vedadi, J. Jin. A Potent, Selective, and Cell-Active Inhibitor of Human Type I Protein Arginine Methyltransferases. ACS Chem Biol 2016, 11, 772-781.
- 31. K. Nakayama, M. M. Szewczyk, C. Dela Sena, H. Wu, A. Dong, H. Zeng, F. Li, R. F. de Freitas, M. S. Eram, M. Schapira, Y. Baba, M. Kunitomo, D. R. Cary, M. Tawada, M., A. Ohashi, Y. Imaeda, K. S. Saikatendu, C. E. Grimshaw, M. Vedadi, C. H. Arrowsmith, D. Barsyte-Lovejoy, A. Kiba, D. Tomita, P. J. Brown. TP-064, a potent and selective small molecule inhibitor of PRMT4 for multiple myeloma. Oncotarget 2018, 9, 18480-18493.
- 32. V. A. Shatrov, M. Ameyar, Z. Cai, A. Bettaieb, S. Chouaib. Methyltransferase inhibitor S-adenosyl-L-homocysteine sensitizes human breast carcinoma MCF7 cells and related TNF-resistant derivatives to TNF-mediated cytotoxicity via the ceramide-independent pathway. Eur Cytokine Netw 1999, 10, 247-252.
- 33. W. W. Yue, M. Hassler, S. M. Roe, V. Thompson-Vale, L. H. Pearl. Insights into histone code syntax from structural and biochemical studies of CARM1 methyltransferase. EMBO J. 2007, 26, 4402-4412.

Chapter 5

Macrocyclic Peptides as Allosteric Inhibitors of Nicotinamide N-Methyltransferase



Published in

RCS Chemical Biology (2021)

DOI.org/10.1039/D1CB00134E

Abstract

Nicotinamide N-methyltransferase (NNMT) methylates nicotinamide to form 1-methylnicotinamide (MNA) using S-adenosyl-L-methionine (SAM) as the methyl donor. The complexity of the role of NNMT in healthy and disease states is slowly being elucidated and provides an indication that NNMT may be an interesting therapeutic target for a variety of diseases including cancer, diabetes, and obesity. Most inhibitors of NNMT described to date are structurally related to one or both of its substrates. In the search for structurally diverse NNMT inhibitors, an mRNA display screening technique was used to identify macrocyclic peptides which bind to NNMT. Several of the cyclic peptides identified in this manner show potent inhibition of NNMT with IC_{50} values as low as 229 nM. The peptides were also found to downregulate MNA production in cellular assays. Interestingly, substrate competition experiments reveal that these cyclic peptide inhibitors are noncompetitive with either SAM or NA indicating they may be the first allosteric inhibitors reported for NNMT.

Introduction

Nicotinamide N-methyltransferase (NNMT) is a cytosolic enzyme that catalyzes the methylation of nicotinamide (NA, vitamin B3) and a variety of other pyridines in the presence of S-adenosyl-L-methionine (SAM) to form 1-methyl nicotinamide (MNA) or the corresponding methylpyridinium ion.^{1,2} Recently, a number of reports have demonstrated that the role of NNMT is not limited to its involvement in xenobiotic metabolism, but rather reveal NNMT to be a master metabolic regulator in a variety of cancers.³⁻⁵ Additionally, NNMT overexpression is found to be a biomarker in an increasing number of cancers and is often linked to poor prognosis. 6-10 Aside from its roles in cancer, NNMT is implicated in Parkinson's Disease (PD), 11,12 vasoprotection, 13,14 pulmonary arterial hypertension (PAH), 15 diabetes 16 and obesity.^{17,18} Interestingly, these involvements can be either protecting, as in PD, PAH, and endothelial function, or damaging as in cancer, diabetes, and obesity. To more fully understand the roles played by NNMT in healthy and disease states, specific NNMT inhibitors are needed. However, despite the increasing interest in NNMT, a limited number of NNMT inhibitors have been described to date and none have entered clinical trials. 19-24

Previous work in both our group and that of others has focused primarily on the design and optimization of bisubstrate inhibitors of NNMT that incorporate structural elements of both the NA and SAM substrates. In this report, we describe the use of an entirely different strategy for the development of NNMT inhibitors. Specifically, we applied a peptide-mRNA display technology known as the random nonstandard peptide integrated discovery (RaPID) system to screen a library of more than 10^{12} macrocyclic peptides binding to NNMT. This mRNA display selection technique has demonstrated promising results against a variety of protein targets and, together with similar screening methods, has led to the identification of numerous peptide macrocycles currently in clinical trials.^{25–27} In the present study, hits from this RaPID screen against NNMT were identified, synthesized by Fmoc solid phase peptide synthesis (SPPS), and tested for inhibition using a convenient LC-MS-based NNMT activity assay previously developed in our group.² Potent NNMT inhibition was found for a number of the macrocyclic peptides identified. Interestingly, this inhibition was found not to be impacted by elevated concentrations of either NA or SAM substrates suggesting that these peptides function as allosteric inhibitors, the first to be reported for NNMT. In cellular assays, the cyclic peptides showed a reduction in the concentration of MNA indicating a target-specific effect.

Results and discussion

To identify macrocyclic peptide binders for NNMT, two parallel selections

employing the RaPID system for reprogrammed mRNA display^{28,29} were performed using purified, N-terminal His-tagged NNMT as the target (Figure. 1). The two selections differed only in the stereochemistry of the initiating amino acid, L-tyrosine or D-tyrosine, as a way of increasing the conformational space of the library. Both initiating tyrosine amino acids also carried an N-terminal chloroacetyl moiety to give spontaneous macrocyclisation³⁰ with a cysteine hard-coded after a stretch of 15 random amino acids. This head-to-sidechain thioether cyclized library showed exponential enrichment of target-binding sequences over the course of 6 rounds. Hits were identified by high-throughput sequencing of the output DNA from each round (see Figure. S1 in the Appendix IV). Within these hits, no clear consensus sequences were visible but it was clear that hydrophobic and positively charged amino acids were overall enriched (see Figure. S2 in the Appendix IV). Based on the results of the two selections performed, 17 unique peptides were selected for chemical synthesis and assessment as NNMT inhibitors (Table 1).

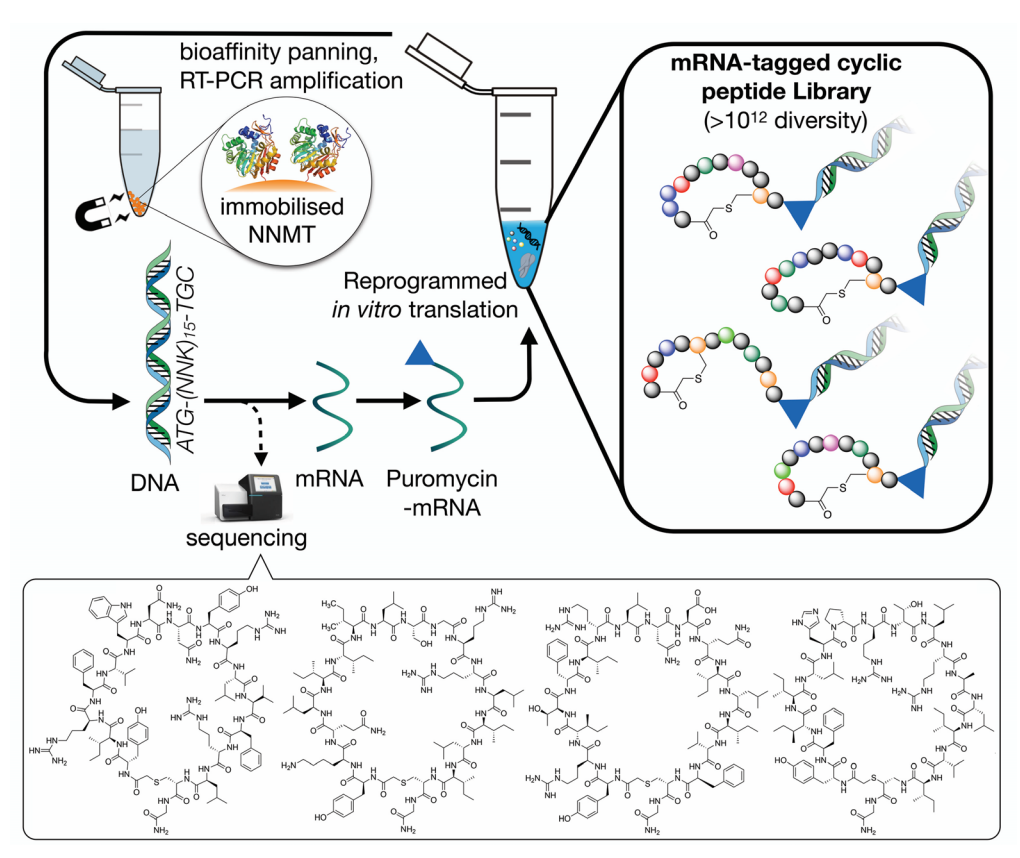


Figure 1. Schematic overview of the RaPID mRNA display system used to translate a random DNA library (>10¹² library members, 17 residues), affording a large peptide library whose members were selected for binding affinity against NNMT. Selections initiated with either N-chloroacetyl-L-tyrosine or N-chloroacetyl-D-tyrosine were performed to introduce additional structural diversity in the library.

Using standard Fmoc-SPPS, the peptides were synthesized on rink amide resin as depicted in Scheme 1. The N-terminus of the linear peptide was subsequently treated with chloroacetyl chloride on the resin. After acidic cleavage and

deprotection of the amino acid side chains, the peptides were cyclized in the presence of base and the macrocyclic peptides then purified using preparative HPLC. Notably, among the 17 peptides synthesized (Table 1) peptides 9 and 10 actually derive from the same sequence containing an additional Cys residue in the variable region of the sequence. For this reason, in peptides 9 and 10, one of the two Cys residues was replaced by Ala to allow for the controlled synthesis of a single macrocyclic species.

The cyclic peptides were subsequently tested for their inhibitory activity against NNMT using an LC-MS based method. The results given in Table 1 show that all 17 peptides identified and selected from the RaPID screenings demonstrate the capacity to inhibit NNMT. For 5 out of the 17 macrocyclic peptides potent inhibition (defined as an IC50 value below 1 μ M) was observed (see the Appendix IV, for full IC50 curves). Notably, no correlation could be found between the degree of enrichment in the RaPID selection and inhibitory activity. On the contrary, the most abundant peptides from the screen (peptides 1, 9 and 10) were found to be only moderate NNMT inhibitors with IC50 values around 5 μ M. These findings suggested that the macrocyclic peptides may be interacting with NNMT at a site(s) not directly involved in the methylating activity of the enzyme.

Scheme 1. General synthesis route for the preparation of cyclic peptides identified from the mRNA display screen. The example presented contains 6 amino acids, whereas the identified peptides all contain 18 amino acids.

Table 1. Sequences, abundance and IC_{50} values for selected macrocyclic peptides initiated with I-tyrosine (Y) or d-tyrosine (DY). The residues in bold and the blue lines highlight the location of the thioether linkage.

Peptide	Sequence	Abundance ^a	IC ₅₀ (μM) ^b
1	Y ARRIILVFRDRLVVI C G	9.5 %	4.964 ± 0.509
2	Y RIVVIHKKLYLLRIG C G	1.4 %	1.584 ± 0.111
3	YIYFILEPGYYARVNV C G	1.1 %	1.115 ± 0.066
4	Y FIILHPRTLRALIVI C G	1.1 %	0.772 ± 0.054
5	YFAIITKNSRWKIIWLCG 0.7 %		1.125 ± 0.076
6	YIRFVWNNYRLYVFRLCG 0.6 %		0.674 ± 0.042
7	Y VYVFSFGGKLYLVRK C G	0.6 %	5.344 ± 0.432
8	Y TIYLIQKRYLFAVHS C G	0.5 %	2.238 ± 0.211
9	^D Y PK C FGIKFRDRFLLLAG	6.6%	4.426 ± 0.428
10	^D Y PKAFGIKFRDRFLLL C G	0.0%	6.241 ± 0.889
11	^D Y TIYVFRFFNKLVLIN C G	5.7 %	1.131 ± 0.080
12	^D Y TIAFILNGRYLAIVR C G	5.4 %	1.209 ± 0.113
13	^D Y KQLIIILSGRRLILI C G	2.6 %	0.241 ± 0.012
14	^D Y RYLFIIAGKKYAIVR C G	1.2 %	7.058 ± 0.530
15	^D Y RITFIRLNDQILIVF C G	1.1 %	0.437 ± 0.023
16	^D Y FVFARFGNHIVIIKA C G	1.1 %	1.238 ± 0.100
17	^D Y SVSIVIRGRYIGIIR C G	0.9 %	0.229 ± 0.007

^aPercentage of total sequences after the sixth round of enrichment. Peptides 1-8 originate from the selection initiated with I-tyrosine or and peptides 9-17 originate from the selection initiated with d-tyrosine. ^bHalf-maximal inhibitory concentration of the compounds tested against human wild-type NNMT (full assay details provided in the supporting information). Values reported in μM are based on triplicate data of at least 10 different concentrations.

To further investigate the mode of inhibition, macrocyclic peptide inhibitors with IC_{50} values below 2 μM were subsequently tested for competition with the substrate binding site(s). In this experiment, the concentration of either NA or SAM was increased 10-fold and the impact on the IC₅₀ value of the macrocyclic peptide inhibitor determined. As can be seen in Figure. 2, none of the cyclic peptides saw a significant change in IC₅₀ in the presence of elevated concentrations of either of the substrates. In comparison and as a control, two known bisubstrate inhibitors, compounds X^{21} and Y, 20 previously reported to bind in the NNMT active site, were also included in the assay. In line with expectation, these bisubstrate NNMT inhibitors did show a marked increase in their IC₅₀ values under higher concentrations of both substrates with a more pronounced competitive effect seen at increased SAM concentrations. These findings suggest that whereas the bisubstrate inhibitors bind in the NNMT active site, the cyclic peptides instead engage with NNMT at an allosteric binding site(s) and as such are not competitive with the NA and SAM substrates. To further assess the non-competitive mechanism of inhibition, the K_M of SAM and V_{max} of NNMT were determined in the presence of cyclic peptides 4 and 13 and bisubstrate inhibitor Y. The results of these investigations support the non-competitive mechanism of inhibition for cyclic peptides 4 and 13. Increasing concentrations of 4 or 13 had no significant effect on the K_M value of SAM but did lead to a decrease in the V_{max} of the enzyme. In contrast, the substrate competitive nature of compound Y was confirmed by the increased K_M values observed with increasing inhibitor concentration but with no significant effect on V_{max} (see Figure. S11 in the Appendix IV).

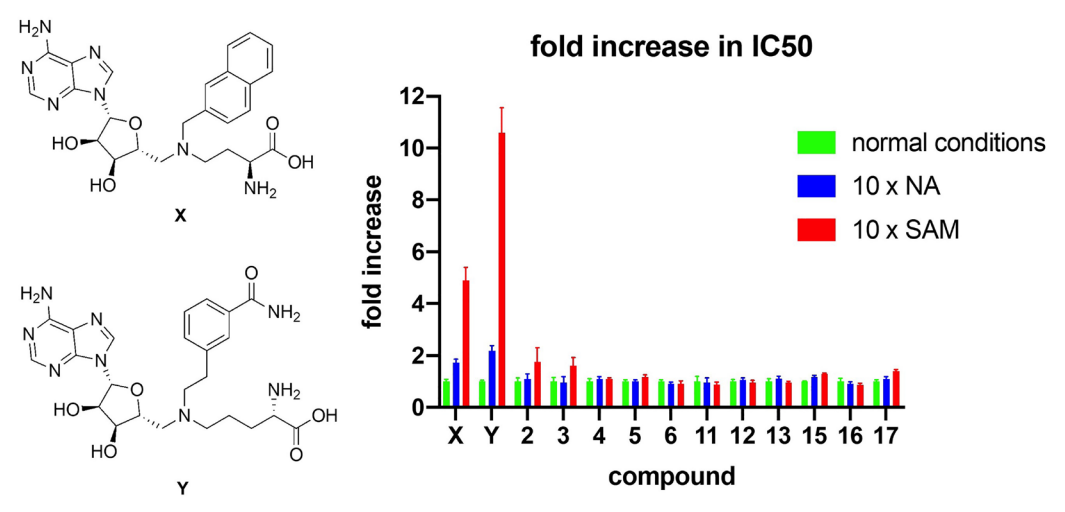


Figure 2. Results of the substrate competition experiment. The data is normalized per compound by setting the IC_{50} under normal assay conditions at 1. Data is based on duplicate data of at least 7 different concentrations. Structures of control compounds X and Y are presented on the left.

Finally, the cyclic peptides were evaluated for their effect on MNA production

in human aortic endothelial cells (HAEC) as well as in A549 lung carcinoma cells. Cyclic peptides 4 and 13 were selected as representative compounds with sequences initiating with either an L-tyrosine or a D-tyrosine residue, respectively. The recently published small molecule nicotinamide analogue 6-methylaminonicotinamide (6-MANA), with a reported IC₅₀ value of 588 \pm 75 nM, was included as a reference compound. The compounds were incubated in the presence of 100 μ M nicotinamide and 10 μ M SAM for 1 h in A549 cells and 3 hours in HAEC cells. As illustrated in Figure. 3, the cyclic peptides produce a dose-dependent reduction of the concentration of MNA in both healthy cells and cancer cells. The observed effect is similar to that found for the small molecule reference inhibitor 6-MANA.

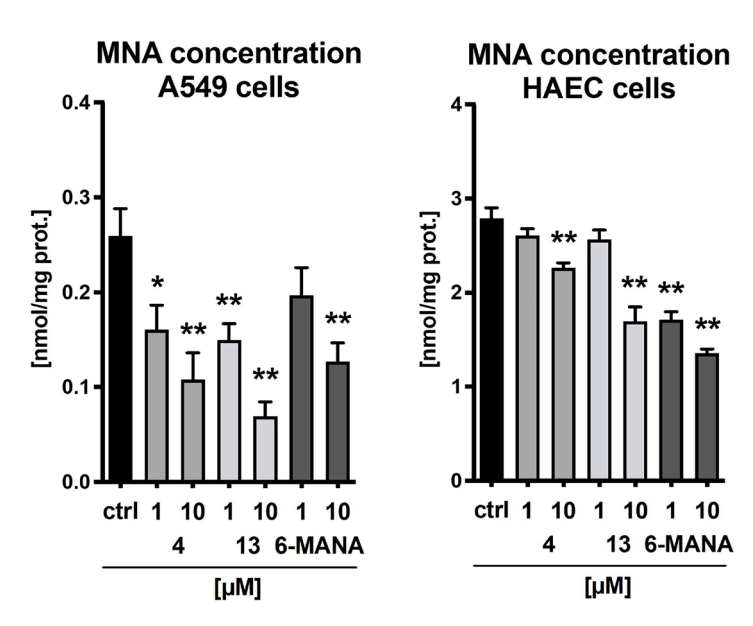


Figure 3. Cellular activity of cyclic peptides 4 and 13 and small molecule reference compound 6-methylamino-nicotinamide (6-MANA) against A549 lung carcinoma cells (left) and human aortic endothelial cells (HAEC, right). Data is based on six replicates. The results indicate a significant reduction of MNA concentration compared to untreated cells.

Conclusions

Using the RaPID mRNA display methodology, a set of macrocyclic peptides were identified with affinity for NNMT. While the hits identified from the RaPID selections did not reveal a clear consensus sequence, all peptides displayed a higher abundance of hydrophobic and positively charged amino acids. To investigate whether binding to NNMT resulted in the inhibition of its methylation activity, the most highly enriched cyclic peptides from both L-tyrosine and D-tyrosine initiating libraries were synthesized using Fmoc-SPPS and subsequently evaluated for their inhibitory activity against NNMT. From the screening hits, five macrocyclic peptides showed potent inhibition with IC₅₀ values between 200 and 800 nM. Of note, while preparing our manuscript a publication appeared in the literature describing a similar strategy for generating peptidomimetic NNMT inhibitors.³² Interestingly, the

most active peptides identified in that study share very little structural similarity to those identified in our investigations aside from the presence of a number of hydrophobic and positively charged residues. In addition, they appear to inhibit NNMT by binding to the enzyme active site as supported by structural studies. In contrast, none of the macrocyclic peptides identified in our study exhibit significant competition with the NNMT, SAM or nicotinamide substrates, indicating that they may instead bind at an allosteric site on the enzyme. This is the first description of allosteric inhibitors of NNMT. Furthermore, in cell-based assays, administration of our macrocyclic peptides was found to result in a significant reduction in the production of MNA by endothelial HAEC cells and A549 lung carcinoma cells. To further elucidate the mode of binding and potential for further optimization of these macrocyclic peptide-based NNMT inhibitors, structural studies are currently being pursued, the results of which will be reported in due course.

Experimental Procedures

All reagents were purchased from Sigma Aldrich or Combi-blocks and used as received. HPLC-grade acetonitrile, peptide grade N,N-dimethylformamide (DMF) and dichloromethane (DCM) for peptide synthesis were purchased from Biosolve Chimie SARL and VWR, respectively. The ultrapure water was obtained from a Veolia Purelab flex3 water purification system. Standard Fmoc-protected amino acids and rink amide resin were purchased from P3 Biosystems.

Liquid Chromatography-Mass Spectrometry (LC-MS) was performed on a Shimadzu LC-20AD system with a Shimadzu Shim-Pack GIST-AQ C18 column (3.0 x 150 mm, 3 mm) at 30 °C. This system was connected to a Shimadzu 8040 triple quadrupole mass spectrometer (ESI ionization). Peptides were eluted with a water–acetonitrile gradient moving from 5% to 100% acetonitrile (0.1% FA) over 12 minutes at a flow rate of 0.5 mL min-1 with UV detection (214 nm and 254 nm) and MS detection.

Preparative reversed-phase high performance liquid chromatography (HPLC) was performed using a BESTA-Technik system with a ECOMFlash UV detector monitoring at 214 nm and 254 nm. Preparative reversed-phase HPLC was performed using a Dr Maisch Reprosil Gold 120 C18 Prep Column (25 x 250 mm, 10 mm) using a mobile phase of water—acetonitrile gradientmoving from Buffer A (5% acetonitrile, 95% water and 0.1% TFA) to 100% Buffer B (95% acetonitrile, 5% water and 0.1% TFA) over 60 minutes at a flow-rate of 12.0mLmin-1 with UV detection at 214 nm and 254 nm.

HRMS analyses were performed on a Thermo Scientific Dionex UltiMate 3000 HPLC system with a Phenomenex Kinetex C18 column (150 mm, 2.6 mm) at 35°C and

equipped with a diode array detector. The following solvent system, at a flow rate of 0.3 mL min⁻¹, was used: solvent A, 0.1% formic acid in water; solvent B, 0.1% formic acid in acetonitrile. Gradient elution was as follows: 95 : 5 (A/B) for 1 min, 95 : 5 to 5 : 95 (A/B) over 9 min, 5 : 95 to 2 : 98 (A/B) over 1 min, 2 : 98 (A/B) for 1 min, then reversion back to 95 : 5 (A/B) over 2 min, 95 : 5 (A/B) for 1 min. This system was connected to a Bruker micrOTOF-Q II mass spectrometer (ESI ionization) calibrated internally with sodium formate.

Reprogrammed mRNA display protocol. Acylation of N-chloroacetyl tyrosine (both L- and D-stereochemistry in separate reactions) onto tRNA^{fMet}_{CAU} was carried out using amino acids synthetically activated as cyanomethyl esters and in vitro transcribed tRNA and catalyst 'enhanced flexizyme' as previously reported^{33,34}, incubating for 2 hours on ice before purifying by ethanol precipitation and storing the dry pellet at -20 °C.

Two parallel selections were carried out using His tag-immobilised NNMT based on a previously published method,³⁵ one with D- and one with L-tyrosine initiation. Briefly, DNA encoding 15 randomised NNK codons followed by a section encoding a CGSGSGS linker was assembled by PCR, and subsequently transcribed in vitro using T7 RNA polymerase (NEB) at 1 mL scale with 25 pmol input DNA (starting diversity ~1.5x10¹³) at 37 °C overnight. This was purified by PAGE, and the resulting library was ligated by T4 RNA ligase at room temperature for 30 min to a short oligonucleotide terminating in puromycin before purifying by ethanol precipitation with 0.25 mg mL⁻¹ RNAse-free glycogen. Translation of 10 pmol of this puromycinmRNA library in vitro using the PURExpress system (combining solution A from Δ (aa/tRNA) and solution B from Δ RF123 kits; NEB) in a 5 μL reaction at 37 °C for 30 min, with methionine omitted and with added initiating acyl-tRNA to 25 µM, gave a cyclic peptide library with covalent mRNA tag. Following translation, the reaction mix was allowed to stand at room temperature for 12 minutes, and then EDTA was added to 16.6 mM and the reaction mix was again incubated at 37 °C for 30 min. This was then reverse-transcribed by Protoscript II reverse transcriptase (NEB) at 42 °C for 1 hour, TBS-T and BSA added from concentrated stocks to 1X and 0.1% final concentrations (respectively), and a 0.5 µL sample diluted to 500 µL. Any background peptides and proteins that bind directly to Dynabeads His-tag isolation and pulldown resin (invitrogen) were removed by three sequential incubations with free resin (5, 2.5, and 2.5 µL) for 10 min at 4 °C. The supernatant following this last pre-clear step was added to immobilised NNMT saturating 0.4 µL of the same His-tag isolation and pulldown resin and incubated for 30 min at 4 °C with constant inversion. Nonspecifically-bound members of the library were removed by stringent washing on ice (3 X 20 µL TBS-T), and any surviving peptides were eluted by incubation in 50 µL RNAse free water at 95 °C for 5 min and then transferring the supernatant to a new tube while hot. The first aliquot of pre-clear beads was washed and eluted in the same way as the selection containing NNMT. All samples (1 µL each of input, positive, negative) were analyzed by qPCR alongside a standard curve produced by reverse transcription of the input library, and recovery was calculated as the percentage of the input found in the positive or negative selection rounds after accounting for dilution factors. The remainder of the eluted specific binders were amplified by PCR to provide a new DNA template that served as the input for the subsequent round (round 1 carried out at double scale to increase initial diversity), and selection was continued until recovery indicated enrichment above the background negative selections (Figure S1 in the Appendix IV).

The DNA output was used for sequencing of all rounds on the Illumina MiSeq platform using a 2 X 150 bp V2 reagent kit at the Utrecht UMC sequencing facility (USEQ). The resulting sequencing output files were analyzed by Python script that searches for exact matches to the T7 promoter and puromycin ligation sequences, translates the coding sequence between these, and tallies at the peptide level the abundance of each unique hit.³⁶

Fmoc-solid-phase Peptide Synthesis (SPPS)

General procedure A; Microwave-assisted Peptide Synthesizer (CEM HT12 Liberty Blue peptide Synthesizer): The Rink Amide AM resin (100 µmol) was swollen in 10 mL of a 1:1 mixture of DMF/DCM for 5 min, drained, and then treated with 20 vol.% piperidine (10 mL) in DMF for 65 seconds at 90°C, drained and washed with DMF (3 x 5 mL). The resin was then treated with a solution of Fmoc-Xaa-OH (0.2 mol/L, 2.5 mL, 5 eq), DIC (1 mol/L, 1 mL, 10 eq) and Oxyma (1 mol/L, 0.5 mL, 5 eq) in DMF (4 mL) at 76°C for 15 s before the temperature was increased to 90°C for an additional 110 s before being drained. The resin was then treated again with the same amount of Fmoc-Xaa-OH, DIC and Oxyma in DMF (4 mL) at 76°C for 15 s before the temperature was increased to 90°C for an additional 110 s before being drained.

General procedure B; Manual coupling (N-terminal chloroacetyl group capping): The resin (25 μ mol) was washed with DMF (3 x 5 mL), treated with chloroacetyl chloride (50 μ mol, 4 μ L, 2 eq) and DIPEA (100 μ mol, 18 μ L, 4 eq) shaking for 1 h at room temperature. The resin was then washed with DMF (3 x 5 mL) and DCM (3 x 5 mL), respectively. The resin was dried with a nitrogen flow and used in the next step without further purification.

General procedure C; Manual cleavage: The peptide was cleaved from the resin using a mixture of TFA/water/TIPS/EDT (92.5:2.5:2.5:2.5) under shaking for 2 hours at room temperature. The resin was filtered over cotton and washed with TFA (2 x 0.5 mL). The crude peptide was precipitated in a mixture of MTBE/Hexane (1:1). The peptide was pelleted by centrifugation (5 min at 4500 rpm), the pellet was washed

twice with MTBE/Hexane (1:1) (50 mL), centrifiuged (5 min at 4500 rpm) and dried under a nitrogen flow.

General procedure D; Manual cyclization: The crude peptide was dissolved in 2 mL DMSO with 10 μ L DIPEA and stirred for 16 hours at room temperature to facilitate cyclization. The reaction was quenched with 10 μ L TFA and the crude mixture was purified by preparative HPLC to afford the pure peptide as a white solid.

Peptide 1: Rink Amide AM resin (146 mg, 100 μ mol, 0.684 mmol g⁻¹) was used for Fmoc solid phase peptide synthesis (Fmoc SPPS) according to general procedure A. After checking the crude peptide by LC-MS, a portion (25 μ mol) of the peptide was capped with chloroacetyl chloride following general procedure B. The peptide was deprotected and cleaved from the resin according to general procedure C. Subsequently, the peptide was cyclized following general procedure D and purified by preparative HPLC (0-100%, buffer B) affording cyclic peptide 1 as a white solid (1.6 mg, 2.9%). HRMS (m/z): $[M+2H]^{2+}$ calculated for $C_{103}H_{173}N_{29}O_{21}S^{2+}$, 1101.1468, found 1101.1462. LC-MS R_t 6.07 min (0 to 100 % B over 12 min, 0.1% FA, λ = 214 nm).

Peptide 2: Rink Amide AM resin (146 mg, 100 μ mol, 0.684 mmol g⁻¹) was used for Fmoc solid phase peptide synthesis (Fmoc SPPS) according to general procedure A. After checking the crude peptide by LC-MS, a portion (25 μ mol) of the peptide was capped with chloroacetyl chloride following general procedure B. The peptide was deprotected and cleaved from the resin according to general procedure C. Subsequently, the peptide was cyclized following general procedure D and purified by preparative HPLC (0-100%, buffer B) affording cyclic peptide 2 as a white solid (3.5 mg, 6.5%). HRMS (m/z): $[M+2H]^{2+}$ calculated for $C_{101}H_{171}N_{31}O_{22}S^{2+}$,1092.1541, found 1092,1534. LC-MS Rt 5.57 min (0 to 100 % B over 12 min, 0.1% FA, λ = 214 nm).

Peptide 3: Rink Amide AM resin (146 mg, 100 μ mol, 0.684 mmol g⁻¹) was used for Fmoc solid phase peptide synthesis (Fmoc SPPS) according to general procedure A. After checking the crude peptide by LC-MS, a portion (25 μ mol) of the peptide was capped with chloroacetyl chloride following general procedure B. The peptide was deprotected and cleaved from the resin according to general procedure C. Subsequently, the peptide was cyclized following general procedure D and purified by preparative HPLC (0-100%, buffer B) affording cyclic peptide 3 as a white solid (4.2 mg, 7.8%). HRMS (m/z): $[M+2H]^{2+}$ calculated for $C_{105}H_{149}N_{23}O_{26}S^{2+}$, 1090.0382, found 1090.0371. LC-MS R, 7.01 min (0 to 100 % B over 12 min, 0.1% FA, λ = 214 nm).

Peptide 4: Rink Amide AM resin (146 mg, 100 μ mol, 0.684 mmol g⁻¹) was used for Fmoc solid phase peptide synthesis (Fmoc SPPS) according to general procedure A. After checking the crude peptide by LC-MS, a portion (25 μ mol) of the peptide was capped with chloroacetyl chloride following general procedure B. The peptide

was deprotected and cleaved from the resin according to general procedure C. Subsequently, the peptide was cyclized following general procedure D and purified by preparative HPLC (0-100%, buffer B) affording cyclic peptide 4 as a white solid (3.6 mg, 6.7%). HRMS (m/z): $[M+2H]^{2+}$ calculated for $C_{107}H_{167}N_{27}O_{21}S^{2+}$, 1069.1275, found 1069.1274. LC-MS R_t 7.01 min (0 to 100 % B over 12 min, 0.1% FA, λ = 214 nm).

Peptide 5: Rink Amide AM resin (146 mg, 100 μ mol, 0.684 mmol g⁻¹) was used for Fmoc solid phase peptide synthesis (Fmoc SPPS) according to general procedure A. After checking the crude peptide by LC-MS, a portion (25 μ mol) of the peptide was capped with chloroacetyl chloride following general procedure B. The peptide was deprotected and cleaved from the resin according to general procedure C. Subsequently, the peptide was cyclized following general procedure D and purified by preparative HPLC (0-100%, buffer B) affording cyclic peptide 5 as a white solid (5.1 mg, 9.1%). HRMS (m/z): $[M+2H]^{2+}$ calculated for $C_{109}H_{165}N_{27}O_{23}S^{2+}$,1126.1146, found 1126.1140. LC-MS R_t 6.54 min (0 to 100 % B over 12 min, 0.1% FA, λ = 214 nm).

Peptide 6: Rink Amide AM resin (146 mg, 100 μ mol, 0.684 mmol g⁻¹) was used for Fmoc solid phase peptide synthesis (Fmoc SPPS) according to general procedure A. After checking the crude peptide by LC-MS, a portion (25 μ mol) of the peptide was capped with chloroacetyl chloride following general procedure B. The peptide was deprotected and cleaved from the resin according to general procedure C. Subsequently, the peptide was cyclized following general procedure D and purified by preparative HPLC (0-100%, buffer B) affording cyclic peptide 6 as a white solid (4.7 mg, 7.8%). HRMS (m/z): $[M+2H]^{2+}$ calculated for $C_{117}H_{167}N_{31}O_{24}S^{2+}$,1211.1260, found 1211.1253. LC-MS R_t 6.35 min (0 to 100 % B over 12 min, 0.1% FA, λ = 214 nm).

Peptide 7: Rink Amide AM resin (146 mg, 100 µmol, 0.684 mmol g⁻¹) was used for Fmoc solid phase peptide synthesis (Fmoc SPPS) according to general procedure A. After checking the crude peptide by LC-MS, a portion (25 µmol) of the peptide was capped with chloroacetyl chloride following general procedure B. The peptide was deprotected and cleaved from the resin according to general procedure C. Subsequently, the peptide was cyclized following general procedure D and purified by preparative HPLC (0-100%, buffer B) affording cyclic peptide 7 as a white solid (6.5 mg, 12.2%). HRMS (m/z): $[M+2H]^{2+}$ calculated for $C_{104}H_{154}N_{24}O_{23}S^{2+}$, 1069.5670, found 1069.5665. LC-MS R_t 5,90 min (0 to 100 % B over 12 min, 0.1% FA, λ = 214 nm).

Peptide 8: Rink Amide AM resin (146 mg, 100 μ mol, 0.684 mmol g⁻¹) was used for Fmoc solid phase peptide synthesis (Fmoc SPPS) according to general procedure A. After checking the crude peptide by LC-MS, a portion (25 μ mol) of the peptide was capped with chloroacetyl chloride following general procedure B. The peptide was deprotected and cleaved from the resin according to general procedure C.

Subsequently, the peptide was cyclized following general procedure D and purified by preparative HPLC (0-100%, buffer B) affording cyclic peptide 8 as a white solid (5.7 mg, 10.4%). HRMS (m/z): $[M+2H]^{2+}$ calculated for $C_{105}H_{158}N_{26}O_{25}S^{2+}$, 1107.5806, found 1107.5807. LC-MS R_t 5,91 min (0 to 100 % B over 12 min, 0.1% FA, λ = 214 nm).

Peptide 9: Rink Amide AM resin (146 mg, 100 μ mol, 0.684 mmol g⁻¹) was used for Fmoc solid phase peptide synthesis (Fmoc SPPS) according to general procedure A. After checking the crude peptide by LC-MS, a portion (25 μ mol) of the peptide was capped with chloroacetyl chloride following general procedure B. The peptide was deprotected and cleaved from the resin according to general procedure C. Subsequently, the peptide was cyclized following general procedure D and purified by preparative HPLC (0-100%, buffer B) affording cyclic peptide 9 as a white solid (4.9 mg, 9.1%). HRMS (m/z): [M+2H]²⁺ calculated for C₁₀₅H₁₆₁N₂₇O₂₂S²⁺, 1092.1015, found 1092.1008. LC-MS R_t 6.07 min (0 to 100 % B over 12 min, 0.1% FA, λ = 214 nm).

Peptide 10: Rink Amide AM resin (146 mg, 100 μ mol, 0.684 mmol g⁻¹) was used for Fmoc solid phase peptide synthesis (Fmoc SPPS) according to general procedure A. After checking the crude peptide by LC-MS, a portion (25 μ mol) of the peptide was capped with chloroacetyl chloride following general procedure B. The peptide was deprotected and cleaved from the resin according to general procedure C. Subsequently, the peptide was cyclized following general procedure D and purified by preparative HPLC (0-100%, buffer B) affording cyclic peptide 10 as a white solid (5.4 mg, 10.2%). HRMS (m/z): [M+2H]²⁺ calculated for $C_{105}H_{161}N_{27}O_{22}S^{2+}$, 1092.1015, found 1092.1006. LC-MS R_t 6.18 min (0 to 100 % B over 12 min, 0.1% FA, λ = 214 nm).

Peptide 11: Rink Amide AM resin (146 mg, 100 μ mol, 0.684 mmol g⁻¹) was used for Fmoc solid phase peptide synthesis (Fmoc SPPS) according to general procedure A. After checking the crude peptide by LC-MS, a portion (25 μ mol) of the peptide was capped with chloroacetyl chloride following general procedure B. The peptide was deprotected and cleaved from the resin according to general procedure C. Subsequently, the peptide was cyclized following general procedure D and purified by preparative HPLC (0-100%, buffer B) affording cyclic peptide 11 as a white solid (6.1 mg, 10.8%). HRMS (m/z): [M+2H]²⁺ calculated for C₁₁₀H₁₆₃N₂₅O₂₄S²⁺, 1125,1012, found 1125.1005. LC-MS Rt 6.67 min (0 to 100 % B over 12 min, 0.1% FA, λ = 214 nm).

Peptide 12: Rink Amide AM resin (146 mg, 100 μ mol, 0.684 mmol g⁻¹) was used for Fmoc solid phase peptide synthesis (Fmoc SPPS) according to general procedure A. After checking the crude peptide by LC-MS, a portion (25 μ mol) of the peptide was capped with chloroacetyl chloride following general procedure B. The peptide

was deprotected and cleaved from the resin according to general procedure C. Subsequently, the peptide was cyclized following general procedure D and purified by preparative HPLC (0-100%, buffer B) affording cyclic peptide 12 as a white solid (4.4 mg, 8.5%). HRMS (m/z): $[M+2H]^{2+}$ calculated for $C_{97}H_{154}N_{26}O_{23}S^{2+}$, 1041.5700, found 1041.5696. LC-MS R_t 6.59 min (0 to 100 % B over 12 min, 0.1% FA, λ = 214 nm).

Peptide 13: Rink Amide AM resin (146 mg, 100 μ mol, 0.684 mmol g⁻¹) was used for Fmoc solid phase peptide synthesis (Fmoc SPPS) according to general procedure A. After checking the crude peptide by LC-MS, a portion (25 μ mol) of the peptide was capped with chloroacetyl chloride following general procedure B. The peptide was deprotected and cleaved from the resin according to general procedure C. Subsequently, the peptide was cyclized following general procedure D and purified by preparative HPLC (0-100%, buffer B) affording cyclic peptide 13 as a white solid (5.2 mg, 10.0%). HRMS (m/z): [M+2H]²⁺ calculated for C₉₈H₁₇₃N₂₇O₂₂S²⁺, 1056.1485, found 1056.1474. LC-MS R_t 6.21 min (0 to 100 % B over 12 min, 0.1% FA, λ = 214 nm).

Peptide 14: Rink Amide AM resin (146 mg, 100 µmol, 0.684 mmol g⁻¹) was used for Fmoc solid phase peptide synthesis (Fmoc SPPS) according to general procedure A. After checking the crude peptide by LC-MS, a portion (25 µmol) of the peptide was capped with chloroacetyl chloride following general procedure B. The peptide was deprotected and cleaved from the resin according to general procedure C. Subsequently, the peptide was cyclized following general procedure D and purified by preparative HPLC (0-100%, buffer B) affording cyclic peptide 14 as a white solid (4.7 mg, 8.7%). HRMS (m/z): $[M+2H]^{2+}$ calculated for $C_{104}H_{163}N_{27}O_{22}S^{2+}$, 1087.1093, found 1087.1088. LC-MS R_t 5.64 min (0 to 100 % B over 12 min, 0.1% FA, λ = 214 nm).

Peptide 15: Rink Amide AM resin (146 mg, 100 μ mol, 0.684 mmol g⁻¹) was used for Fmoc solid phase peptide synthesis (Fmoc SPPS) according to general procedure A. After checking the crude peptide by LC-MS, a portion (25 μ mol) of the peptide was capped with chloroacetyl chloride following general procedure B. The peptide was deprotected and cleaved from the resin according to general procedure C. Subsequently, the peptide was cyclized following general procedure D and purified by preparative HPLC (0-100%, buffer B) affording cyclic peptide 15 as a white solid (5.9 mg, 10.6%). HRMS (m/z): $[M+2H]^{2+}$ calculated for $C_{104}H_{165}N_{27}O_{25}S^{2+}$, 1112.1095, found 1112.1095. LC-MS R_t 6.87 min (0 to 100 % B over 12 min, 0.1% FA, λ = 214 nm).

Peptide 16: Rink Amide AM resin (146 mg, 100 μmol, 0.684 mmol g⁻¹) was used for Fmoc solid phase peptide synthesis (Fmoc SPPS) according to general procedure

A. After checking the crude peptide by LC-MS, a portion (25 µmol) of the peptide was capped with chloroacetyl chloride following general procedure B. The peptide was deprotected and cleaved from the resin according to general procedure C. Subsequently, the peptide was cyclized following general procedure D and purified by preparative HPLC (0-100%, buffer B) affording cyclic peptide 16 as a white solid (4.7 mg, 9.0%). HRMS (m/z): $[M+2H]^{2+}$ calculated for $C_{101}H_{150}N_{26}O_{21}S^{2+}$, 1047.5595, found 1047.5594. LC-MS R_t 6.10 min (0 to 100 % B over 12 min, 0.1% FA, λ = 214 nm).

Peptide 17: Rink Amide AM resin (146 mg, 100 µmol, 0.684 mmol g^{-1}) was used for Fmoc solid phase peptide synthesis (Fmoc SPPS) according to general procedure A. After checking the crude peptide by LC-MS, a portion (25 µmol) of the peptide was capped with chloroacetyl chloride following general procedure B. The peptide was deprotected and cleaved from the resin according to general procedure C. Subsequently, the peptide was cyclized following general procedure D and purified by preparative HPLC (0-100%, buffer B) affording cyclic peptide 17 as a white solid (5.6 mg, 10.9%). HRMS (m/z): $[M+2H]^{2+}$ calculated for $C_{93}H_{156}N_{28}O_{23}S^{2+}$, 1032.5809, found 1032.5797. LC-MS R_t 6.01 min (0 to 100 % B over 12 min, 0.1% FA, λ = 214 nm).

Inhibition Studies. Expression and purification of full-length human wild-type NNMT protein (hNNMTwt) were performed as previously described.³⁷ The purity of the enzyme was confirmed using sodium dodecyl sulfate-polyacrylamide gel electrophoresis (SDS-PAGE) with Coomassie blue staining, and NNMT identity was confirmed using SDS-PAGE and Western blotting. Catalytic activity of the recombinant protein was evaluated with 1 unit of enzyme activity representing the formation of 1 nmol of MNA/h of incubation at 37°C. The specific activity of the batch used in the inhibitory activity assays was 15064 units per mg of protein at a protein concentration of 8.4 mg mL⁻¹. NNMT was used at a final concentration of 50 nM diluted in assay buffer (50 mM Tris buffer (pH 8.4) and 1 mM dithiothreitol). The compounds were dissolved in DMSO and diluted with water to concentrations ranging from 1 nM to 100 µM (DMSO was kept constant at 1.25% final concentration). The compounds were incubated with the enzyme for 10 min at room temperature before initiating the reaction with a mixture of NA and SAM at their K_M values of 200 and 8.5 µM, respectively. The formation of MNA was measured after 30 min at room temperature. The reaction was quenched by addition of 30 µL of the sample to 70 µL of acetonitrile containing 50 nM deuteromethylated nicotinamide as internal standard. The enzymatic activity assays were performed using Multiple Reaction Monitoring (MRM) on a Shimadzu LC-20AD system with a Waters Acquity BEH Amide HILIC column (3.0x100 mm, 1.7 µm particle size, Waters, Milford) at 65°C using water containing 300 mM formic acid and 550 mM NH4OH (pH 9.2) at 40% v/v and acetonitrile at 60% v/v isocratically

at a flowrate of 0.6 mL min⁻¹, with a runtime of 1.7 min. Calibration samples were prepared using 70 μ L of internal standard d₃-MNA at 50 nM in acetonitrile and 30 μ L of an aqueous solution of reference standard MNA with concentrations ranging from 1 to 1024 nM. Ratios of the sums of the MNA and d₃-MNA transitions were used to calculate concentrations of MNA. Concentrations of MNA were plotted against concentration of inhibitor and the results were subsequently normalized with the highest value in the concentration range defined as 100% inhibition. The percentage of inhibitory activity was plotted as a function of inhibitor concentration and fit using non-linear regression analysis of the sigmoidal dose-response curve generated using the normalized data and a variable slope in Graphpad Prism 8. IC₅₀ curves are presented in the Appendix IV .

Substrate competition study. Substrate competition was performed under three different conditions; (1) normal conditions with both substrates at K_M values, (2) NA at 2 mM and SAM at its K_M of 8.5 μ M and (3) NA at its K_M of 200 μ M and SAM at 85 μ M. All peptides were tested under these conditions at concentrations between 20 μ M and 27 nM in duplicate using 200 nM hNNMTwt. The slightly higher concentration of enzyme compared to the initial inhibition testing was used to achieve more signal for enhanced discrimination between high and low values. Results were normalized to indicate the fold change in IC₅₀ value compared to the normal conditions.

Cell-based assays. Human aortic endothelial cell line (HAEC, ATCC, VA, USA) and human lung adenocarcinoma line (A549, ATCC, VA, USA) were cultured according to the provider's indications and seeded in 6-well or 24-well format. After 24h-stabilization, when cells reached about 100% confluence, culture medium was removed and cells were pre-incubated for 1h in normal Hank's buffer (HBSS). After the buffer change, cells were treated with NNMT peptide inhibitors or reference compound at concentrations of 1 and 10 μ M. The compounds were incubated in the presence of nicotinamide (100 μ M) and S-adenosyl-L-methionine 10 μ M (Sigma Aldrich, MO, USA) for 3 hours in HAEC cells and for 1 hour in A549 cells. Effluent samples were collected after incubation and frozen (-80 °C) for further measurement of exogenous MNA. Cells were collected using scraper, centrifuged (2 x 500 G/5 min.) and frozen for BCA protein assay.

MNA measurement in buffer samples. The quantification of 1-methylnicotinamide (MNA), nicotinamide (NA), nicotinic acid (NicA), 1-methyl-2-pyridone-5-carboxamide (Met-2Pyr) and 1-methyl-4-pyridone-5-carboxamide (Met-4Pyr) was performed applying ultra-pressure liquid chromatography coupled to tandem mass spectrometry (UPLC-MS) according to the methodology previously described with minor modifications.¹⁵ A UPLC-MS system comprised of an UPLC Ultimate 3000 (Dionex, Thermo Scientific, USA) connected to a TSQ Quantum Ultra mass

spectrometer (Thermo Scientific, USA) equipped with a heated electrospray ionization interface (HESI-II Probe) was used. Chromatographic separation of analytes was carried out on an Aquasil C18 analytical column (4.6 mm x 150 mm, 5 µm; Thermo Scientific) under isocratic elution using acetonitrile with 0.1% of formic acid (A) and 5 mM ammonium formate in water (B) as mobile phases delivered at the flow rate of 0.8 ml min⁻¹ (A:B, 80:20, v/v). 50 µl of effluent sample was used for the measurement of exogenous MNA. The internal standard (IS) containing MNA-d₃ was added to each sample (5 µL) obtaining the final concentration of 500 ng mL⁻¹. After sample mixing, the proteins were precipitated using 100 µL of acidified acetonitrile (0.1% of formic acid), and samples were mixed (10 min), cooled at 4°C (15 min) and finally centrifuged (15000 x g, 15 min, 4°C). A clear supernatant was transferred to a chromatographic vial and directly injected (5 µL) into UPLC-MS system. The mass spectrometer was operating in the positive ionization using selected reactions monitoring (SRM) mode monitoring the following ion transitions for analyzed metabolite: m/z 137 \rightarrow 94 for MNA and 140 \rightarrow 97 for MNA-d₃. The concentration of MNA was calculated based on the calibration curve plotted for the analyte as the relationship between the peak area ratios of analyte/IS to the nominal concentration of the analyte. The concentration of analytes was normalized to mg of proteins, which was assessed using Pierce[™] BCA Protein Assay Kit (Thermo Fisher, Waltham, MA, USA) and Synergy4 multiplate reader (BioTek, Winooski, VT, USA). MNA was obtained from Sigma-Aldrich, MO, USA. Deuterated standard MNA-d₃ was synthesized by Dr. Adamus (Technical University, Lodz, Poland). LC-MS-grade acetonitrile, ammonium formate and formic acid were purchased from Sigma-Aldrich. Ultrapure water was obtained from a Millipore system (Direct-Q 3UV).

References

- 1. T. A. Alston and R. H. Abeles, Substrate specificity of nicotinamide methyltransferase isolated from porcine liver, Arch. Biochem. Biophys., 1988, 260, 601–608.
- 2. M. J. van Haren, J. Sastre Toraño, D. Sartini, M. Emanuelli, R. B. Parsons and N. I. Martin, A Rapid and Efficient Assay for the Characterization of Substrates and Inhibitors of Nicotinamide N -Methyltransferase, Biochemistry, 2016, 55, 5307–5315.
- 3. O. A. Ulanovskaya, A. M. Zuhl and B. F. Cravatt, NNMT promotes epigenetic remodeling in cancer by creating a metabolic methylation sink, Nat. Chem. Biol., 2013, 9, 300–306.
- M. A. Eckert, F. Coscia, A. Chryplewicz, J. W. Chang, K. M. Hernandez, S. Pan, S. M. Tienda, D. A. Nahotko, G. Li, I. Blaženović, R. R. Lastra, M. Curtis, S. D. Yamada, R. Perets, S. M. McGregor, J. Andrade, O. Fiehn, R. E. Moellering, M. Mann and E. Lengyel, Proteomics reveals NNMT as a master metabolic regulator of cancerassociated fibroblasts, Nature, 2019, 569, 723–728.
- A. Kanakkanthara, K. Kurmi, T. L. Ekstrom, X. Hou, E. R. Purfeerst, E. P. Heinzen, C. Correia, C. J. Huntoon, D. O'Brien, A. E. Wahner Hendrickson, S. C. Dowdy, H. Li, A. L. Oberg, T. Hitosugi, S. H. Kaufmann, S. J. Weroha and L. M. Karnitz, BRCA1 Deficiency Upregulates NNMT, Which Reprograms Metabolism and Sensitizes Ovarian Cancer Cells to Mitochondrial Metabolic Targeting Agents, Cancer Res., 2019, 79, 5920–5929.
- 6. Y. Xu, P. Liu, D.-H. Zheng, N. Wu, L. Zhu, C. Xing and J. Zhu, Expression profile and prognostic value of NNMT in patients with pancreatic cancer, Oncotarget, 2016, 7, 19975–19981.
- 7. C. Chen, X. Wang, X. Huang, H. Yong, J. Shen, Q. Tang, J. Zhu, J. Ni and Z. Feng, Nicotinamide N-methyltransferase: a potential biomarker for worse prognosis in gastric carcinoma, Am. J. Cancer Res., 2016, 6, 649–663.
- 8. Y. Wang, J. Zeng, W. Wu, S. Xie, H. Yu, G. Li, T. Zhu, F. Li, J. Lu, G. Y. Wang, X. Xie and J. Zhang, Nicotinamide N-methyltransferase enhances chemoresistance in breast cancer through SIRT1 protein stabilization, Breast Cancer Res., 2019, 21, 1–17.
- 9. S. Holstein, S. Venz, H. Junker, R. Walther, M. B. Stope and U. Zimmermann, Nicotinamide N-methyltransferase and its precursor substrate methionine directly and indirectly control malignant metabolism during progression of renal cell carcinoma, Anticancer Res., 2019, 39, 5427–5436.
- 10. M. Mascitti, A. Santarelli, D. Sartini, C. Rubini, G. Colella, E. Salvolini, G. Ganzetti, A. Offidani and M. Emanuelli, Analysis of nicotinamide N-methyltransferase in oral malignant melanoma and potential prognostic significance, Melanoma Res., 2019, 29, 151–156.
- 11. R. B. Parsons, M.-L. Smith, A. C. Williams, R. H. Waring and D. B. Ramsden,

- Expression of Nicotinamide N-Methyltransferase (E.C. 2.1.1.1) in the Parkinsonian Brain, J. Neuropathol. Exp. Neurol., 2002, 61, 111–124.
- 12. R. B. Parsons, S. W. Smith, R. H. Waring, A. C. Williams and D. B. Ramsden, High expression of nicotinamide N-methyltransferase in patients with idiopathic Parkinson's disease, Neurosci. Lett., 2003, 342, 13–16.
- 13. L. Mateuszuk, A. Jasztal, E. Maslak, M. Gasior-Glogowska, M. Baranska, B. Sitek, R. Kostogrys, A. Zakrzewska, A. Kij, M. Walczak and S. Chlopicki, Antiatherosclerotic effects of 1-methylnicotinamide in apolipoprotein e/low-density lipoprotein receptor-deficient mice: A comparison with nicotinic acid, J. Pharmacol. Exp. Ther., 2016, 356, 514–524.
- 14. R. Campagna, Ł. Mateuszuk, K. Wojnar-Lason, P. Kaczara, A. Tworzydło, A. Kij, R. Bujok, J. Mlynarski, Y. Wang, D. Sartini, M.Emanuelli and S. Chlopicki, Nicotinamide N-methyltransferase in endothelium protects against oxidant stress-induced endothelial injury, Biochim. Biophys. Acta, Mol. Cell Res., 2021, 184, 119082.
- 15.A. Fedorowicz, Ł. Mateuszuk, G. Kopec, T. Skórka, B. Kutryb-Zaj⊠c, A. Zakrzewska, M. Walczak, A. Jakubowski, M. Łomnicka, E. Słomińska and S. Chlopicki, Activation of the nicotinamide N-methyltransferase (NNMT)-1-methylnicotinamide (MNA) pathway in pulmonary hypertension, Respir. Res., 2016, 17, 108.
- 16. S. Brachs, J. Polack, M. Brachs, K. Jahn-Hofmann, R. Elvert, A. Pfenninger, F. Bärenz, D. Margerie, K. Mai, J. Spranger and A. Kannt, Genetic Nicotinamide N-Methyltransferase (Nnmt) Deficiency in Male Mice Improves Insulin Sensitivity in Diet-Induced Obesity but Does Not Affect Glucose Tolerance, Diabetes, 2019, 68, 527–542.
- 17. D. Kraus, Q. Yang, D. Kong, A. S. Banks, L. Zhang, J. T. Rodgers, E. Pirinen, T. C. Pulinilkunnil, F. Gong, Y. Wang, Y. Cen, A. A. Sauve, J. M. Asara, O. D. Peroni, B. P. Monia, S. Bhanot, L. Alhonen, P. Puigserver and B. B. Kahn, Nicotinamide N-methyltransferase knockdown protects against diet-induced obesity, Nature, 2014, 508, 258–262.
- 18. R. Giuliante, C. Polidori, R. Rocchetti, D. Sartini, M. Emanuelli, I. Klöting, T. Bacchetti and G. Ferretti, Potential Involvement of Nicotinamide N -Methyltransferase in the Pathogenesis of Metabolic Syndrome, Metab. Syndr. Relat. Disord., 2015, 13, 165–170.
- 19.19 M. J. Van Haren, R. Taig, J. Kuppens, J. Sastre Toraño, E. E. Moret, R. B. Parsons, D. Sartini, M. Emanuelli and N. I. Martin, Inhibitors of nicotinamide: N -methyltransferase designed to mimic the methylation reaction transition state, Org. Biomol. Chem., 2017, 15, 6656–6667.
- 20.20 N. Babault, A. Allali-Hassani, F. Li, J. Fan, A. Yue, K. Ju, F. Liu, M. Vedadi, J. Liu and J. Jin, Discovery of Bisubstrate Inhibitors of Nicotinamide N -Methyltransferase (NNMT), J. Med. Chem., 2018, 61, 1541–1551.

- 21. Y. Gao, M. J. Van Haren, E. E. Moret, J. J. M. M. Rood, D. Sartini, A. Salvucci, M. Emanuelli, P. Craveur, N. Babault, J. Jin and N. I. Martin, Bisubstrate Inhibitors of Nicotinamide N -Methyltransferase (NNMT) with Enhanced Activity, J. Med. Chem., 2019, 62, 6597–6614.
- 22. R. L. Policarpo, L. Decultot, E. May, P. Kuzmič, S. Carlson, D. Huang, V. Chu, B. A. Wright, S. Dhakshinamoorthy, A. Kannt, S. Rani, S. Dittakavi, J. D. Panarese, R. Gaudet and M. D. Shair, High-Affinity Alkynyl Bisubstrate Inhibitors of Nicotinamide N -Methyltransferase (NNMT), J. Med. Chem., 2019, 62, 9837–9873.
- 23. D. Chen, L. Li, K. Diaz, I. D. Iyamu, R. Yadav, N. Noinaj and R. Huang, Novel Propargyl-Linked Bisubstrate Analogues as Tight-Binding Inhibitors for Nicotinamide N-Methyltransferase, J. Med. Chem., 2019, 62, 10783–10797.
- 24. A. Kannt, S. Rajagopal, M. S. Hallur, I. Swamy, R. Kristam, S. Dhakshinamoorthy, J. Czech, G. Zech, H. Schreuder and S. Ruf, Novel Inhibitors of Nicotinamide-N-Methyltransferase for the Treatment of Metabolic Disorders, Molecules, 2021, 26, 991.
- 25. A. Zorzi, K. Deyle and C. Heinis, Cyclic peptide therapeutics: past, present and future, Curr. Opin. Chem. Biol., 2017, 38, 24–29.
- 26. C. Morrison, Constrained peptides' time to shine?, Nat. Rev. Drug Discov., 2018, 17, 531–533.
- 27. A. A. Vinogradov, Y. Yin and H. Suga, Macrocyclic Peptides as Drug Candidates: Recent Progress and Remaining Challenges, J. Am. Chem. Soc., 2019, 141, 4167–4181.
- 28.T. Passioura and H. Suga, A RaPID way to discover nonstandard macrocyclic peptide modulators of drug targets, Chem. Commun., 2017, 53, 1931–1940.
- 29. C. J. Hipolito and H. Suga, Ribosomal production and in vitro selection of natural product-like peptidomimetics: The FIT and RaPID systems, Curr. Opin. Chem. Biol., 2012, 16, 196–203.
- 30.Y. Goto, A. Ohta, Y. Sako, Y. Yamagishi, H. Murakami and H. Suga, Reprogramming the translation initiation for the synthesis of physiologically stable cyclic peptides, ACS Chem. Biol., 2008, 3, 120–129.
- 31. S. Ruf, M. S. Hallur, N. K. Anchan, I. N. Swamy, K. R. Murugesan, S. Sarkar, L. K. Narasimhulu, V. P. R. K. Putta, S. Shaik, D. V. Chandrasekar, V. S. Mane, S. V. Kadnur, J. Suresh, R. K. Bhamidipati, M. Singh, R. R. Burri, R. Kristam, H. Schreuder, J. Czech, C. Rudolph, A. Marker, T. Langer, R. Mullangi, T. Yura, R. Gosu, A. Kannt, S. Dhakshinamoorthy and S. Rajagopal, Novel nicotinamide analog as inhibitor of nicotinamide N-methyltransferase, Bioorg. Med. Chem. Lett., 2018, 28, 922–925.
- 32. K. Hayashi, S. Uehara, S. Yamamoto, D. R. Cary, J. Nishikawa, T. Ueda, H. Ozasa, K. Mihara, N. Yoshimura, T. Kawai, T. Ono, S. Yamamoto, M. Fumoto and H. Mikamiyama, Macrocyclic Peptides as a Novel Class of NNMT Inhibitors: A SAR Study Aimed at Inhibitory Activity in the Cell, ACS Med. Chem. Lett., 2021, 12,

1093-1101.

- 33. Y. Goto, T. Katoh and H. Suga, Flexizymes for genetic code reprogramming, Nat. Protoc., 2011, 6, 779–790.
- 34. H. Murakami, A. Ohta, H. Ashigai and H. Suga, A highly flexible tRNA acylation method for non-natural polypeptide synthesis, Nat. Methods, 2006, 3, 357–359.
- 35. Y. Hayashi, J. Morimoto and H. Suga, In vitro selection of anti-Akt2 thioether-macrocyclic peptides leading to isoform-selective inhibitors, ACS Chem. Biol., 2012, 7, 607–613.
- 36. S. A. K. Jongkees, S. Caner, C. Tysoe, G. D. Brayer, S. G. Withers and H. Suga, Rapid discovery of potent and selective glycosidase-inhibiting de novo peptides, Cell Chem. Biol., 2017, 24, 381–390.
- 37. Y. Peng, D. Sartini, V. Pozzi, D. Wilk, M. Emanuelli and V. C. Yee, Structural Basis of Substrate Recognition in Human Nicotinamide N -Methyltransferase, Biochemistry, 2011, 50, 7800–7808.

Chapter 6

Summary Samenvatting

Summary

The work described in this thesis focuses on the development of linear and cyclized peptide probes targeting protein arginine N-methyltransferases (PRMTs) and nicotinamide N-methyltransferase (NNMT). These probes were used to characterize the recognition of specific substrate(s) by PRMTs and NNMT and in so doing providing further insights into inhibitor design and assessment.

In Chapter 1 a general introduction is given on peptide based inhibitors of protein methyltransferases (PMTs). A detailed overview is provided on the work that has been done with respect to the development of the peptide inhibitors of the specific PRMTs. The dysfunction of PMTs are involved in a wide range of diseases, including many forms of cancer. All reported inhibitors were derived from their natural substates which are generally highly specific for the corresponding enzyme. After modification and optimization, the inhibitors' affinity and stability were largely increased also enabling new structural insights into PMT substrate binding. While the endogenous substrates of PMTs are by definition peptide/protein based, peptide-based probes and inhibitors can be of value guiding the development of more drug-like small molecular inhibitors.

Chapter 2 describes the synthesis and evaluation of transition state mimics of PRMT1 and PRMT6, marking the extended application of a methodology recently developed in our group for the production of peptide-based transition state mimicking PRMT inhibitors. Using this approach, an adenosine moiety, mimicking that of the S-adenosyl-L-methionine (AdoMet) cofactor, is covalently linked to the guanidine side chain of a target arginine residue contained in a peptidic fragment derived from a PRMT substrate protein (Figure 1). Histone H4 tail peptide-based transition state mimics were synthesized wherein the adenosine group was linked to the Arg3 residue of a H4 tail peptide based on the first seven amino acids (Figure 1). H4R3 is a substrate for multiple PRMTs, including PRMT1 and PRMT6. The inhibition results obtained with these new H4-based transition state mimics show low micromolar IC₅₀ values against PRMT1 and PRMT6, indicating that the methodology is applicable to the broader family of PRMTs.

Another PRMT family member, PRMT4, also known as coactivator-associated arginine methyltransferase 1 (CARM1), was investigated in Chapter 3. Peptidomimetics that recapitulate the transition state of protein arginine N-methyltransferases were designed based on the H3 peptide wherein the target Arg¹⁷ was flanked by either a free or an acetylated lysine. The inclusion of the acetylated or non-acetylated Lys¹⁸ residue allowed us to also probe the impact of lysine acetylation on CARM1 substrate binding. Structural studies with these peptidomimetics and the catalytic domain of CARM1 provide new insights into the

binding of the H3 peptide within the enzyme active site (Figure 2). While the cocrystal structures reveal that lysine acetylation results in minor conformational differences for both CARM1 and the H3 peptide, acetylation of Lys18 does lead to additional interactions (Van der Waals and hydrogen bonding) and likely reduces the cost of desolvation upon binding, resulting in increased affinity. Informed by these findings a series of smaller peptidomimetics were also prepared and found to maintain potent and selective CARM1 inhibition.

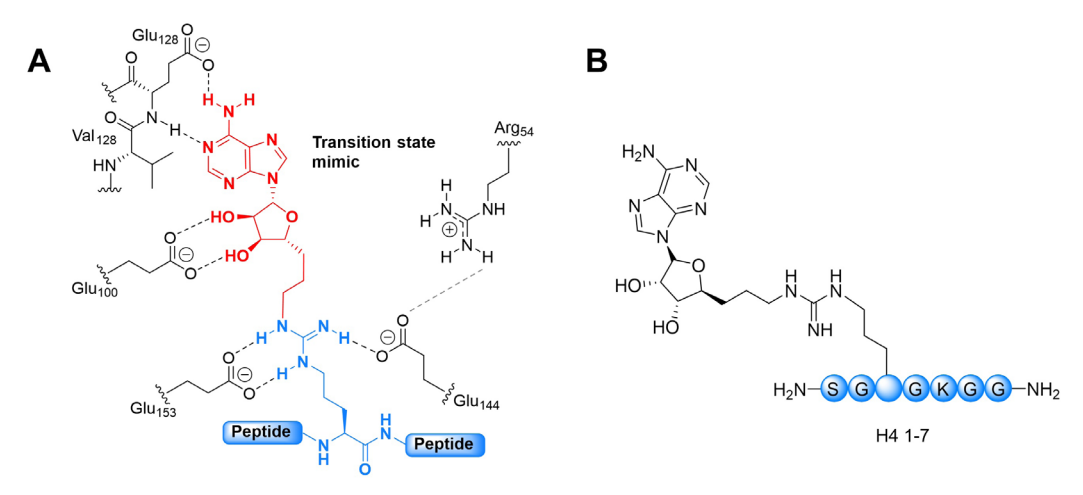


Figure 1. A) The design of the transition state mimics is based on the covalent linkage of the adenosine group (as shown in red) to the arginine sidechain in a peptide (as shown in blue). B) Transition state mimic based on histone H4¹⁻⁷

The aberrant expression of CARM1 has been linked to tumorigenesis, leading to increased interest in targeting CARM1 as a potential therapeutic target. In order to evaluate the effects of inhibitors and tool compounds on the activity of CARM1, sensitive and specific analytical methods are needed. Chapter 4 describes the development of a convenient assay employing peptide substrates derived from poly(A)-binding protein 1 (PABP1), a natural substrate of CARM1. This operationally straightforward LC-MS/MS-based approach allows for the direct detection of substrate methylation with minimal workup. The method was validated and its value in characterizing CARM1 activity and inhibition demonstrated through a comparative analysis involving a set of established small molecule and peptide-based CARM1 inhibitors.

Chapter 5 focusses on the screening, synthesis, and assessment of cyclic peptide inhibitors of nicotinamide N-methyltransferase (NNMT). The complexity of the role of NNMT in healthy and disease states is slowly being elucidated with indications that it may be an interesting therapeutic target for a variety of diseases. The small molecule NNMT inhibitors developed to date are typically structurally related to one or both of its substrates. In the search for structurally diverse NNMT inhibitors, an mRNA display screening technique was used to identify macrocyclic peptides which bind to NNMT. Several of the cyclic peptides identified in this manner showed

potent inhibition of NNMT in biochemical assays and some were also found to reduce nicotinamide methylation in cellular assays. Notably, substrate competition experiments reveal that these cyclic peptide inhibitors are noncompetitive with either AdoMet or nicotinamide indicating they may be the first allosteric inhibitors reported for NNMT.

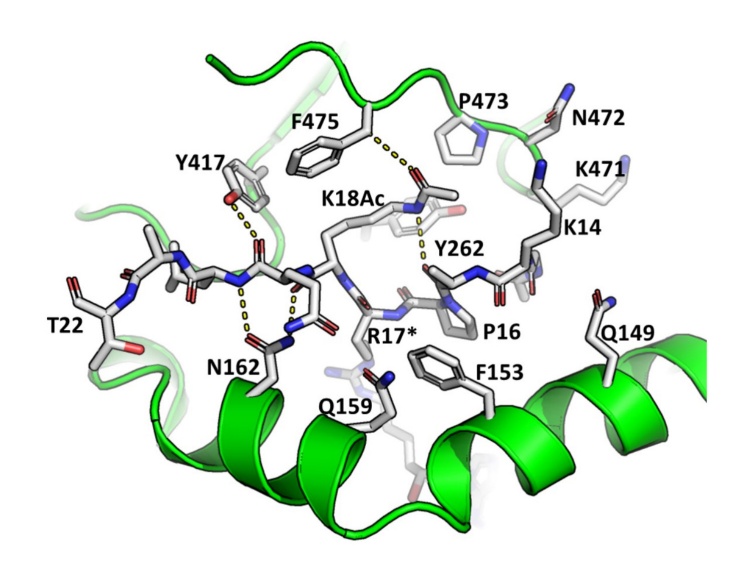
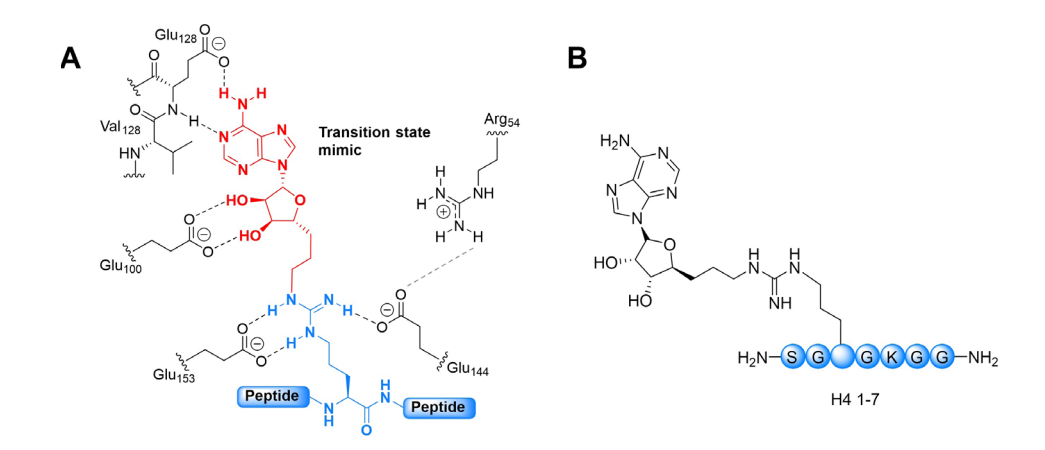


Figure 2. Co-crystal structure of H3¹³⁻³¹ Lys¹⁸Ac peptide bound to CARM1 catalytic domain (PDB code 7OKP.) H-bonds are shown as dash lines with cartoon and stick representation of the peptidomimetics bound to mmCARM1.

Samenvatting

Het werk beschreven in dit proefschrift richt zich op de ontwikkeling van lineaire en gecycliseerde peptidesondes die zich richten op proteïne arginine N-methyltransferases (PRMT's) en nicotinamide N-methyltransferase (NNMT). Deze sondes werden gebruikt om de herkenning van specifieke substraten door PRMT's en NNMT te karakteriseren en op deze manier meer inzicht te verschaffen in het ontwerp en de beoordeling van remmers van deze enzymen.

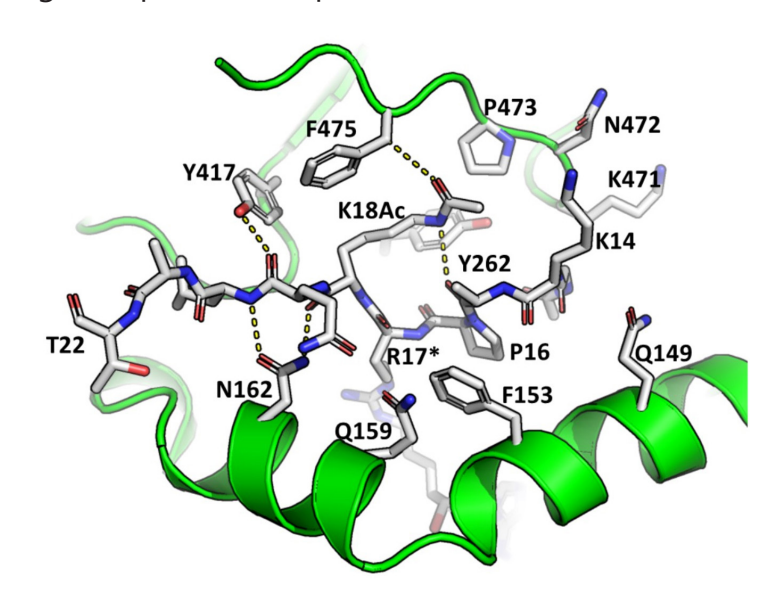
In Hoofdstuk 1 wordt een algemene inleiding gegeven over op peptiden gebaseerde remmers van proteïne methyltransferases (PMT's). Er wordt een gedetailleerd overzicht gegeven van het werk dat is gedaan met betrekking tot de ontwikkeling van peptideremmers van de specifieke PRMT's. De verstoorde werking van PMT's is betrokken bij een breed scala aan ziekten, waaronder vele vormen van kanker. Alle gerapporteerde remmers waren afgeleid van hun natuurlijke substraten die over het algemeen zeer specifiek zijn voor het overeenkomstige enzym. Na modificatie en optimalisatie waren de affiniteit en stabiliteit van de remmers grotendeels verhoogd, wat ook nieuwe structurele inzichten in PMT-substraatbinding mogelijk maakte. Hoewel de natuurlijke substraten van PMT's per definitie op peptiden/eiwitten zijn gebaseerd, kunnen op peptiden gebaseerde probes en remmers waardevol zijn bij de ontwikkeling van meer geneesmiddelachtige kleine moleculaire remmers.



Figuur 1. A) Het ontwerp van de mimetica van de overgangstoestand is gebaseerd op de covalente koppeling van de adenosinegroep (zoals weergegeven in rood) aan de argininezijketen in een peptide (zoals weergegeven in blauw). B) Overgangstoestand mimeticum op basis van histon H4¹⁻⁷.

Hoofdstuk 2 beschrijft de synthese en evaluatie van mimetica van overgangstoestanden van PRMT's gericht op PRMT1 en PRMT6, wat de uitgebreide toepassing laat zien van een methodologie die recentelijk in onze groep is ontwikkeld voor de productie van op peptiden gebaseerde overgangstoestanden

die deze PRMT-remmers nabootsen. Met behulp van deze benadering wordt een adenosine-eenheid, zoals aanwezig in de S-adenosyl-L-methionine (AdoMet) cofactor, covalent gekoppeld aan de guanidine-zijketen van een geselecteerd arginine-residu dat zich in een peptide fragment bevindt dat is afgeleid van een PRMT-substraateiwit (Figuur 1). Op het histon H4-peptide gebaseerde mimetica van de overgangstoestand werden gesynthetiseerd waarbij de adenosinegroep was gekoppeld aan de Arg3-residu van een H4-peptide op basis van de eerste zeven aminozuren van de N-terminus van histon H4 (Figuur 1). H4R3 is een substraat voor meerdere PRMT's, waaronder PRMT1 en PRMT6. De remmingsresultaten die zijn verkregen met deze nieuwe op H4-gebaseerde overgangstoestand-nabootsers vertonen laag-micromolaire IC₅₀-waarden tegen PRMT1 en PRMT6, wat aangeeft dat de methodologie toepasbaar is op de bredere familie van PRMT's.



Figuur 2. Co-kristalstructuur van H3¹³⁻³¹ Lys¹⁸Ac-peptide gebonden aan CARM1-katalytisch domein (PDB-code 7OKP.) H-bindingen worden weergegeven als streepjeslijnen met cartoon- en stokweergave van de peptidomimetica gebonden aan mmCARM1.

Een ander lid van de PRMT-familie, PRMT4, ook bekend als co-activator-geassocieerde arginine methyltransferase 1 (CARM1), werd onderzocht in hoofdstuk 3. Peptidomimetica die de overgangstoestand van de eiwit arginine N-methyltransferasen recapituleren werden ontworpen op basis van het H3-peptide waarin het doelwit Arg17 was geflankeerd door een vrij of een geacetyleerd lysine residu. De inclusie van het geacetyleerde of niet-geacetyleerde Lys18-residu stelde ons in staat om ook de impact van lysine acetylering op CARM1-substraatbinding te onderzoeken. Structurele studies met deze peptidomimetica en het katalytische domein van CARM1 bieden nieuwe inzichten in de binding van het H3-peptide in de actieve site van het enzym (Figuur 2). Terwijl de co-kristalstructuren onthullen dat lysine-acetylering resulteert in kleine verschillen in conformatie voor zowel CARM1

als het H3-peptide, leidt acetylering van Lys18 tot extra interacties (Van der Waals interacties en waterstofbruggen) en vermindert het waarschijnlijk de kosten van desolvatie bij binding, resulterend in een verhoogde affiniteit. Geïnformeerd door deze bevindingen werd ook een reeks kleinere peptidomimetica gesynthetiseerd welke krachtige en selectieve CARM1-remming wisten te behouden.

De afwijkende expressie van CARM1 is in verband gebracht met tumorigenese, wat heeft geleid tot een verhoogde interesse in onderzoek naar CARM1 als een potentieel therapeutisch doelwit. Om de effecten van remmers en gereedschapsverbindingen op de activiteit van CARM1 te evalueren, zijn gevoelige en specifieke analytische methoden nodig. Hoofdstuk 4 beschrijft de ontwikkeling van een geschikte test die gebruik maakt van peptidesubstraten afgeleid van poly(A)-bindend eiwit 1 (PABP1), een natuurlijk substraat van CARM1. Deze operationeel eenvoudige LC-MS/MS-gebaseerde aanpak zorgt voor de directe detectie van substraat-methylering met minimale monsteropwerking. De methode werd gevalideerd en de waarde ervan bij het karakteriseren van CARM1-activiteit en -remming werd aangetoond door een vergelijkende analyse met een reeks bekende CARM1-remmers op basis van kleine moleculen en peptiden.

Hoofdstuk 5 richt zich op de screening, synthese en beoordeling van cyclische peptideremmers van nicotinamide N-methyltransferase (NNMT). De complexiteit van de rol van NNMT in gezonde en ziektetoestanden wordt langzaam opgehelderd met aanwijzingen dat het een interessant therapeutisch doelwit kan zijn voor een verscheidenheid aan ziekten. De tot nu toe ontwikkelde NNMT-remmers met kleine moleculen zijn doorgaans structureel verwant aan één of beide substraten. Bij het zoeken naar structureel diverse NNMT-remmers, werd een mRNA-display screeningtechniek gebruikt om macrocyclische peptiden te identificeren die aan NNMT binden. Verschillende van de op deze manier geïdentificeerde cyclische peptiden vertoonden krachtige remming van NNMT in biochemische testen en sommige bleken ook de methylering van nicotinamide in cellulaire testen te verminderen. Met name blijkt uit substraatcompetitie-experimenten dat deze cyclische peptideremmers niet-competitief zijn met AdoMet of nicotinamide, wat aangeeft dat ze mogelijk de eerste allosterische remmers zijn die zijn gerapporteerd voor NNMT.

Supplementary materials for Chapter 2-5 Appendix I - IV

Δ

Appendix I Supplementary materials for Chapter 2

High resolution Mass Spectrometry (HRMS) data for compounds 1-6:

1: HRMS (m/z): $[M+H]^+$ calculated for $C_{35}H_{60}N_{17}O_{11}^{+}$, 894.4653, found 894.4670.

2: HRMS (m/z): $[M+H]^+$ calculated for $C_{37}H_{62}N_{17}O_{12}^{+}$, 936.4758, found 936.4782.

3: HRMS (m/z): $[M+H]^+$ calculated for $C_{41}H_{72}N_{19}O_{12}^{+}$, 1022.5602, found 1022.5621.

4: HRMS (m/z): $[M+H]^+$ calculated for $C_{43}H_{74}N_{19}O_{13}^+$, 1064.5708, found 1064.5730.

5: HRMS (m/z): $[M+H]^+$ calculated for $C_{25}H_{48}N_{12}O_{8}^+$, 645.3796, found 645.3795.

6: HRMS (m/z): $[M+H]^+$ calculated for $C_{31}H_{60}N_{14}O_9^+$, 773.4746, found 773.4759.

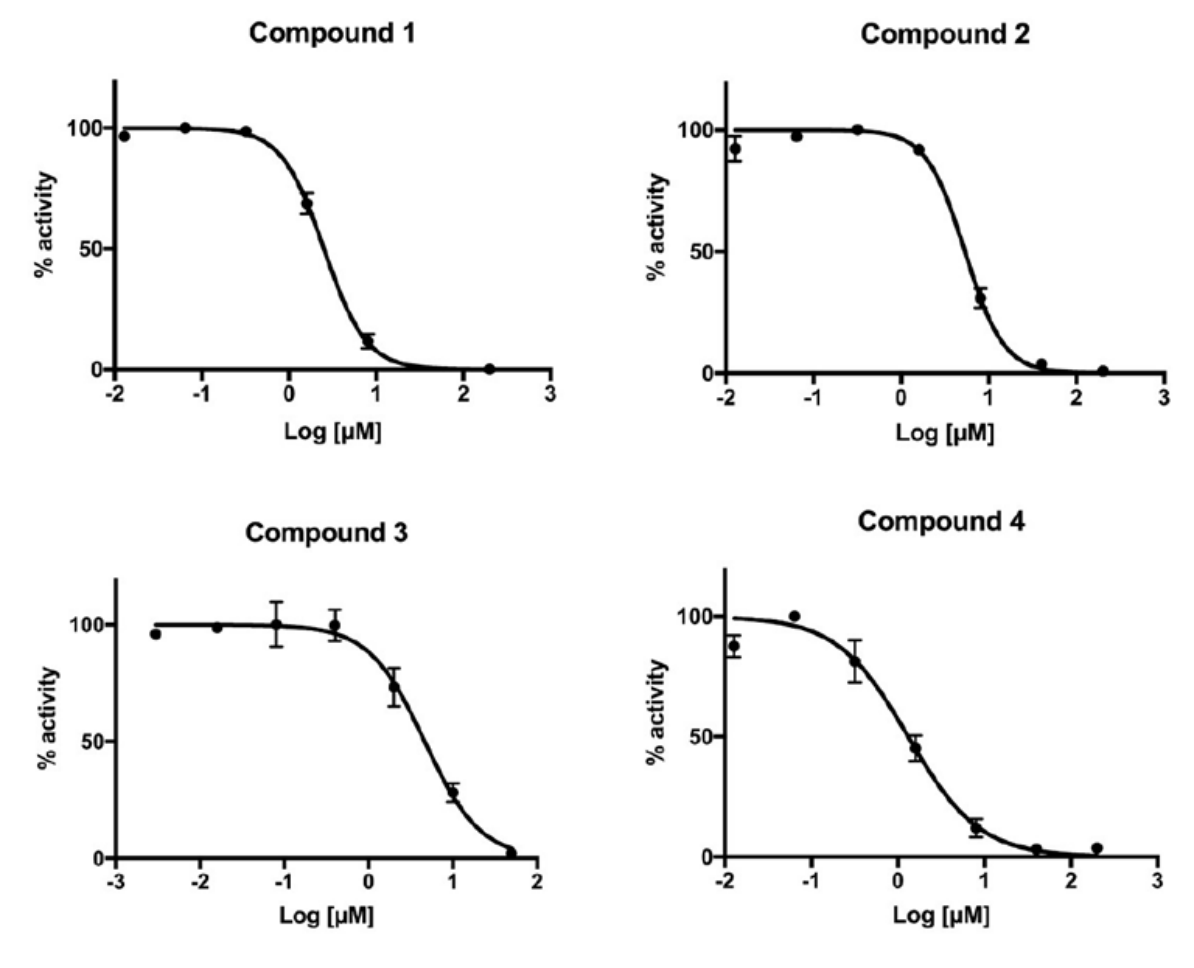


Figure S1a. IC₅₀ curves for compounds 1-4 against PRMT1

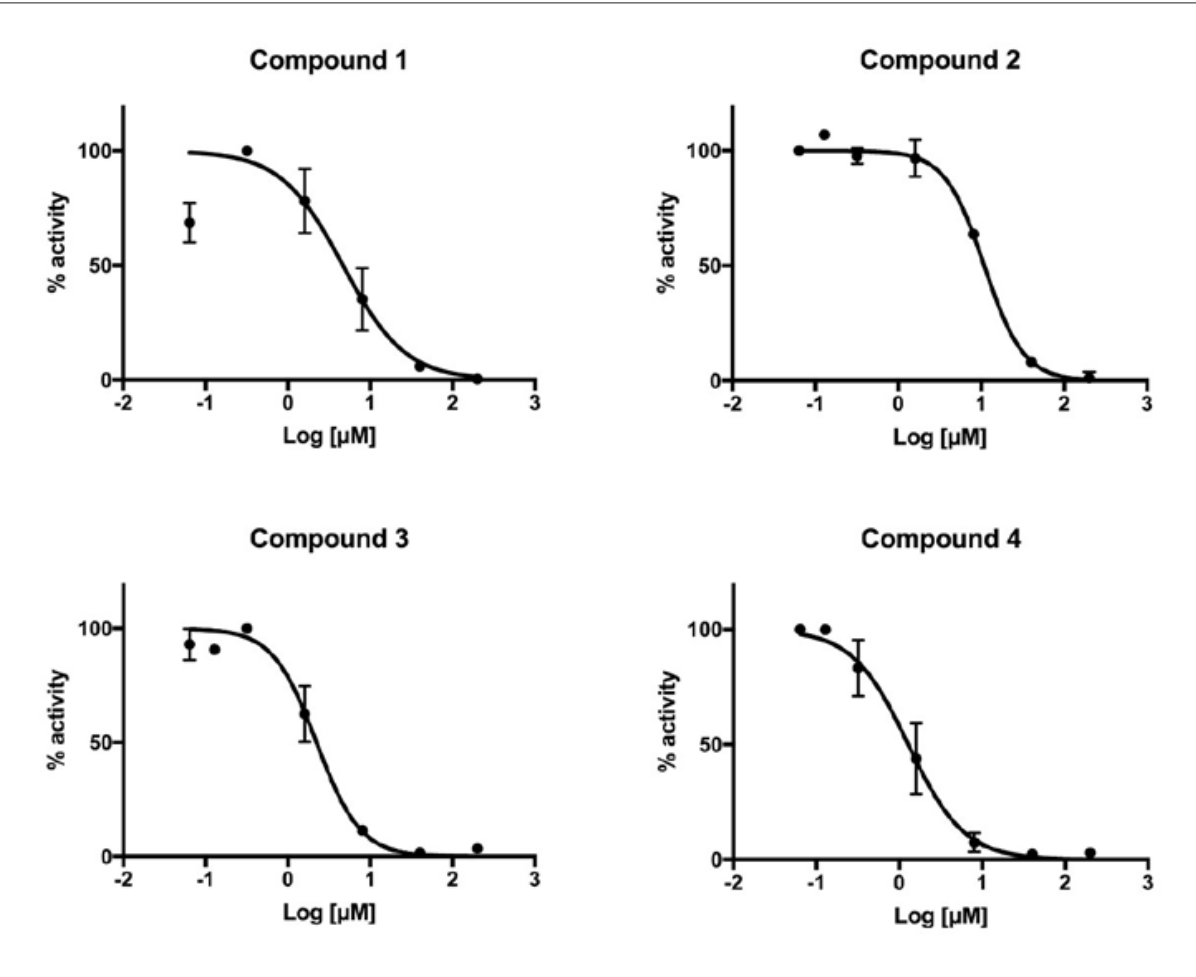
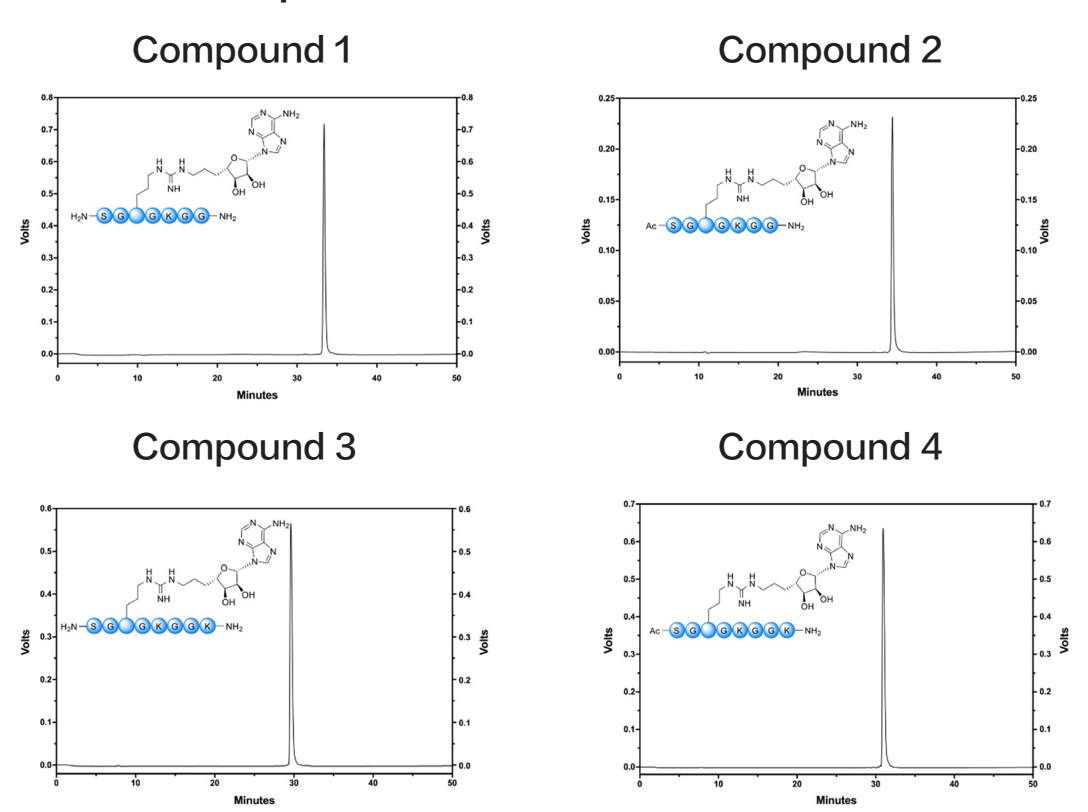
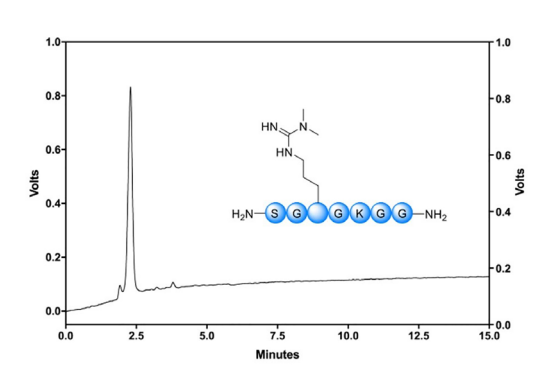


Figure S1b. IC_{50} curves for compounds 1-4 against PRMT6

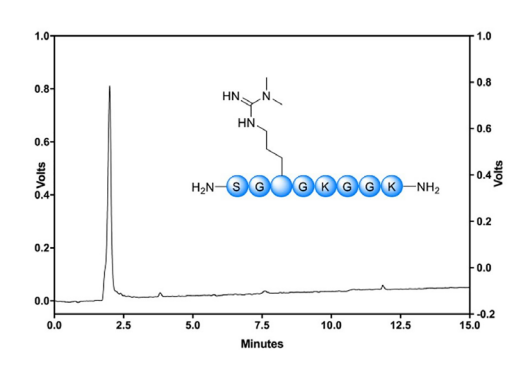
HPLC traces of final compounds



Compound 3



Compound 4



A

Appendix II Supplementary materials for Chapter 3

High Resolution Mass Spectrometry data and purified yields of compounds 1-14

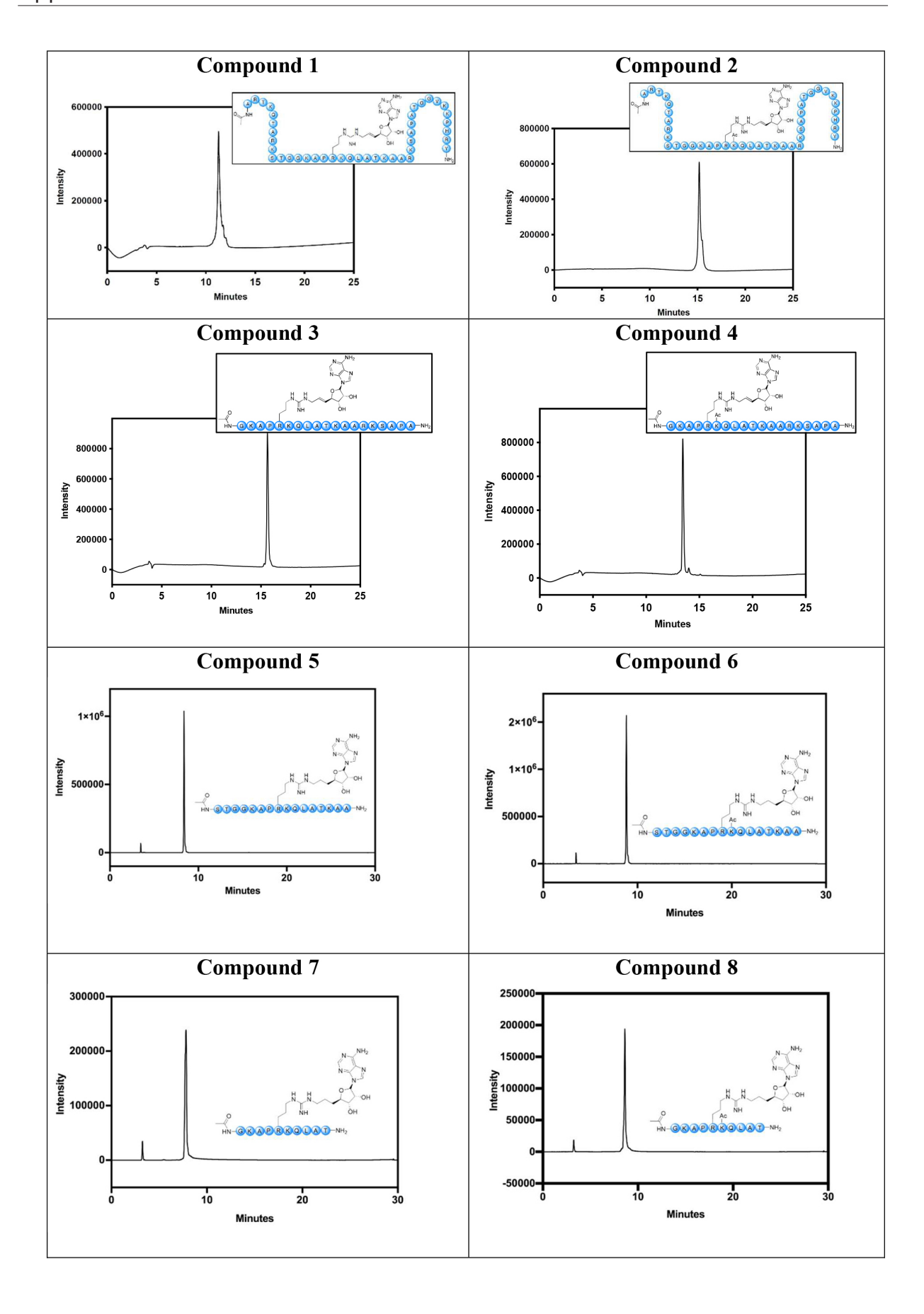
Table S1. High Resolution Mass Spectrometry data and purified yields of compounds 1-14

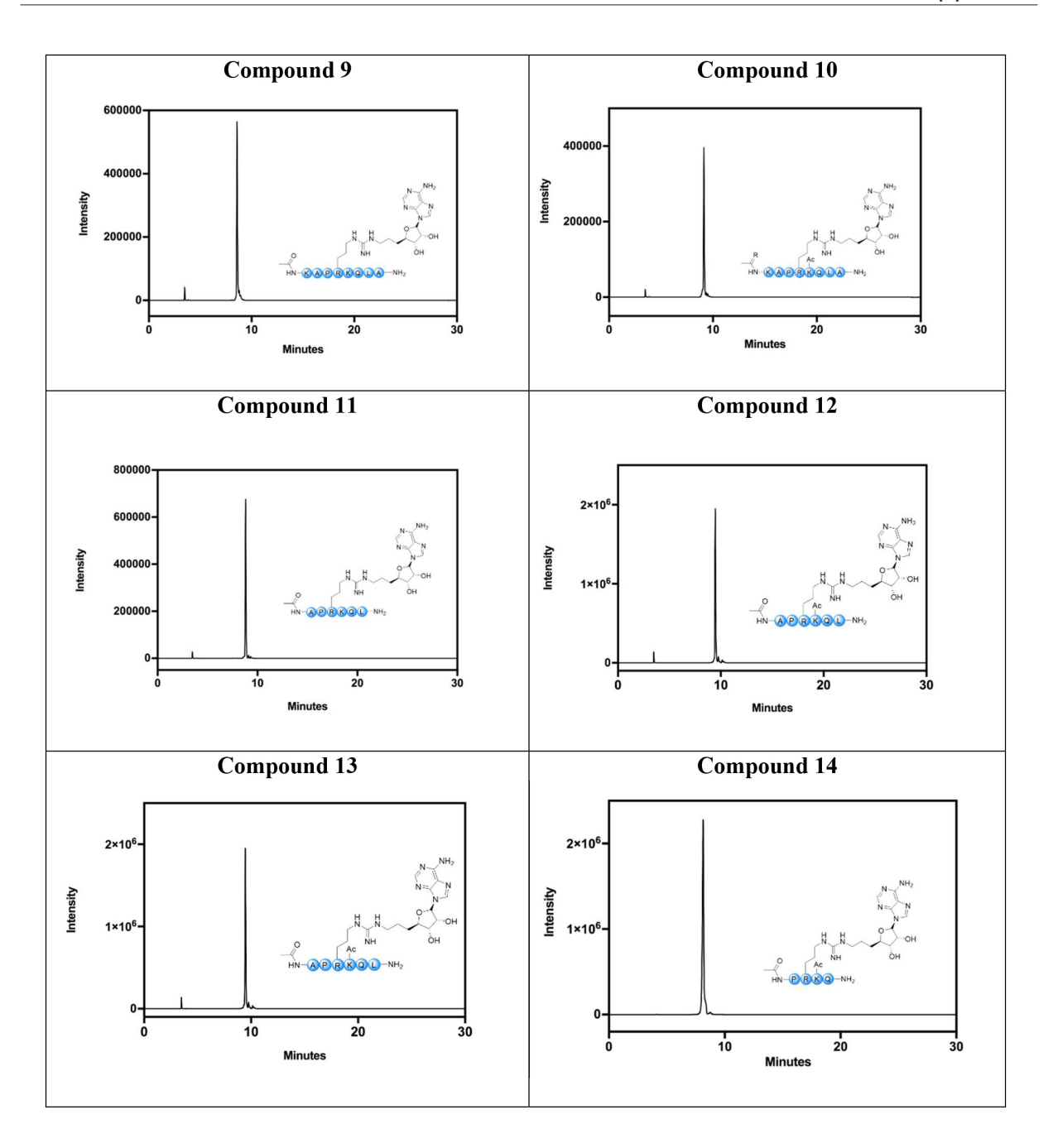
Compound	Chemical formula	Calculated Mass	Found	Yield
1	$C_{201}H_{347}N_{74}O_{55}^{3+}$	1559.2205	1559.2210	11%
2	$C_{203}H_{350}N_{74}O_{56}^{4+}$	1180.1698	1180.1703	8%
3	$C_{98}H_{170}N_{36}O_{26}^{2+}$	1134.1555	1134.1544	23%
4	$C_{100}H_{172}N_{36}O_{27}^{2+}$	1155.1608	1155.1606	26%
5	$C_{81}H_{141}N_{29}O_{24}^{2+}$	952.0297	952.0274	40%
6	$C_{83}H_{143}N_{19}O_{13}^{2+}$	973.0349	973.0330	39%
7	$C_{60}H_{103}N_{22}O_{16}^{}$	1387.7922	1387.7912	47%
8	$C_{62}H_{105}N_{22}O_{17}^{+}$	1429.8082	1429.8052	41%
9	$C_{54}H_{93}N_{20}O_{13}^{+}$	1229.7231	1229.7223	50%
10	$C_{56}H_{95}N_{20}O_{14}^{+}$	1271.7336	1271.7340	50%
11	$C_{45}H_{76}N_{17}O_{11}^{+}$	1030.5910	1030.5907	51%
12	$C_{47}H_{78}N_{17}O_{12}^{+}$	1072.6070	1072.6012	50%
13	$C_{36}H_{60}N_{15}O_9^+$	846.4698	846.4697	53%
14	$C_{38}H_{62}N_{15}O_{10}^{+}$	888.4804	888.4812	55%

HPLC traces of compounds 1-14

HPLC chromatograms of compounds 1-4 were obtained by analytical RP-HPLC using a Phenomenex Kinetex C18 column (250×4.6 mm, 5 µm particle size) with UV detection at 214 nm. The following solvent system, at a flow rate of 0.7 mL/min, was used: solvent A, 0.1 % formic acid in water; solvent B, methanol. Gradient elution was as follows: 95:5 (A/B) for 5 min, 95:5 to 50:50 (A/B) over 15 min, then reversion back to 95:5 (A/B) over 1 min, 95:5 (A/B) for 4 min.

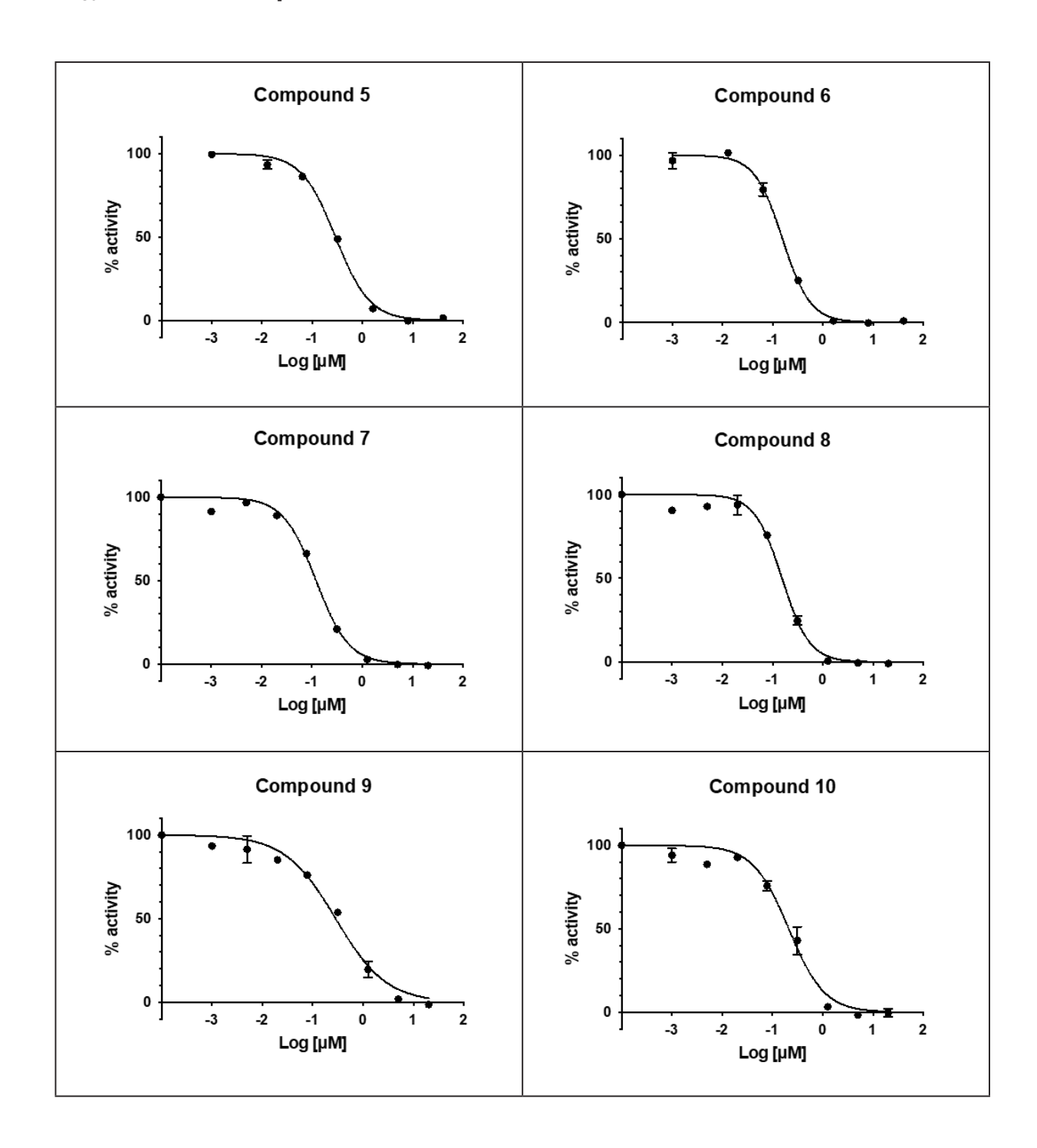
HPLC chromatograms of compounds 5-14 were obtained by LCMS using a Shimadzu Shim-Pack GIST-AQ C18 column (3.0 x 150 mm, 3 µm particle size) with UV detection at 214 nm. The following solvent system, at a flow rate of 0.5 mL/min, was used: solvent A, 0.1 % formic acid in water; solvent B, acetonitrile. Gradient elution was as follows: 95:5 (A/B) for 2 min, 95:5 to 0:100 (A/B) over 23 min, 0:100 (A/B) for 1 min, then reversion back to 95:5 (A/B) over 1 min, 95:5 (A/B) for 3 min.

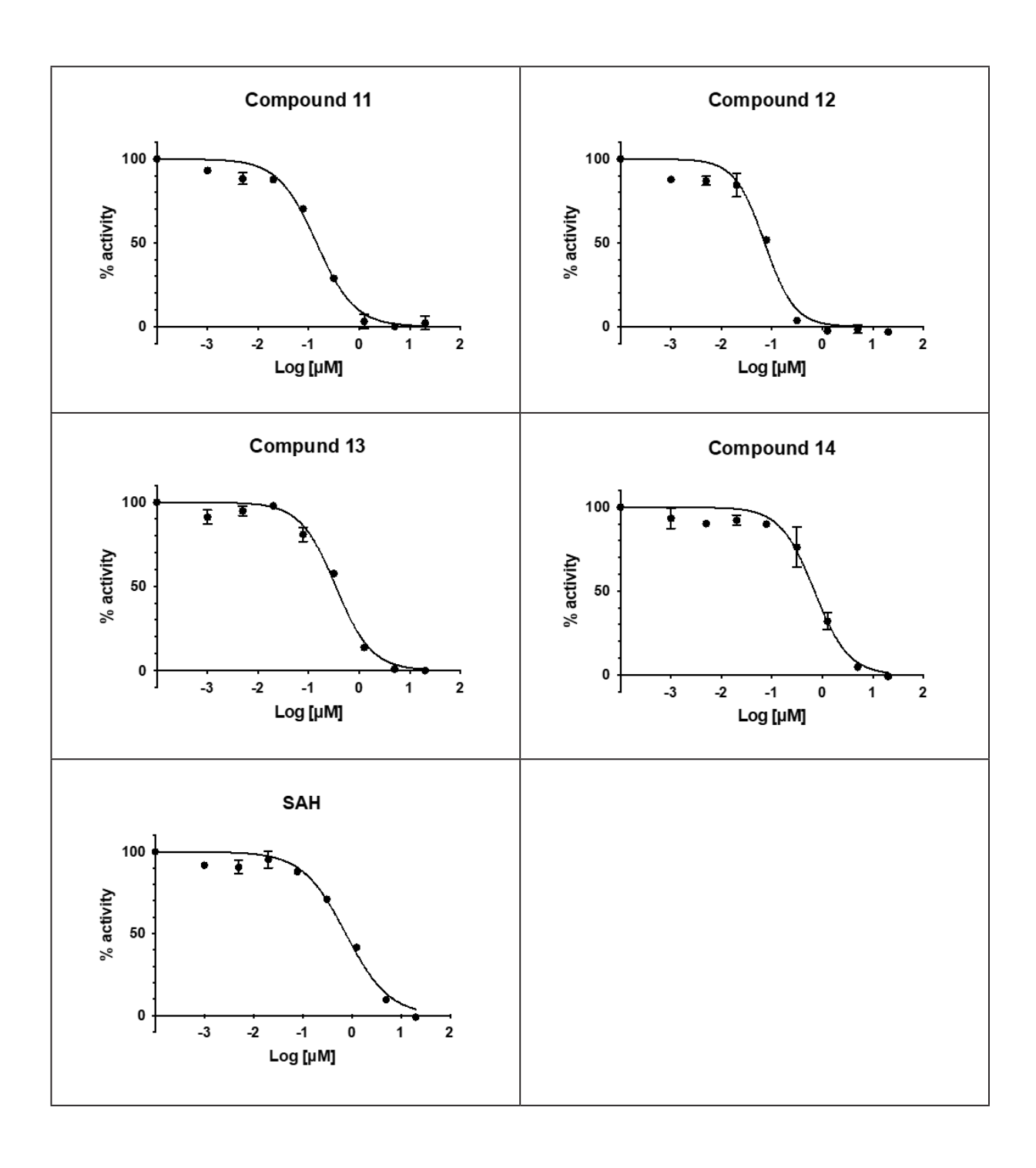




A

IC₅₀ curves for compounds 5-14 and SAH





A

Comparative table of IC₅₀ values and Ki values for compounds 5-14 and SAH

 IC_{50} values were determined as described in the experimental section. Briefly, normalized luminescence data from the activity assay was plotted as a function of inhibitor concentration and analyzed using the following equation:

$$Y = \frac{100}{(1 + 10^{((logIC 50 - X) \times Hill Slope}))}$$

Where Y = percentage activity, X = the logarithmic concentration of the inhibitors, Hill Slope= slope factor or Hill coefficient. The IC_{50} value was determined by the half maximal inhibitory concentration. The IC_{50} values measured for SAH, which served as a reference compound, are similar to those reported.

The K_1 values were determined using the same normalized luminescence data from the activity assay using the following equation:

$$Y = Vo * (1 - \frac{\left(Et + X + \left(Ki * \left(1 + \left(\frac{S}{Km}\right)\right)\right)\right) - \sqrt{((Et + X + \left(Ki * \left(1 + \left(\frac{S}{Km}\right)\right)\right))^2 - 4 * Et * X)}}{(2 * Et)}$$

Where Y = percentage activity, X = Concentration of inhibitor, Et = Enzyme concentration in micromolar, KM: Michealis-Menten constant of enzyme, KI: Dissociation constant of inhibitor in micromolar. Equation 9.6, in R.A. Copeland, Enzymes, 2nd edition, Wiley, 2001.

The enzyme concentration was fixed at 0.2 μ M and the substrate concentration was 12 μ M for the PABP1 peptide, which is equal to its KM value.

Table S2. IC₅₀ values and Ki values for compounds 5-14

Compound		CARM1 Inhibition (μM) ^a	
		IC ₅₀	$\mathbf{K}_{\mathbf{I}}$
SAH		0.756 ± 0.089	0.391 ± 0.040
5	H3 ¹⁰⁻²⁵	0.290 ± 0.015	0.096 ± 0.009
6	$H3^{10-25}(K^{18}Ac)$	0.155 ± 0.007	0.028 ± 0.004
7	H3 ¹³⁻²²	0.121 ± 0.007	0.020 ± 0.002
8	$H3^{13-22}(K^{18}Ac)$	0.155 ± 0.012	0.030 ± 0.005
9	H3 ¹⁴⁻²¹	0.287 ± 0.034	0.137 ± 0.018
10	$H3^{14-21}(K^{18}Ac)$	0.211 ± 0.023	0.066 ± 0.011
11	H3 ¹⁵⁻²⁰	0.143 ± 0.014	0.036 ± 0.005
12	$H3^{15-20}(K^{18}Ac)$	0.072 ± 0.008	0.001 ± 0.002
13	H3 ¹⁶⁻¹⁹	0.346 ± 0.031	0.130 ± 0.017
14	H3 ¹⁶⁻¹⁹ (K ¹⁸ Ac)	0.699 ± 0.081	0.320 ± 0.051
	. ,		

Supplemental table and figures for structural studies

Table S3. X-ray data collection and refinement statistics for mmCARM1 complexes with H313-31 peptidomimetics 3 and 4

PDB ID TS Mimic		70KP H313-31 K18Ac	70\$4
13 MIIIIC		HOLO-OL MICAL	
			H313-31 K18
	Resolution (Å)	46.11-2.20 (2.25-	45.76-2.54 (2.62-
		2.20)	2.54)
-	space group	P21212	P21212
	cell		74.37 98.61 206.61
	Total reflections	406216 (16351)	315674 (22239)
	Unique reflections	77281 (4317)	49843 (4042)
<u> </u>	Rmerge	0.092 (0.693)	0.129 (2.284)
Data processing	Rmeas	0.101 (0.809)	0.140 (2.501)
Data processing	Rpim	0.040 (0.406)	0.055 (0.996)
	Ι/σΙ	9.3 (1.5)	8.6 (0.6)
	CC1/2	0.998 (0.690)	0.999 (0.475)
	Completeness (%)	97.1 (93.7)	97.9 (87.4)
	Multiplicity	5.3 (3.8)	6.3 (5.5)
	Wilson B (Ų)	35.2	63.5
	Resolution limit for $I//\sigma$ (I) > 2.0 (A)	2.36	2.96
	Resolution (Å)	45.32 – 2.2 (2.28 -	45.76 - 2.542 (2.632 -
		2.2)	2.54)
	Rwork (%)	21.08 (31.08)	0.71 (35.19)
	Rfree (%	25.45 (34.88)	25.94 (36.78)
Refinement	Number of non-hy- drogen atoms	12185	11675
	macromolecules	11589	11504
	ligands	297	266
	solvent	425	21
	RMS(bonds)	0.003	0.003
	RMS(angles)	0.59	0.54
	Ramachandran fa- vored (%)	95.64	95.49
Validation	Ramachandran out- liers (%)	0.00	0.00
	Rotamer outliers (%)	0.32	2.00
	Average B-factor	47.62	64.83

Statistics for the highest-resolution shell are shown in parentheses. The resolution limits for I/ σ (I) > 2 are reported.

 $^{^{}a}$ IC₅₀ and KI values reported in μ M from duplicate data obtained from a minimum of 7 different concentrations \pm standard error of the mean (s.e.m.).

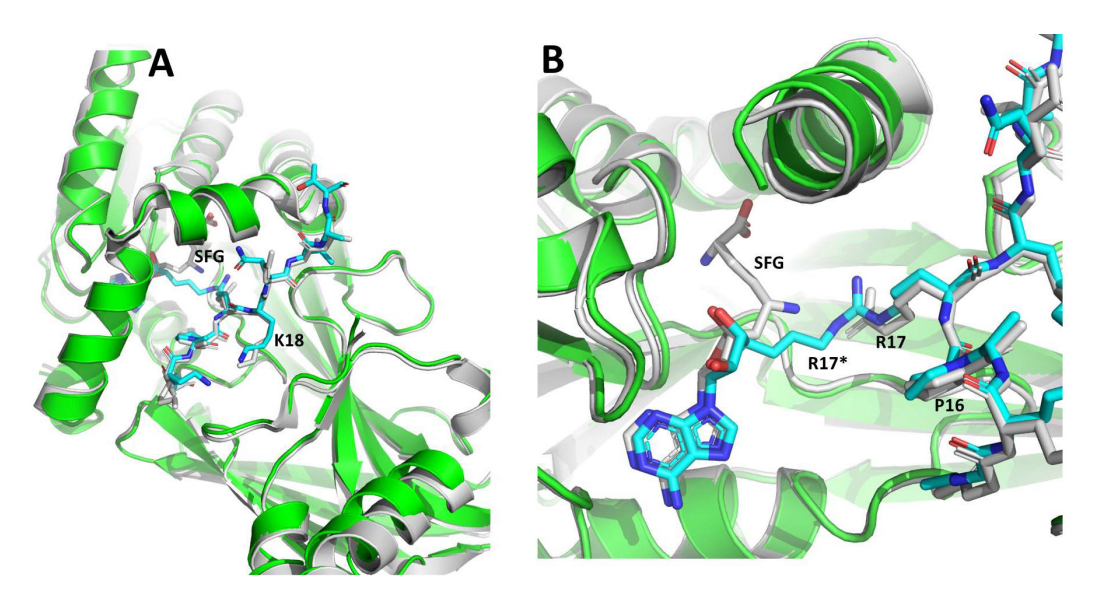


Figure S1. Structure of transition state mimic overlaid with isolated peptide in presence of SFG. (A) H3¹³⁻³¹ K¹⁸ peptidomimetic 3 in complex with mmCARM1 (green cartoon and blue sticks, PDB code 7OS4) superimposed with structure of SFG-H3R17 bound to hs-CARM1 (gray cartoon/sticks, PDB code 5DX0). (B) Close-up around the SFG binding site. For clarity, the N-terminal helices of mmCARM1 and hsCARM1 are not shown.

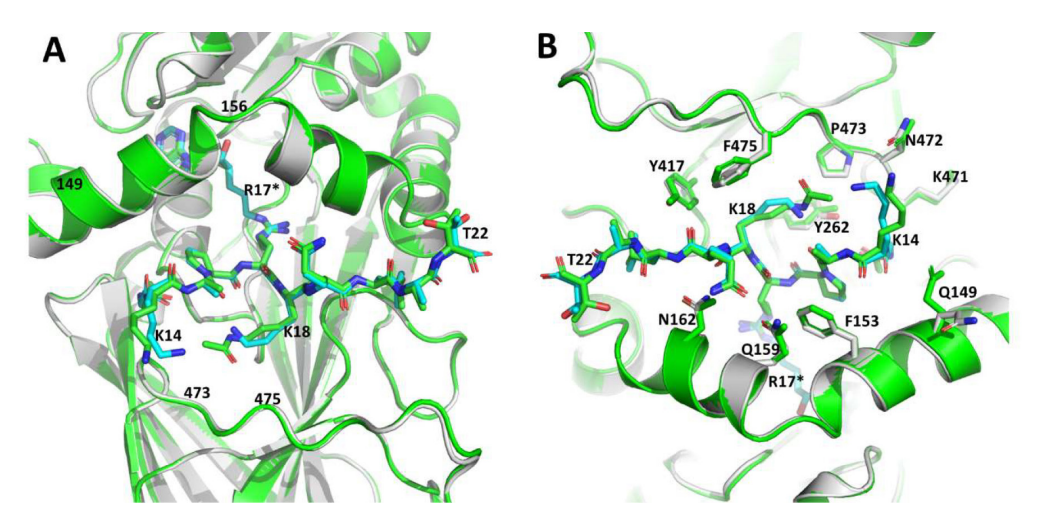


Figure S2. Superimposition of H3¹³⁻³¹(Lys¹⁸NH₂) and H3¹³⁻³¹(Lys¹⁸Ac) complexes with mmCARM1 (only local view of monomer A shown). (A) Superposition of H3¹³⁻³¹(Lys¹⁸NH₂) (blue sticks) and H3¹³⁻³¹(Lys¹⁸Ac) (green sticks) bound to mmCARM1 (gray/green cartoon) (monomer A), PDB codes 7OS4 and 7OKP respectively. (B) Close-up view of recognition mode for H3¹³⁻³¹(Lys¹⁸NH₂) and H3¹³⁻³¹(Lys¹⁸Ac).

Appendix III Supplementary materials for Chapter 4

LC-MS traces of analyte and internal standard

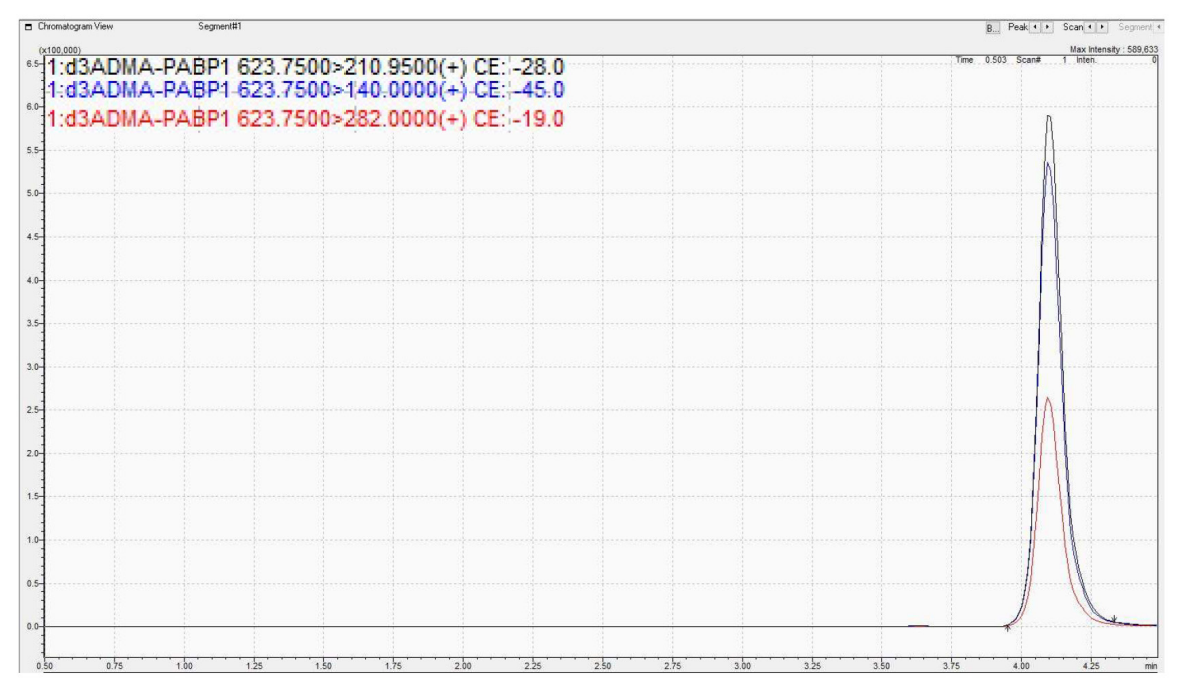


Figure S1. LC-MS/MS traces of PABP1 $^{456-466}$ R 460 -d $_6$ -aDMA (internal standard). MS method: 0.5-4.5 min; retention time 4.101 min, Q1 mass detection; 623.75; Q3 mass detection: 282.00, 210.95, 140.00.



Figure S2. LC-MS/MS traces of PABP1 $^{456-466}$ R 460 -aDMA (methylated product). MS method: 0.5-4.5 min; retention time 4.101 min, Q1 mass detection; 620.85; Q3 mass detection: 282.00, 211.00, 140.00.

Kinetic analysis of CARM1 substrates

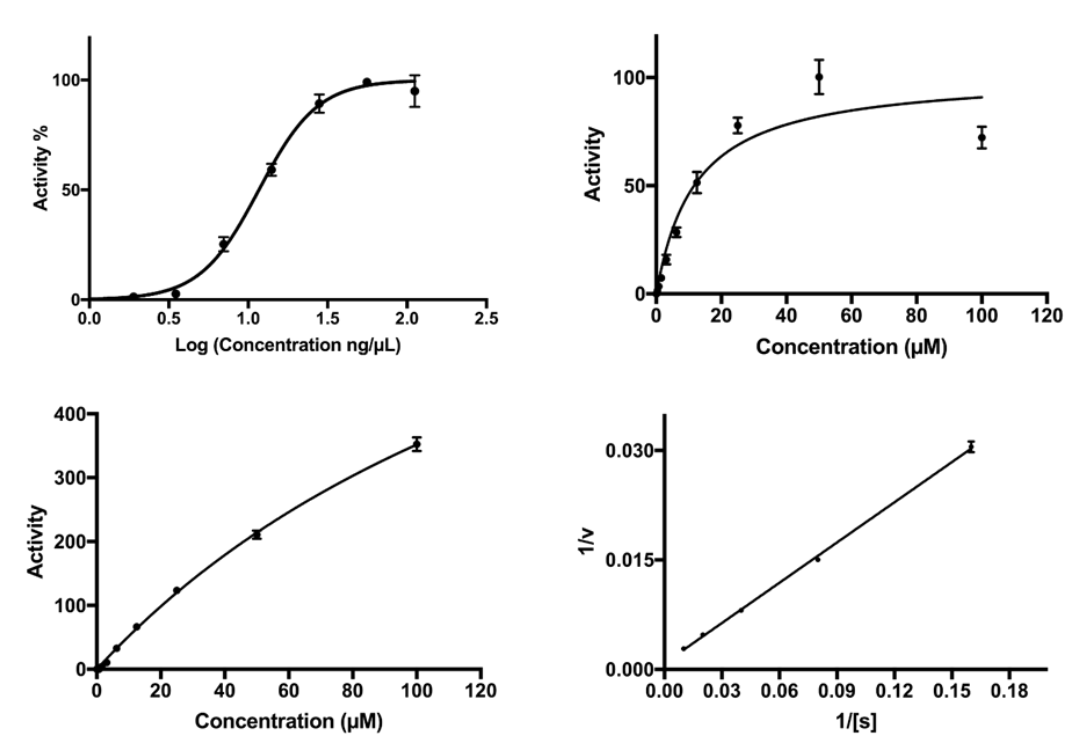
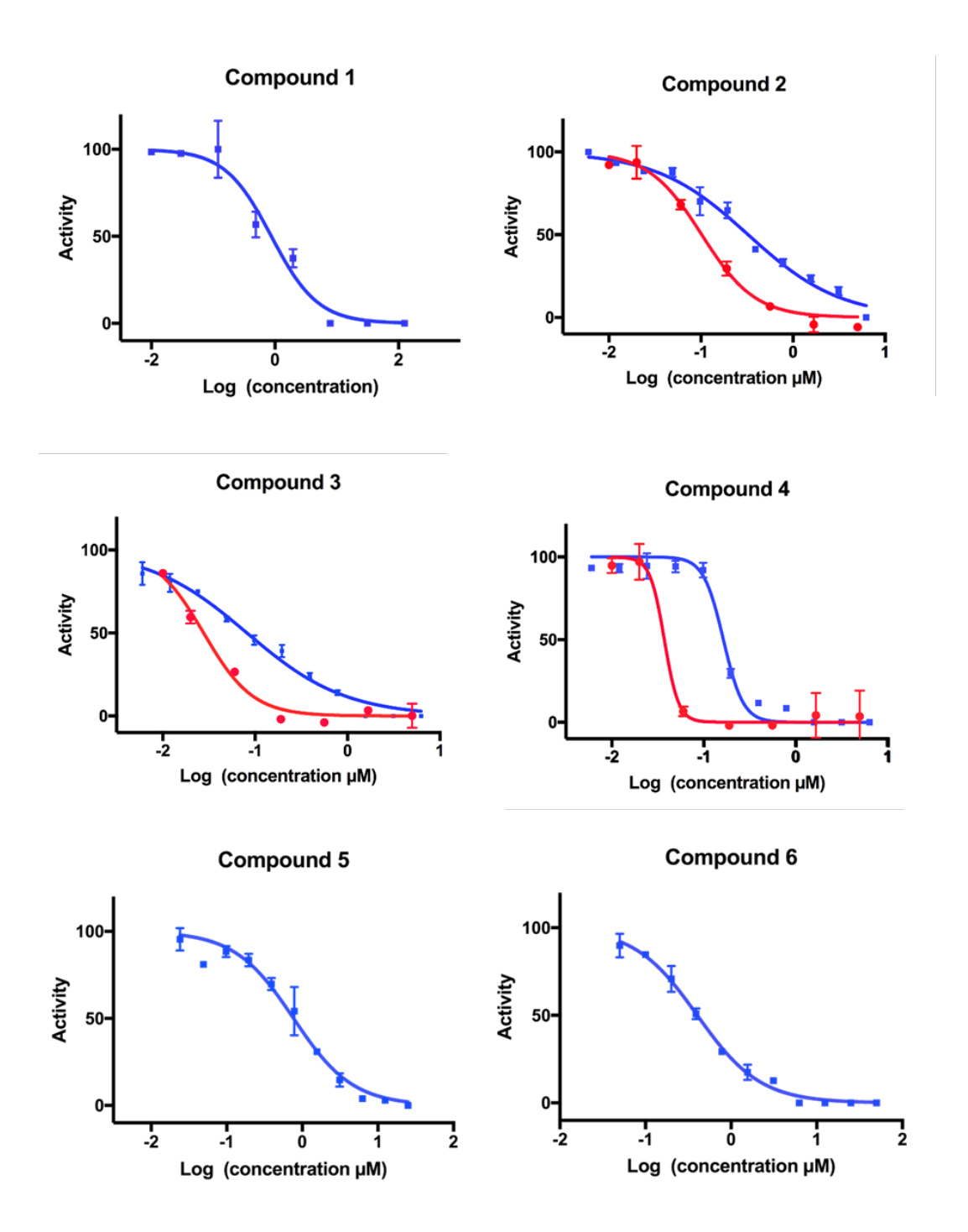


Figure S3. A. EC₅₀ curve for CARM1, EC₅₀ = 11.68 ± 0.33 ng/ μ L. B. Michaelis-Menten Plot for K_M value determination of PABP1⁴⁵⁶⁻⁴⁶⁶, K_{M, PABP1 456-466} = 12.03 ± 2.28 μ M. C. Michaelis-Menten Plot and Lineweaver Burk plot (D) for K_M value determination of AdoMet, K_{M, AdoMet} = 5.46 ± 0.01 μ M.

A

IC50 curves for compounds 1-9



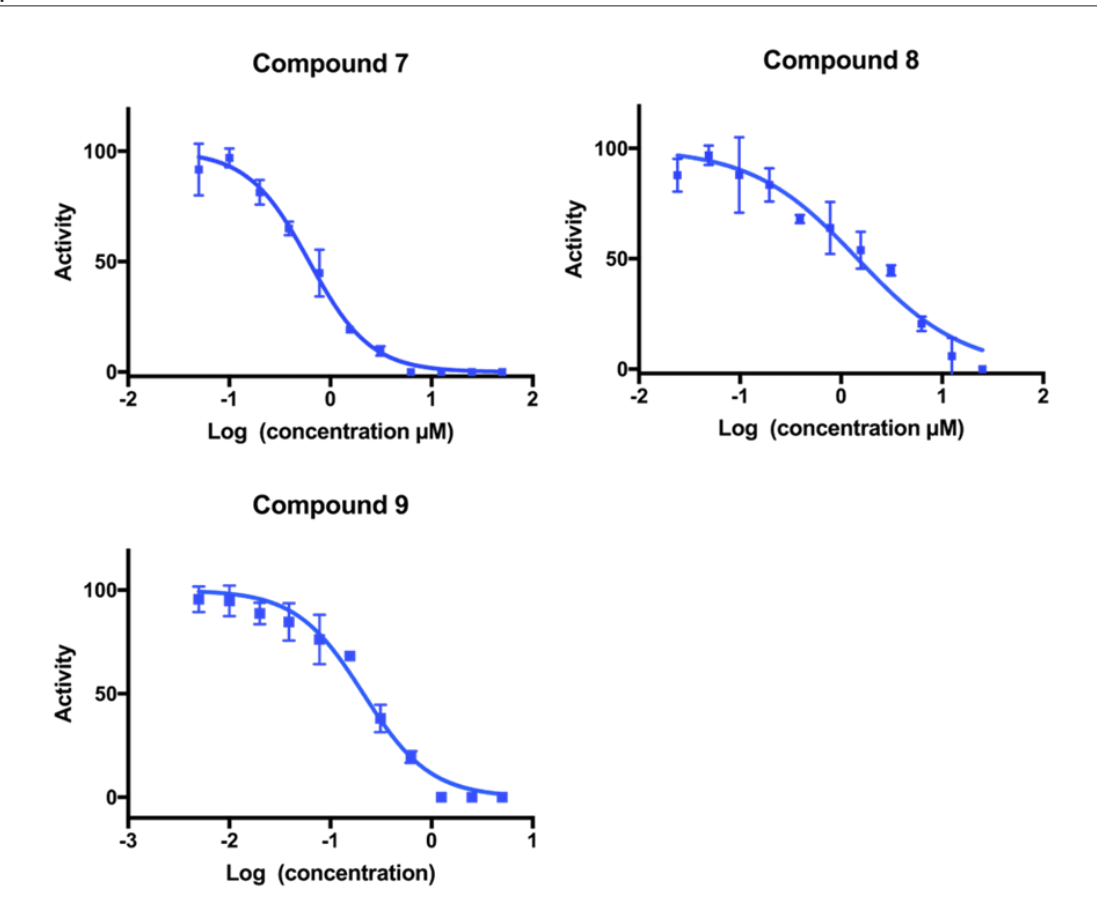


Figure S4. IC₅₀ curves of inhibitors 1-9. Blue curves represent the measurements obtained using the MRM LC-MS assay and red curves correspond to measurements obtained using commercially available the ELISA assay kit. The ELISA assay based IC₅₀ values for compounds 1, 5-9 presented in Table 3 of the manuscript are taken from our previously published work and the corresponding inhibition curves can be found there (refs 27 and 20).

HPLC and High Resolution Mass Spectrometry data for PABP1⁴⁵⁶⁻⁴⁶⁶ peptides High Resolution Mass Spectrometry (HRMS)

PABP1⁴⁵⁶⁻⁴⁶⁶ (m/z):

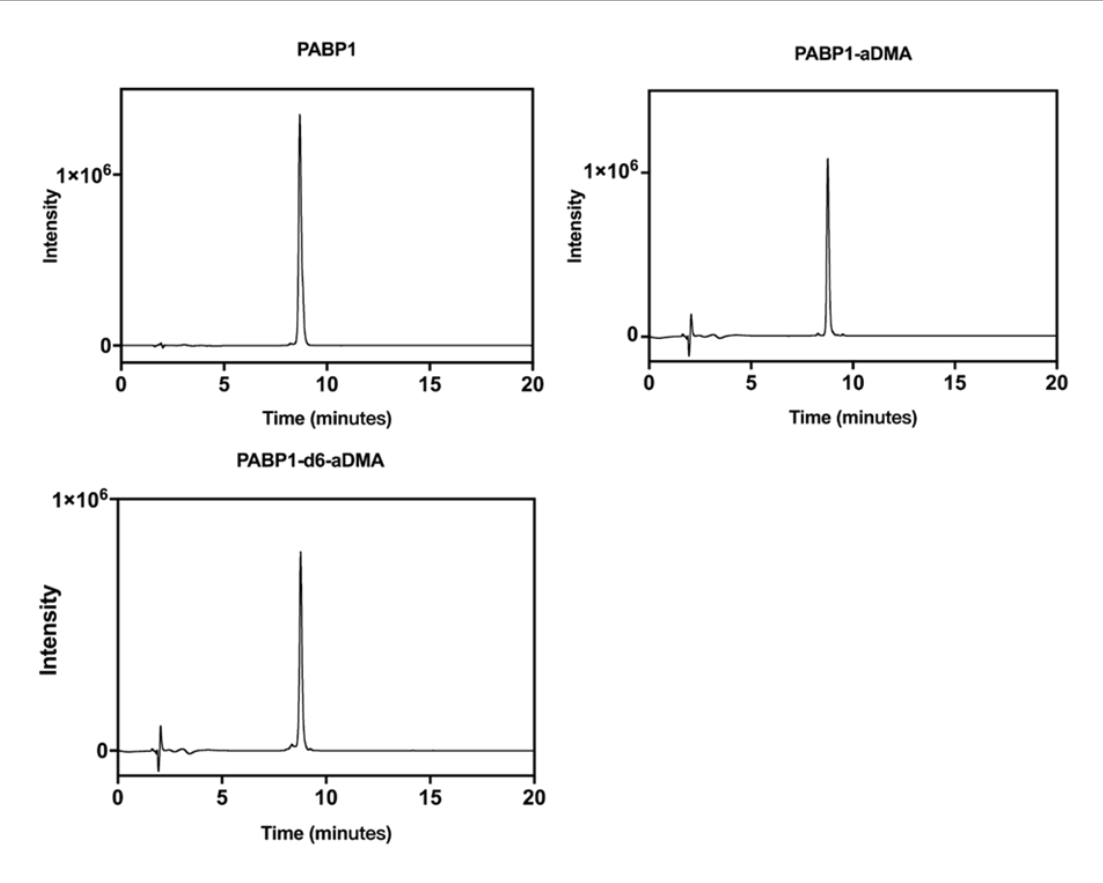
 $[M+H]^+$ calculated for $C_{55}H_{86}N_{15}O_{14}S^+$, 1212.6199, found 1212.6206.

PABP1⁴⁵⁶⁻⁴⁶⁶R⁴⁶⁰-aDMA (m/z):

 $[M+H]^+$ calculated for $C_{57}H_{90}N_{15}O_{14}S^+$, 1240.6512, found 1240.6516.

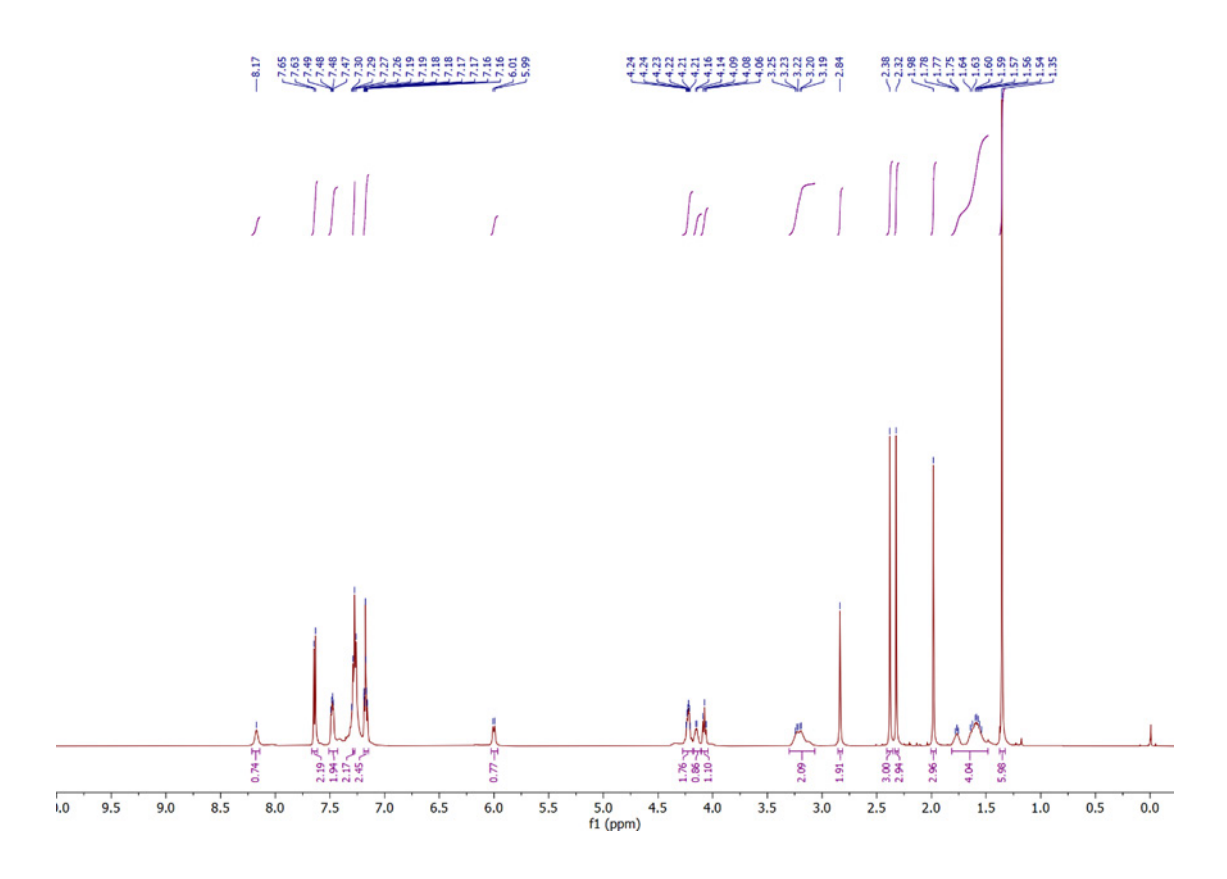
PABP1 $^{456-466}$ R 460 -d $_{6}$ -aDMA (m/z):

 $[M+H]^{+}$ calculated for $C_{57}H_{84}D_{6}N_{15}O_{14}S^{+}$, 1246.6889, found 1246.6894

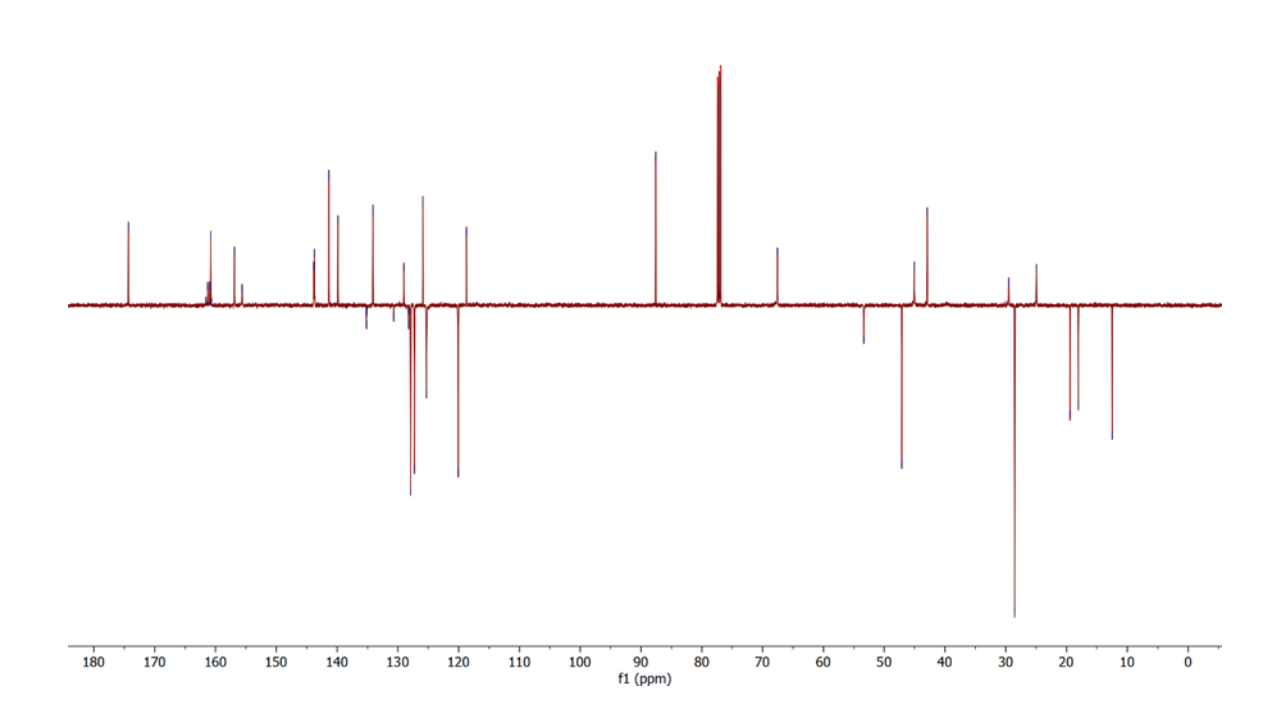


NMR Data of Fmoc-d₆-aDMA-OH

¹H NMR (500 MHz, CDCl₃)









Appendix IV Supplementary materials for Chapter 5

Reprogrammed mRNA display protocol

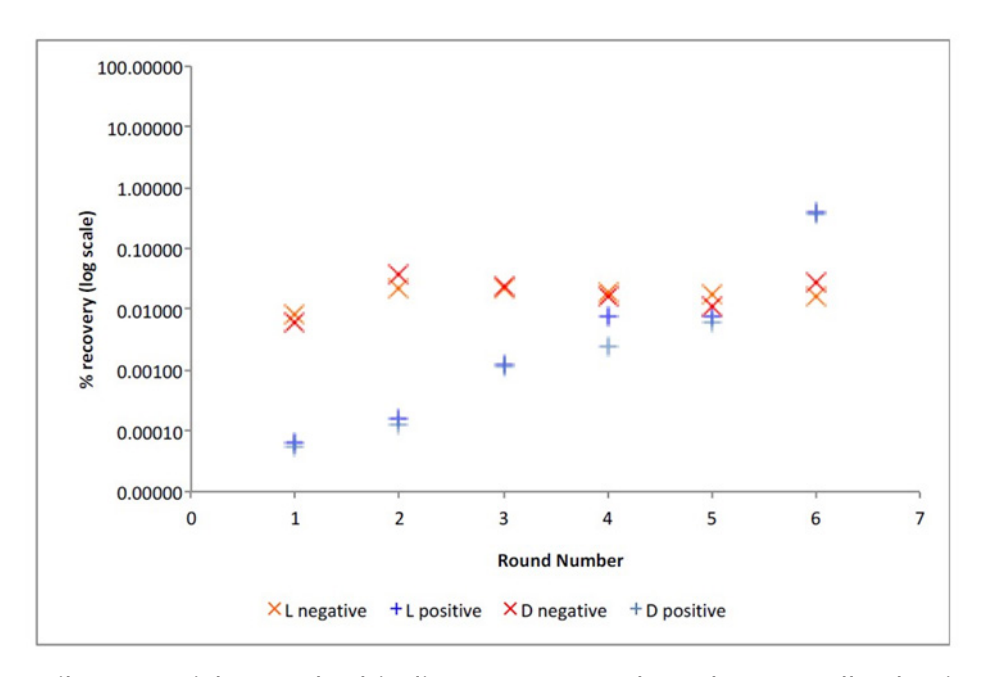


Figure S1. Library enrichment by binding to NNMT plotted across all selection rounds (log scale on Y-axis), showing binding against both immobilised NNMT ('positive', blue/ light blue plus symbol) and against the immobilisation medium alone ('negative', orange/red cross symbol) for both the L- and D-tyrosine initiated libraries (respectively).

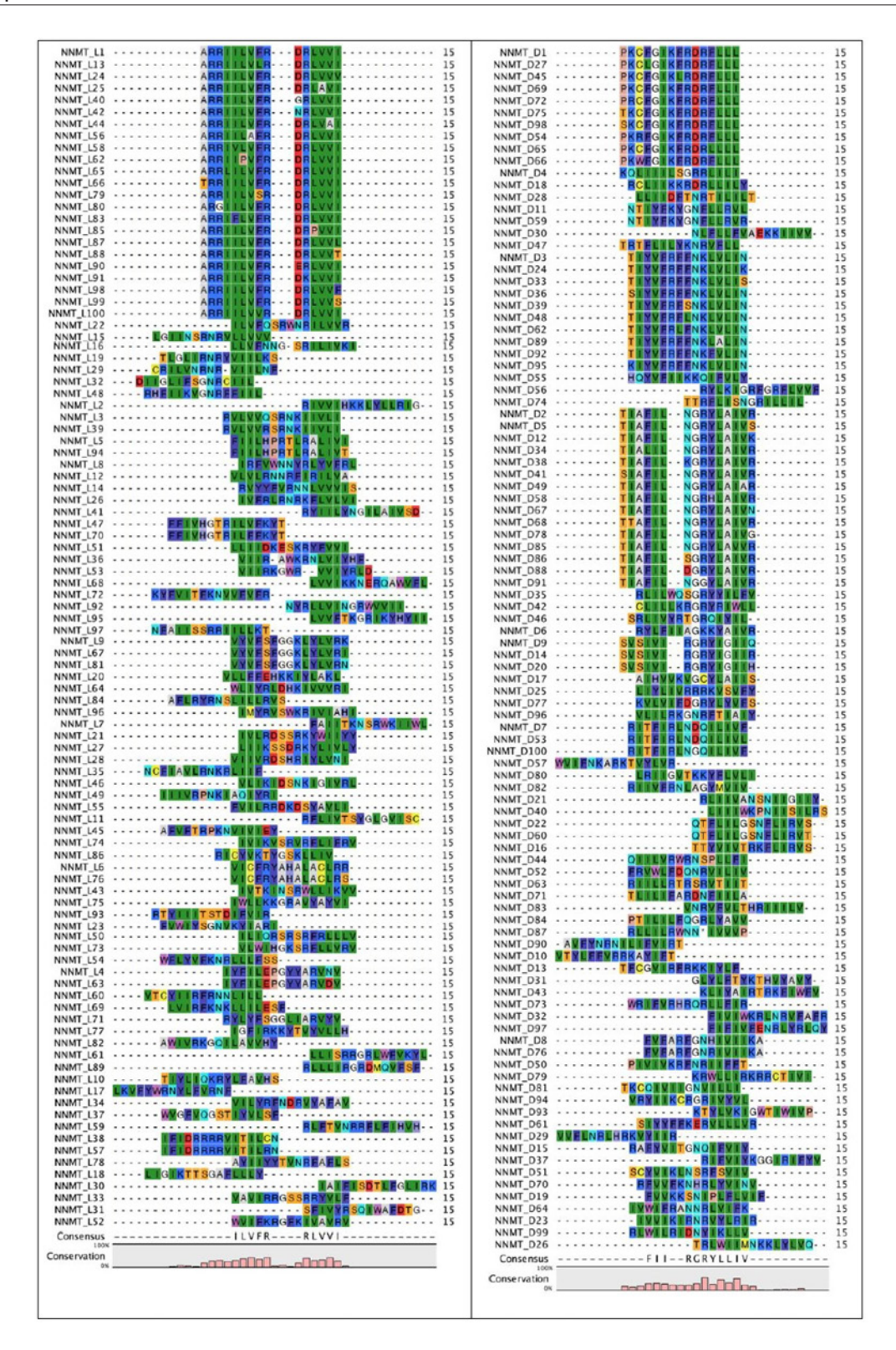


Figure S2. Sequence alignment of the L-tyrosine library (left) and D-tyrosine library (right). Colors indicate the properties of the respective amino acids. In both libraries hydrophobic (green) and positively charged (blue) amino acids are enriched.

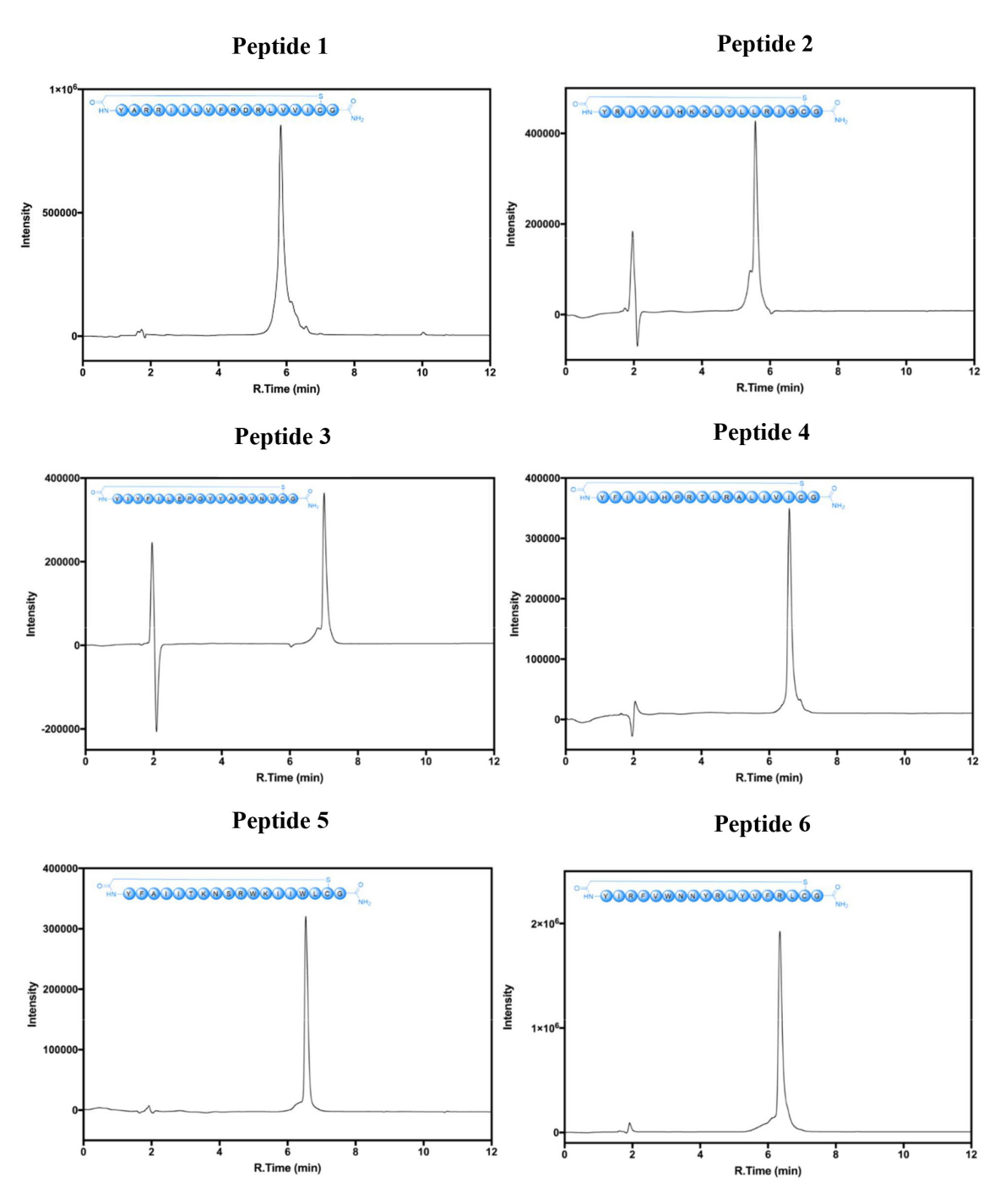


Figure S3. HPLC purity traces for peptides 1-6 over 12 minutes (5-100% acetonitrile).

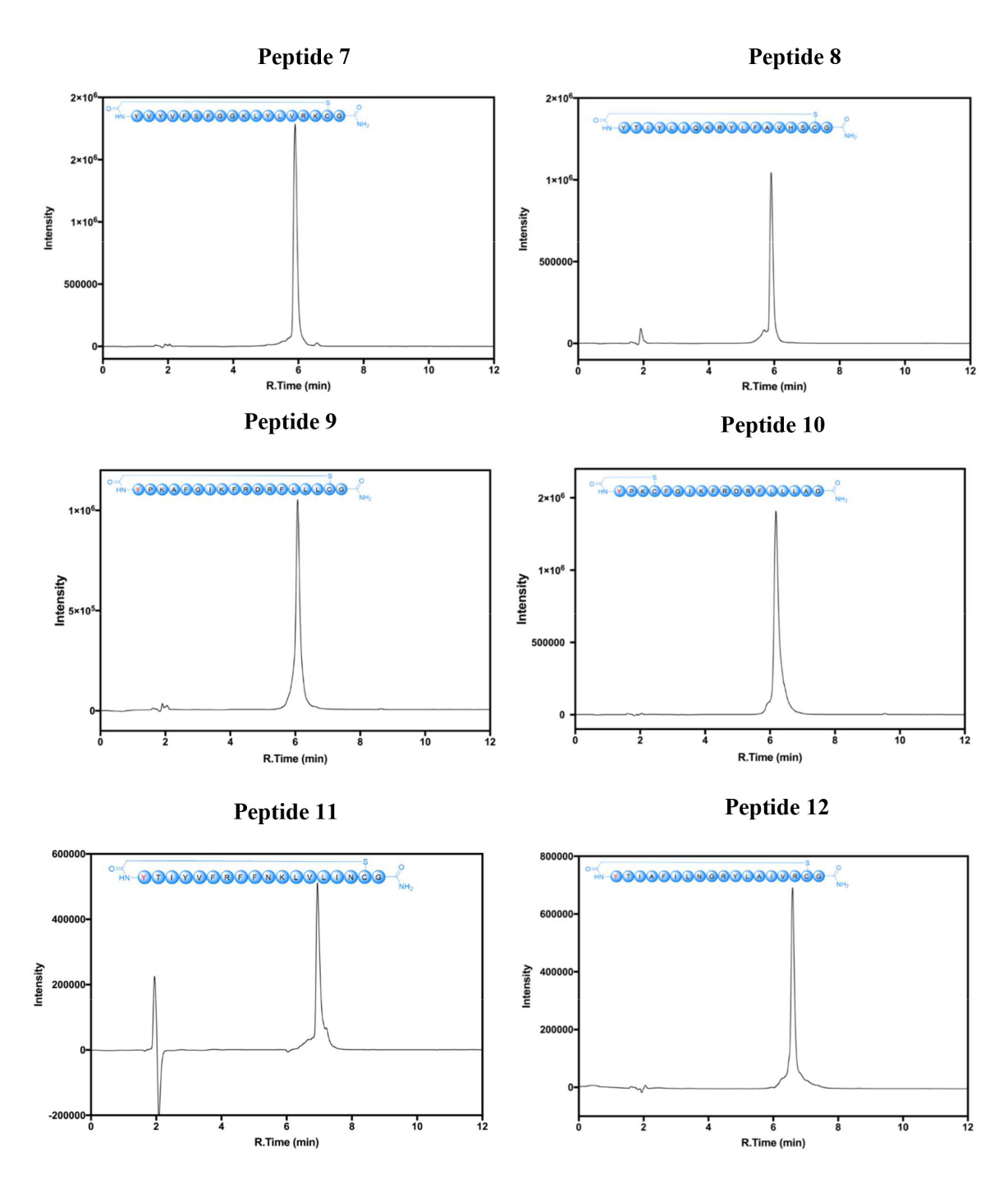


Figure S4. HPLC purity traces for peptides 7-12 over 12 minutes (5-100% acetonitrile).

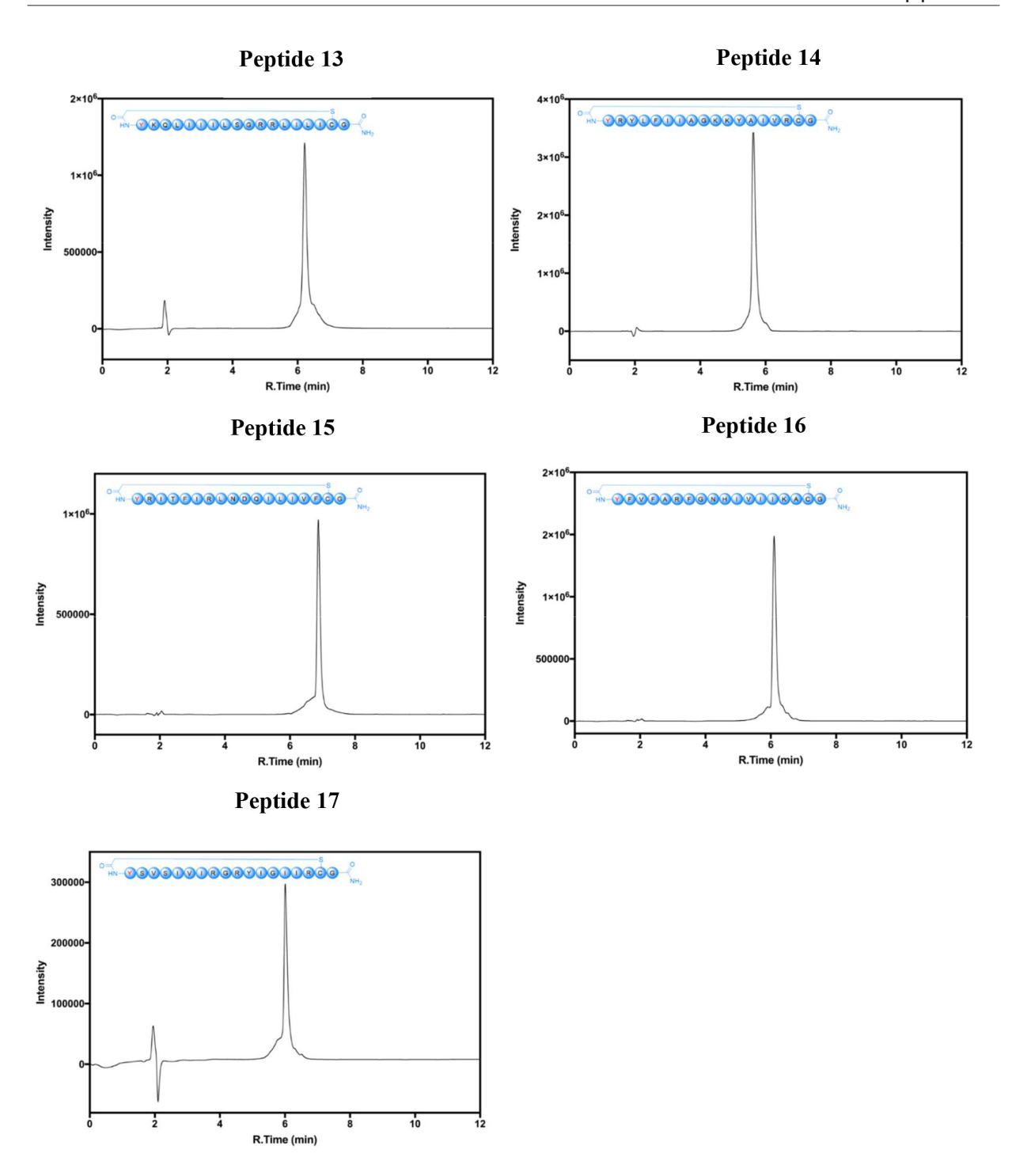


Figure S5. HPLC purity traces for peptides 13-17 over 12 minutes (5-100% acetonitrile).

IC₅₀ curves

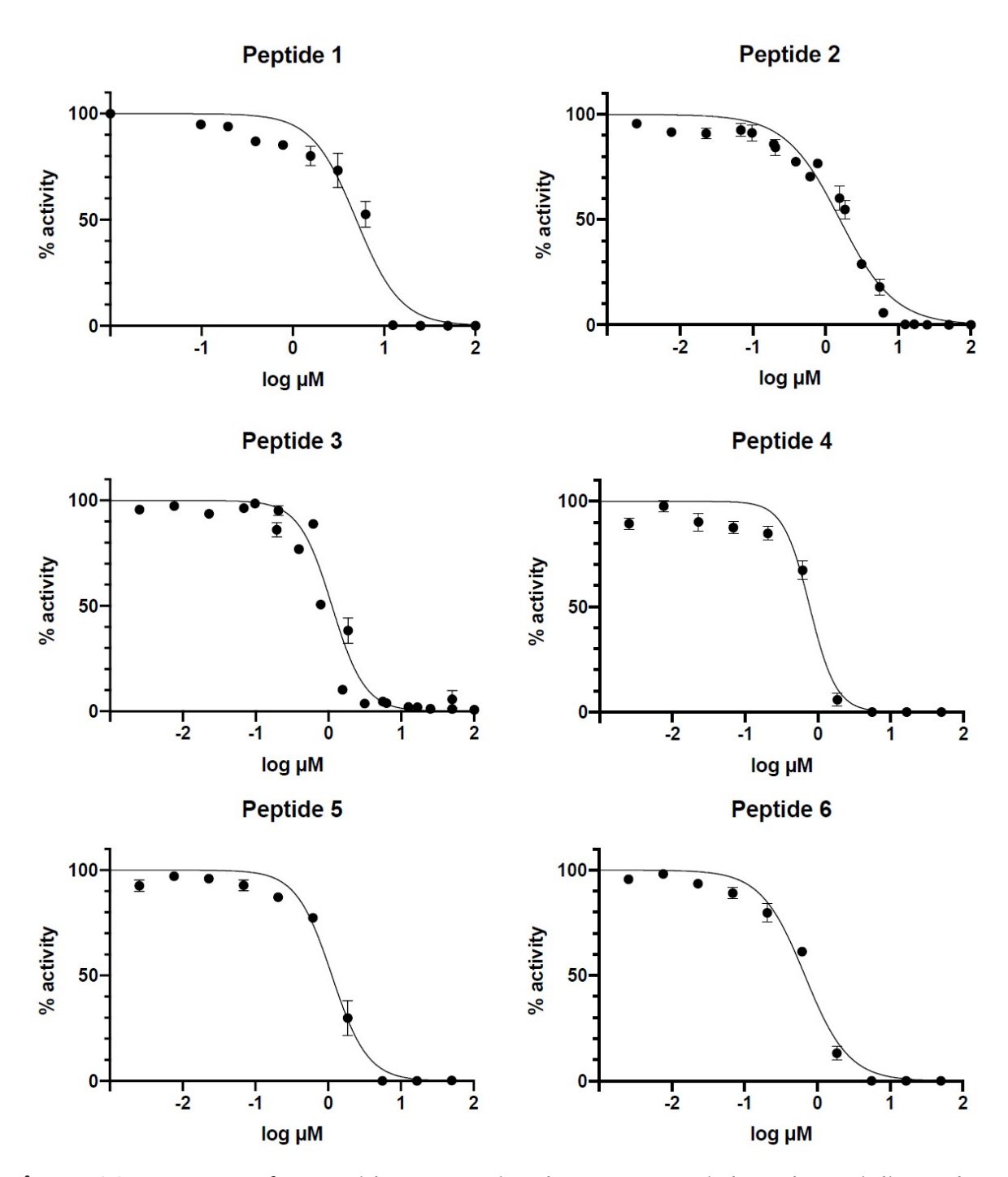


Figure S6. IC₅₀ curves for peptides 1-6 against hNNMT. Data is based on triplicate data of at least 10 different concentrations

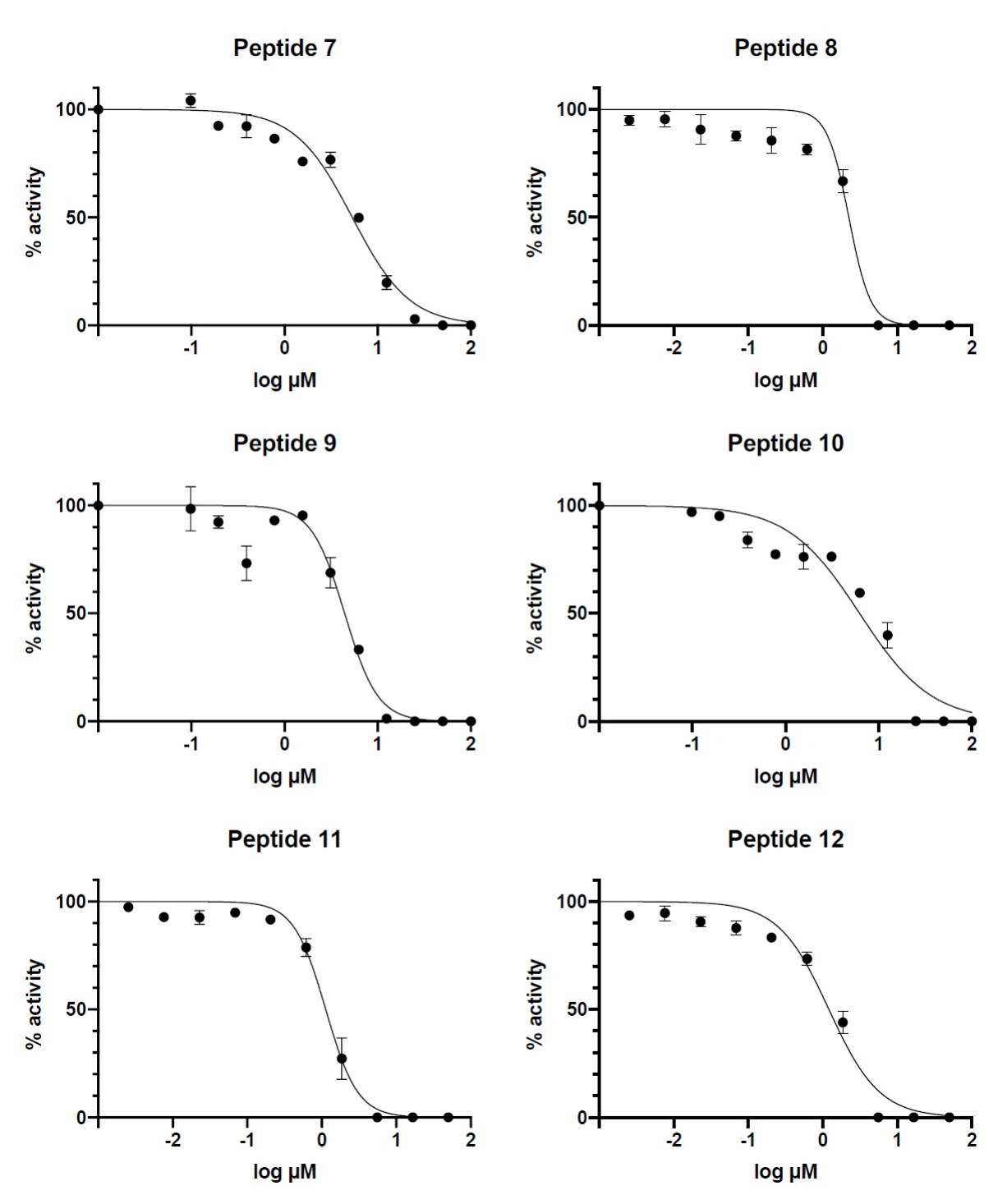


Figure S7. IC_{50} curves for peptides 7-12 against hNNMT. Data is based on triplicate data of at least 10 different concentrations

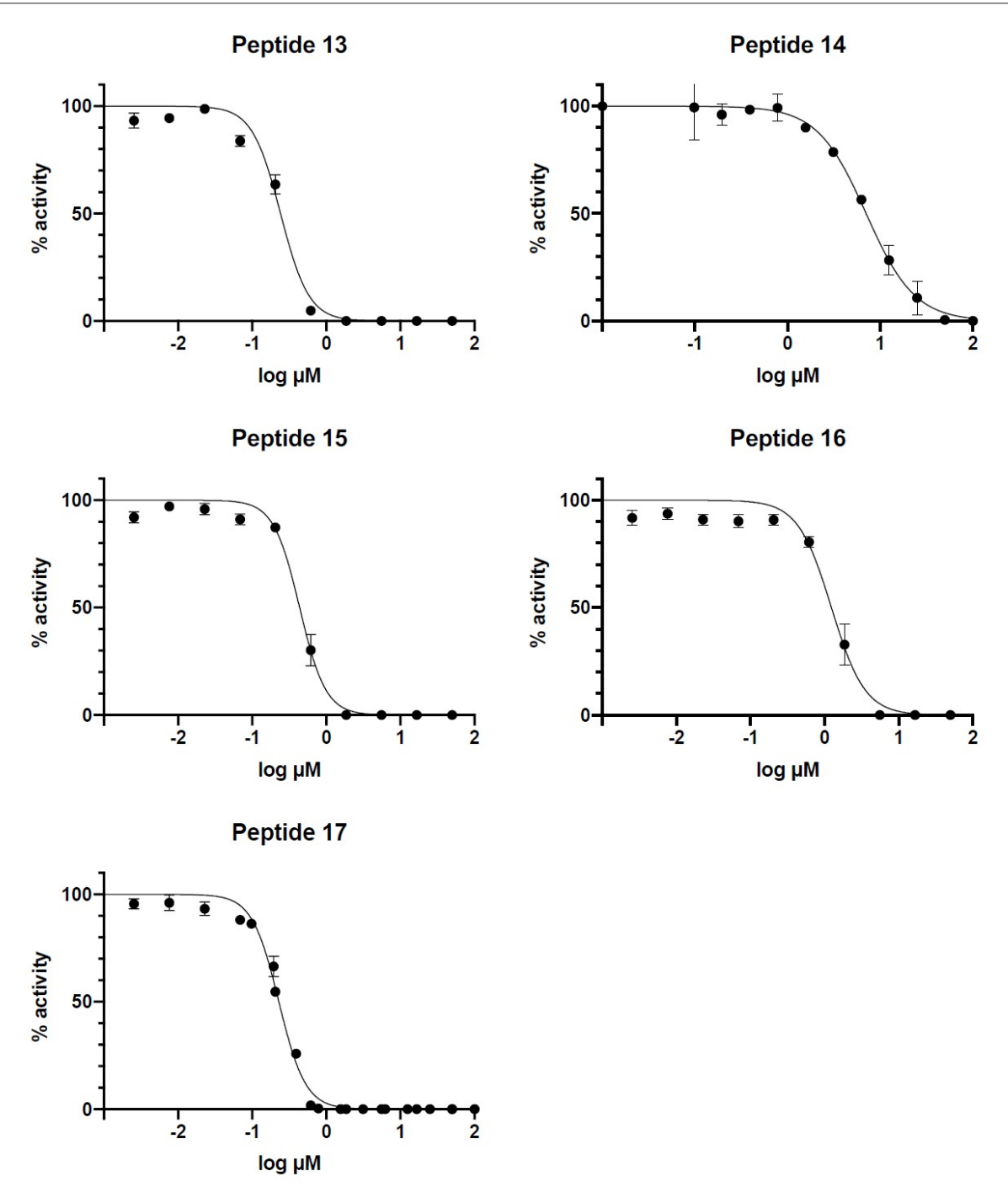


Figure S8. IC₅₀ curves for peptides 13-17 against hNNMT. Data is based on triplicate data of at least 10 different concentrations

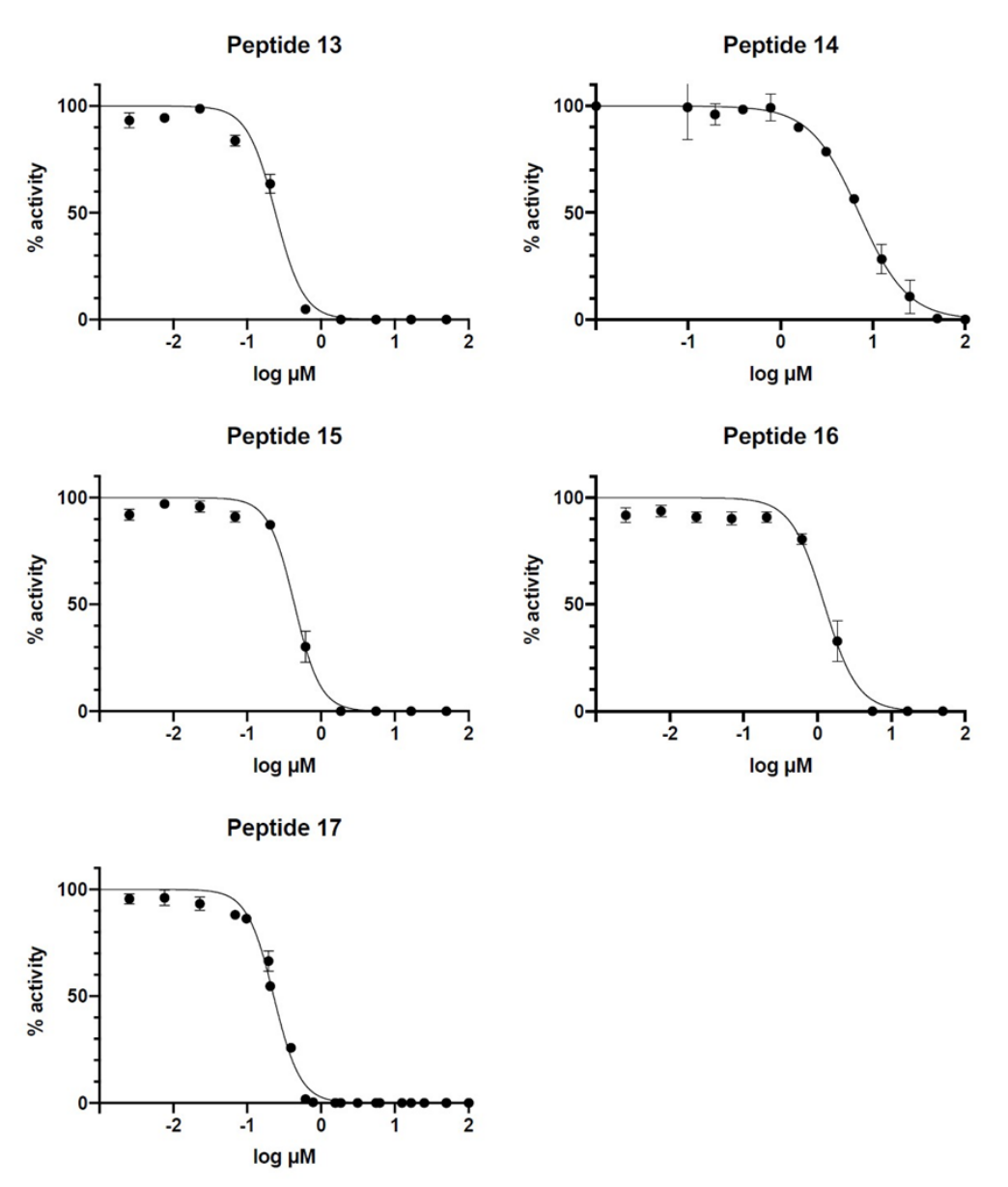


Figure S8. IC₅₀ curves for peptides 13-17 against hNNMT. Data is based on triplicate data of at least 10 different concentrations

IC₅₀ curves substrate competition

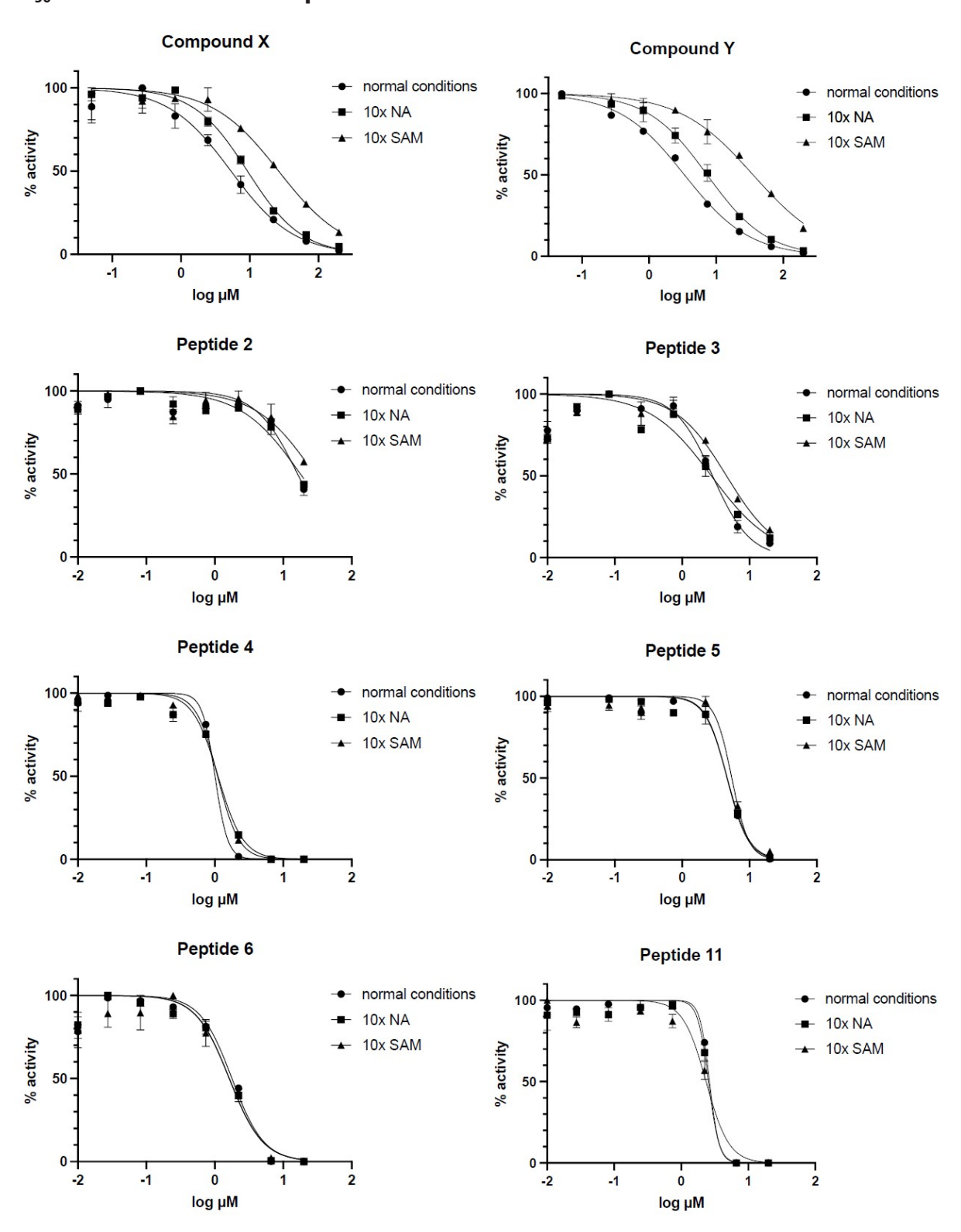


Figure S9. IC₅₀ curves for compounds X and Y and peptides 2-6 and 11 against hNNMT. Compounds were tested using normal conditions (substrates at their K_M value), or in the presence of 10-fold higher concentration of either nicotinamide (NA) or Sadenosyl-L-methionine (SAM). Data is based on duplicate data of at 8 different concentrations.

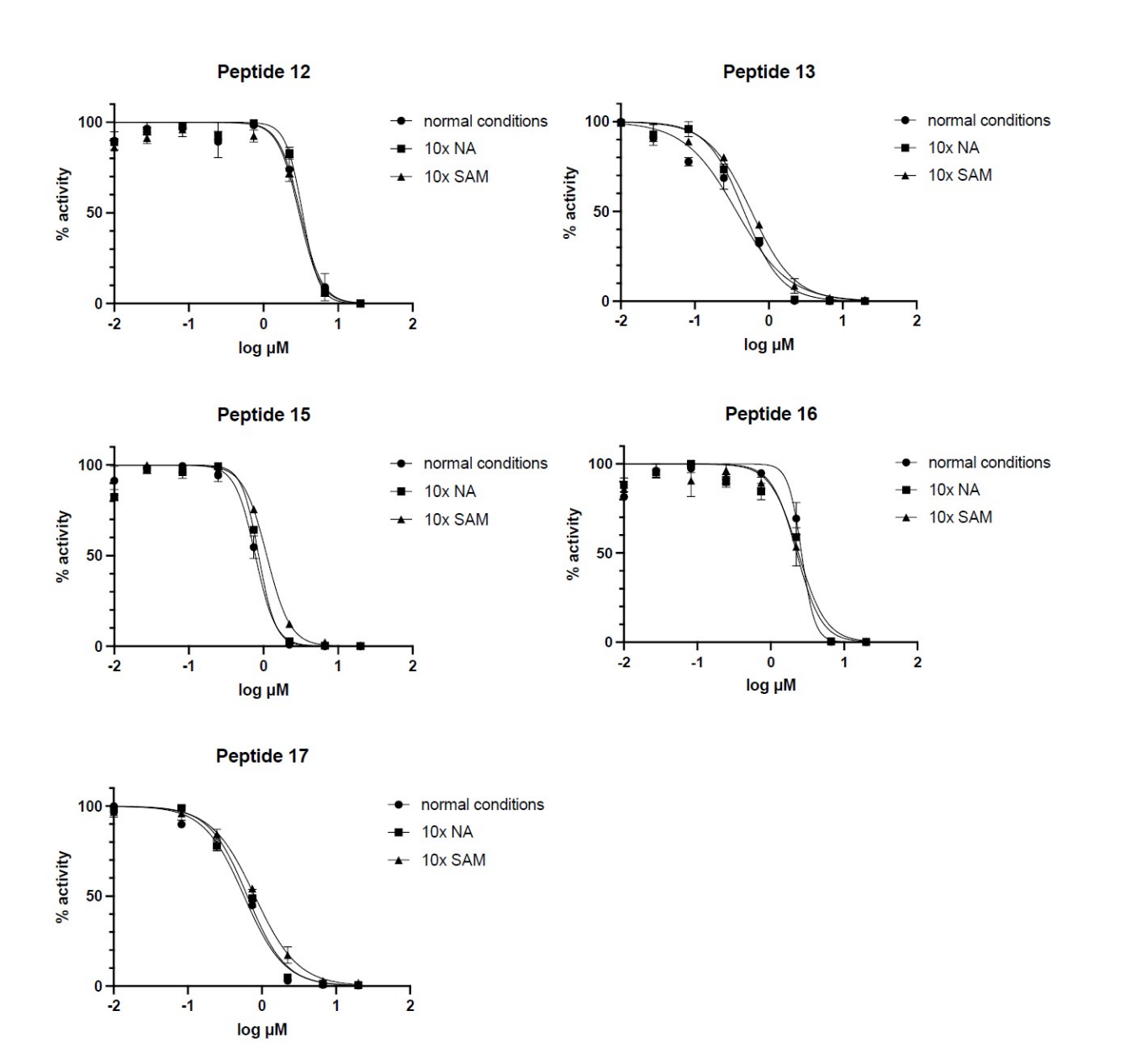
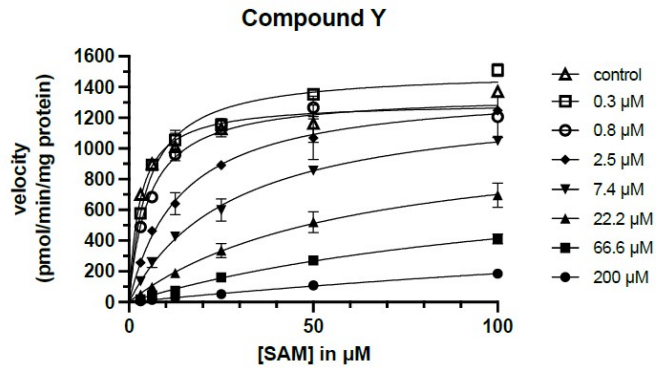
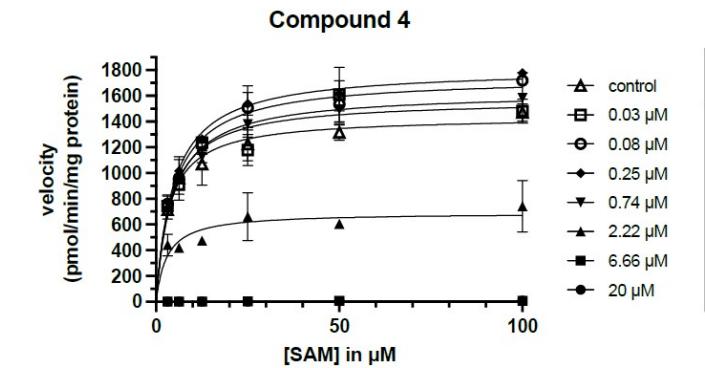


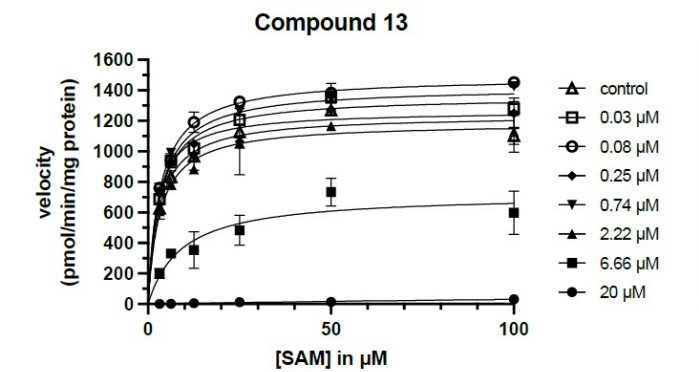
Figure S10. IC₅₀ curves for peptides 12-13 and 15-17 against hNNMT. Peptides were tested using normal conditions (substrates at their K_M value), or in the presence of 10-fold higher concentration of either nicotinamide (NA) or S-adenosyl-L-methionine (SAM). Data is based on duplicate data of at 8 different concentrations.



	V _{max}	
Compound Y	(pmol/min/mg)	$K_M(\mu M)$
200 μΜ	853,66 ± 280,87	359,80 ± 144,56
66.6 μM	920,18 ± 95,95	122,58 ± 20,00
22.2 μM	1115,25 ± 107,57	59,12 ± 11,21
7.4 µM	1337,44 ± 47,71	28,24 ± 2,52
2.5 μM	1396,86 ± 50,82	14,00 ± 1,58
0.8 μM	1350,80 ± 43,44	5,42 ± 0,72
0.3 μM	1503,99 ± 40,47	5,03 ± 0,58
control	1299,61 ± 42,57	2,93 ± 0,50



Compound 4	V _{max} (pmol/min/mg)	<i>K_M</i> (μM)
20 μM	-	-
6.66 µM		-
2.22 μM	690.79 ± 60.07	2.92 ± 1.34
0.74 μM	1627.80 ± 52.10	4.51 ± 0.64
0.25 μΜ	1811.27 ± 40.56	4.73 ± 0.46
0.08 μΜ	1744.78 ± 50.42	4.74 ± 0.59
0.03 μΜ	1568.55 ± 79.20	4.00 ± 0.93
control	1437.15 ± 55.94	3.41 ± 0.65



	V _{max}	
Compound 13	(pmol/min/mg)	$K_M(\mu M)$
20 μΜ	-	-
6.66 µM	719,53 ± 76,43	9,08 ± 3.39
2.22 μΜ	1186,86 ± 32,66	3,23 ± 0.45
0.74 μΜ	1421,84 ± 47,38	3,29 ± 0.55
0.25 μM	1266,71 ± 47,37	2,41 ± 0.52
0.08 μM	1487,49 ± 18,05	3,22 ± 0.20
0.03 μΜ	1360,22 ± 32,96	3,11 ± 0.39
control	1237,38 ± 37,19	3,03 ± 0.47

Figure S11. V_{max} and K_M values for NNMT and SAM respectively after treatment of varying concentrations of compound Y, 4 or 13. The change in K_M observed for SAM after treatment with compound Y supports competitive inhibition. The unchanged K_M and changing V_{max} observed for compounds 4 and 13 supports the non-competitive or allosteric mode of inhibition for the cyclic peptides.

C

Curriculum vitae

Yurui Zhang was born on 28 November 1991 in Datong, China. He started a bachelor's program in pharmaceutic science at Hebei medical University. Since 2011, he started his internship in the laboratory of Prof. Caiqing Yang, studying the preparation of Oleanolic Acid Co-crystals and analysis. After spending two years on bench work, he obtained a bachelor's degree (with distinction). Later, he was enrolled in Peking Union Medical College of TsingHua University in 2014. He conducted his scientific research under Prof. dr. Wenqing Xu, studying in radio protection and radio therapy in vivo and in vitro. In 2017, he was granted his Ph.D. studies from China Scholarship Council (CSC). He subsequently joins the Martin group under the supervision of Prof. dr. Nathaniel I. Martin and Dr. Matthijs J. van Haren. Most of his Ph.D. work is presented in this thesis.

P

List of Publications

Zhang, Y., van Haren, M.J., Marechal, N., Troffer-Charlier, N., Cura, V., Cavarelli, J., Martin, N.I. A Direct Assay for Measuring Activity and Inhibition of Coactivator Associated Arginine Methyltransferase 1. Biochemistry (Accepted in press)

Zhang, Y., Marechal, N., van Haren, M.J., Troffer-Charlier, N., Cura, V., Cavarelli, J., Martin, N.I. Structural studies provide new insights into the role of lysine acetylation on substrate recognition by CARM1 and inform the design of potent peptidomimetic inhibitors. ChemBioChem. (2021)

van Haren, M.J., Zhang, Y., Thijssen, V., Buijs, N., Gao, Y., Mateuszuk, L., Fedak, F.A., Kij, A., Campagna, R., Sartini, D., Emanuelli, M., Chlopicki, S., Jongkees, S.A.K., Martin, N.I. Macrocyclic Peptides as Allosteric Inhibitors of Nicotinamide N-Methyltransferase (NNMT). RSC Chemical Biology. (2021)

Gao, Y., van Haren, M.J., Buijs, N., Innocenti, P., Zhang, Y., Sartini, D., Campagna, R., Emanuelli, M., Parsons, R.B., Jespers, W., Gutiérrez-de-Terán, H., van Westen, G., Martin, N.I. Potent inhibition of nicotinamide N-methyltransferase by alkene linked bisubstrate mimics bearing electron deficient aromatics. Journal of Medicinal Chemistry. (2021)

Zhang, Y., van Haren, M.J., Martin, N.I. Peptidic transition state analogues as PRMT inhibitors. Methods. (2020)

Zhang, Y., Wang, J., Li, Y., Meng, Y., Zhang, Y., Yang, F., Xu, W. Design and Synthesis a Mitochondria-Targeted Dihydronicotinamide as Radioprotector. Free Radical Biology & Medicine. (2019)

Zhang, Y., Li, Y., Wang, J., Li, Wang, H., Wang, H., Kang, X., Xu, W. Synthesis and characterizaion of a rosmarinic acid derivative that targets mitochondria and protects against radiation-induced damage in vitro. Radiation Research. (2017)

Zhang Y, Wang, J., Li, Y., Wang, F., Yang, F., Xu, W. Synthesis and Radioprotective Activity of Mitochondria Targeted Dihydropyridines. International Journal of Molecular Science. (2017)

Liu, Y., Zhang, C., Zhang, H., Li, M., Yuan, J., Zhang, Y., Zhou, J., Guo, H., Zhao, L., Du, Y., Wang, L., Ren, L. Synthesis and antitumor activity of a novel series of 6-substituted pyrrolo[2,3-d]pyrimidines as potential nonclassical antifolates targeting both thymidylate and purine nucleotide biosynthesis. European Journal of Medicinal Chemistry. (2015)